

**DISSECTING THE ROLE OF B2 SINE RNA PROCESSING IN
ACTIVATION OF STRESS RESPONSE GENES IN MOUSE BRAIN
AMYLOID AND AGING PATHOLOGY**

CHRISTOPHER R. ISAAC
Bachelor of Science, University of Lethbridge, 2017

A thesis submitted
in partial fulfilment of the requirements for the degree of

MASTER OF SCIENCE

in

BIOCHEMISTRY

Department of Chemistry and Biochemistry
University of Lethbridge
LETHBRIDGE, ALBERTA, CANADA

DISSECTING THE ROLE OF B2 SINE RNA PROCESSING IN ACTIVATION
OF STRESS RESPONSE GENES IN MOUSE BRAIN AMYLOID AND AGING
PATHOLOGY

CHRISTOPHER R. ISAAC

Date of Defence: July 30, 2020

Dr. Athanasios Zovoilis Thesis Supervisor	Assistant Professor	Ph.D.
--	---------------------	-------

Dr. Marc Roussel Thesis Examination Committee Member	Professor	Ph.D.
---	-----------	-------

Dr. Trushar Patel Thesis Examination Committee Member	Associate Professor	Ph.D.
--	---------------------	-------

Dr. Michael Gerken Chair, Thesis Examination Committee	Professor	Ph.D.
---	-----------	-------

Dedication

I would like to dedicate this thesis to my family.

Abstract

Alzheimer's disease (AD) is a neurodegenerative disorder that results in impairment of learning and memory. Previous work in mice has shown that learning correlates with hippocampus-specific changes in expression of stress response genes (SRGs) and that excess expression of SRGs results in apoptosis. Many mouse SRGs are regulated by a non-coding SINE RNA called B2, but it is unclear how SINE RNAs contribute to AD overall. In this work we show via RNAseq that there is abnormal hyperactivation of SRGs caused by dysregulation of the B2-mediated stress response mouse amyloid-aging pathology. We also show that B2 RNA degradation is abnormally high during active neurodegeneration and that the increase in B2 degradation is due to Hsf1-mediated cleavage of B2 RNA during amyloid beta-induced stress. Our research reveals a novel connection between abnormal SINE RNA processing, SRG hyperactivation, and amyloid-aging pathology. Further study of SINE RNAs may elucidate new AD therapies.

Contributions of Authors

I would like to acknowledge that this work has been made possible through a collaborative effort among the following individuals with whom I share the respective IP and any future authorship resulting from this work. Dr. Athanasios Zovoilis contributed to the overall design of the experiments, data analysis, and figure preparation. Luke Saville assisted with experiments in the wet lab and also helped with data analysis and figure preparation. Dr. Babita Gollen performed the library preparations for the RNA sequencing. Yubo Cheng performed RNA-Seq data analysis and contributed to figure preparation.

Acknowledgments

I would like to thank the lab members that have been with me through the entirety of this journey: Dr. Athanasios Zovoilis for his guidance and insight, Luke Saville for his assistance and long hours in the lab, Dr. Babita Gollen for her steady hand and library preparations, and Yubo Cheng for her computational expertise. In addition, I would like to thank our collaborators Dr. Jogender Mehla and Dr. Majid Mohajerani from the Canadian Centre for Behavioral Neuroscience. I would also like to thank Adam Christiansen for his help with the \LaTeX formatting.

Contents

Contents	vii
List of Tables	x
List of Figures	xi
List of Abbreviations	xiii
1 Introduction	1
1.1 Amyloid Pathology and Alzheimer's Disease	1
1.1.1 Alzheimer's Disease	1
1.1.2 Impact of Alzheimer's Disease	2
1.2 Alzheimer's Disease Pathogenesis and Aetiology	4
1.2.1 Amyloid Pathology	4
1.2.2 Tau Fibrils	6
1.2.3 Alpha Synuclein	7
1.2.4 Apolipoprotein E4	8
1.2.5 Mitochondrial Deficiency	9
1.3 The Transcriptomic Angle	10
1.3.1 Stress Response Genes	10
1.3.2 Non-Coding RNAs	12
1.3.3 B2 SINE RNAs	12
1.4 Hypothesis and Objectives	14
1.4.1 Rationale	14
1.4.2 Hypothesis	16
2 Methods	19
2.1 Transgenic Mouse Model	19
2.1.1 Genetic Background and Age	19
2.1.2 Sample Acquisition	20
2.2 Cell Culture	21
2.2.1 HT22 Cell Line	21
2.2.2 Counting Cells	22
2.2.3 Amyloid-Beta Oligomers	22
2.2.4 LNA Transfections	22
2.3 In Vitro Methods	24
2.3.1 B2 RNA In Vitro Transcription	24
2.3.2 RNA-Protein Incubations	24

2.4	Gel Electrophoresis Methods	25
2.4.1	Agarose Gels	25
2.4.2	Urea PAGE	25
2.4.3	Quantification of Processing Rates	26
2.5	Quantitative Polymerase Chain Reaction	26
2.5.1	Sample Preparation	26
2.6	RNA Sequencing	26
2.6.1	Library Preparation of Hippocampal Samples	26
2.6.2	Long RNA-Seq	27
2.6.3	Short RNA-Seq	28
2.6.4	Preparation for Cell Culture Samples	28
2.7	Bioinformatics Analysis	28
3	Results	31
3.1	Gene Networks Controlled by B2 have Diverse Functions	31
3.1.1	GO Terms and KEGG Pathways of PreHS B2 Binding Genes	31
3.1.2	PreHS B2 Binding Genes and Learning-Associated Genes have Overlap	33
3.2	B2 RNA Processing and SRG Activation in RNA-Seq Data	38
3.2.1	B2 RNA Processing is Increased in Mouse Models of AD	38
3.2.2	Alzheimer's Disease and Old Age Results in Aberrant Tran- scription of Stress Response Genes	40
3.2.3	B2 is Colocalized with Transcriptionally Active Regions	41
3.3	B2 Processing in APP Mice using Short RNA-seq	42
3.3.1	RNA Sequencing Reveals Increased Processing of the B2 RNA in AD Mice	42
3.3.2	RNA Sequencing Reveals Increased Transcription of Hsf1 in AD Mice	43
3.3.3	AD Causes Abnormally High Expression of SRGs	44
3.3.4	AD Also Causes a Depression in Overall Transcription	45
3.4	B2 RNA Processing In Vitro	46
3.4.1	B2 RNA is Not Degraded by Amyloid Beta Fragments	46
3.4.2	B2 is Degraded by Hsf1 Over Time In Vitro	47
3.4.3	The Processing Rate of B2 is Dose-Dependent on Hsf1	48
3.5	Cell Culture and LNA and Amyloid Challenges	50
3.5.1	Incubation of Hippocampal Neurons with Amyloid Results in an Increase in FOSB Transcription	50
3.5.2	The Downregulation of Hsf1 Limits the Activation of FOSB by Amyloid Beta During Amyloid Toxicity	51
4	Discussion	55
4.1	The Link Between Learning, Stress, and Memory	55
4.2	B2 RNA is Aberrantly Processed in AD	56
4.3	B2 RNA Processing is Related to Abnormal SRG Activation	57
4.4	The Role of Hsf1 and FOSB	58

4.5 Future Directions	60
5 Conclusion	63
Bibliography	64
Appendix A Reagents	79
Appendix B Gene Lists	81
B.1 Pre-Heatshock Genes	81
B.2 Learning Associated Genes	85
B.3 APP Upregulated Genes	88
B.4 PreHS and Learning Genes	89

List of Tables

2.1	Effects of introduced Swedish, Arctic, and Iberian familial AD mutations in humanized APP mice.	19
2.2	Genotypes, ages, and number of sampled mice.	20
2.3	Bioinformatic software and version numbers used in this research. . .	30
2.4	Links to the bioinformatic software used in this thesis.	30
A.1	Forward primer sequences used in this study for qPCR.	79
A.2	Reverse primer sequences used in this study for qPCR.	79
A.3	Locked nucleic acid sequences used in cell culture experiments.	80
A.4	Protein sequences of $A\beta$ fragments.	80
A.5	Nucleic acid reagents for in vitro transcription of B2 RNA.	80

List of Figures

1.1	Predicted distribution of ages in the populations of Canada and the world in 2050.	3
1.2	Amyloid precursor protein is differentially cleaved by β -secretase and α -secretase.	4
1.3	The classical hypothesis of the influence of amyloid on the brain. . . .	6
1.4	A simplified model of insoluble protein aggregation. Monomeric unstructured proteins form structures oligomers, protofibrils, and long tangles or aggregations depending on the protein. Proteins known to aggregate in neurodegenerative disorders include $A\beta$, tau, and α -synuclein	7
1.5	Simplified diagram of stress response gene activation	11
1.6	The cycle of SRGs increasing production of miR-34c and pro-apoptotic proteins.	15
1.7	Fragments of B2 can be observed at approximately 98 bases downstream of the transcriptional start site.	16
1.8	A possible model of how the B2 RNA may be influence by factors like $A\beta$ or Hsf1 to produce the symptoms of Alzheimer's disease.	18
2.1	Schematic representation of the progression of amyloidogenesis in mice	20
2.2	Cortical histology shows significantly increased plaque density on aged transgenic mice relative to controls.	21
2.3	Layout of cell culture wells treated with $A\beta$	23
2.4	Layout of cell culture wells treated with LNA	23
2.5	Layout of cell culture wells treated with LNA and $A\beta$	24
3.1	KEGG pathways of preHS genes created using DAVID 6.8 gene ontology analysis.	32
3.2	Inflammatory mediator regulation of TRP channels KEGG pathway diagram created from DAVID 6.8 gene ontology analysis of preHS genes.	32
3.3	KEGG calcium signalling pathway diagram created from DAVID 6.8 gene ontology analysis of preHS genes.	33
3.4	KEGG glutamatergic synapse pathway diagram created from DAVID 6.8 gene ontology analysis of preHS genes.	34
3.5	Venn diagram representing the number of genes common that were unique or common between preHS genes and learning-associated genes.	35
3.6	PANTHER Overrepresentation Test of genes common to preHS and learning	36

3.7	DAVID 6.8 Functional Annotations of genes common to preHS and learning	37
3.8	TSS plot of RNA reads mapped to the full length B2 RNA from wild-type and Alzheimer model mice.	38
3.9	Increased cleavage of the B2 RNA is observed in the unstimulated hippocampi of aging mice	39
3.10	TSS plot of randomly selected gene reads in WT and AD mice.	40
3.11	TSS plot of stress response gene reads in WT and AD mice.	41
3.12	CHARTseq data shows increased B2 reads in H4K12 acetylated regions.	42
3.13	Short RNA-seq reveals increased processing of SINE RNAs in 6-month-old AD mice models.	43
3.14	Long RNA-seq of mouse brain tissue shows an increase in levels of Hsf1 produced in APP+ 6-month-old mice.	44
3.15	Long RNA-seq of mouse brain tissue shows an increase of transcription of stress response genes in 6-month-old APP+ mice.	45
3.16	Long RNA-seq of mouse brain tissue shows a generalized depression of transcription in 6-month-old APP+ mice.	46
3.17	B2 is not degraded by amyloid fragments	47
3.18	B2 RNA is degraded by Hsf1 over time.	48
3.19	B2 is degraded by increasing amounts of Hsf1	49
3.20	Densitometric quantification of the bands of remaining B2 RNA.	50
3.21	FOSB is strongly upregulated in the presence of $A\beta_{1-42}$ after 1 hour of incubation in $1\mu\text{M}$ of protein.	51
3.22	FOSB gene expression under amyloid stress is dependent on the availability of Hsf1.	53
3.23	$A\beta_{1-42}$ is sufficient to cause processing of B2 RNA when treated with scrambled LNA but not when depleted of Hsf1.	54
4.1	Summary figure of the role of B2 RNA in amyloid-aging pathology	60

List of Abbreviations

$A\beta$	Amyloid beta
$A\beta_{1-40}$	Amyloid beta amino acids 1-40
$A\beta_{1-42}$	Amyloid beta amino acids 1-42
$A\beta_{\text{rev}}$	Amyloid beta reversed peptide sequence
AD	Alzheimer's Disease
APS	Ammonium persulfate
APOE	Apolipoprotein E
$APOE\epsilon 4$	Apolipoprotein E polymorphism 4
APP	Amyloid Precursor Protein
$APP_{\text{NL-G-F}}$	Amyloid precursor protein mutant NL-G-F
APP_{SWE}	Amyloid precursor protein with Swedish mutation
α -synuclein	Alpha synuclein
CCBN	Canadian Centre for Behavioral Neuroscience
CHART	Capture Hybridization Analysis of RNA Targets
DMSO	Dimethyl Sulfoxide
EDTA	Ethylenediaminetetraacetic acid
ERK	Extracellular Signal-Related Kinase
H4K12	Histone 4 Lysine 12
H4K12ac	Histone 4 lysine 12 acetylation
Hsf1	Heat Shock Factor 1

HT22	Mouse Hippocampal Neuron Cell Line
LBD	Lewy-Body Dementia
LINE	Long Interspersed Nuclear Element
LNA	Locked Nucleic Acid
LTR	Long Terminal Repeat
MAPK	Mitogen Activated Protein Kinase
NGS	Next Generation Sequencing
PAGE	Polyacrylamide Gel Electrophoresis
PCR	Polymerase Chain Reaction
preHS	Pre-Heat Shock
<i>PS1ΔE9</i>	Presenillin-1 minus glutamic acid 9
qPCR	Quantitative Polymerase Chain Reaction
<i>sAPPα</i>	Soluble amyloid precursor protein alpha
<i>sAPPβ</i>	Soluble amyloid precursor protein beta
SINE	Small Interspersed Nuclear Element
SRG	Stress Response Gene
TBE	Tris base, boric acid, EDTA
TEMED	N, N, N', N'-tetramethylethylenediamine
TSS	Transcriptional Start Site
WT	Wild-Type

Chapter 1

Introduction

1.1 Amyloid Pathology and Alzheimer’s Disease

1.1.1 Alzheimer’s Disease

Alzheimer’s Disease (AD) is a chronic neurodegenerative disorder first studied in 1901 by Dr. Alois Alzheimer [1]. The first presentation of AD was observed in Auguste Deter of Kassel, Germany. She was experiencing memory loss, irritability, and delusions—common symptoms of dementia. This case was unique in that classical presentations of dementia often occur in much older patients, known as senile dementia [2]. Auguste Deter was a mere 51 years old. When first examined by Alzheimer she could recount her name, but when questioned further would repeat “I have lost myself, so to say.”, indicating an awareness of her condition [3]. Her mental state further declined over time until her sense of self had been totally eroded.

When Auguste Deter died, Alzheimer examined her brain with staining techniques and identified senile plaques, neurofibrillary tangles, and marked cortical shrinkage which would later become accepted indicators for the disease [4]. These findings were presented at a conference of German psychiatrists in 1906. Following publication of the case summary, many incidents of presenile dementia were documented in the medical literature until “Alzheimer’s disease” was coined in 1910 [5].

As research into the disease progressed, a clinical definition of the disease was established [2]. Broadly, symptoms of the disease include: issues with memory, executive function, and changes in personality [6]. Psychosocial symptoms of AD include:

depression, apathy, mood swings, distrust and paranoia, irritability and aggressiveness, changes in sleep, wandering, loss of inhibitions, and delusions [7]. Individuals with AD may also become withdrawn and isolate themselves from friends and family [2]. Symptoms of the disease appear slowly and increase in severity over time. There is no cure for Alzheimer's Disease [8].

Despite knowing the symptoms of the disease, conclusive clinical diagnosis of AD may only be achieved after post-mortem examination. Brains of those affected with AD are often shriveled, small, and contain aggregations of proteins like amyloid beta ($A\beta$), α -synuclein, and tau [9].

With many diseases, prevention and early intervention are important to securing positive clinical outcomes. Unfortunately, there are very few biomarker assays available for conclusive early detection of AD. Studies have been conducted that examine cerebrospinal fluid for markers related to AD [10]. However, these tests are not standardized and not widely available. Accordingly, it will be valuable to develop effective liquid biopsy methods to accurately determine a patient's post-test probability of AD. Pre-test risks for developing AD are varied and include genetics, poor lifestyle and chronic stress, and most notably, progression to advanced age [11, 12].

1.1.2 Impact of Alzheimer's Disease

Elderly people are most at risk of developing a variety of neurodegenerative disorders and age-related dementia. Populations all around the world are progressing to advanced age. As of 2016, 16.9% of Canadians were 65 years of age or older [13]. Approximately 25% of Canadians will be age 65 or older age by 2050 [13]. Worldwide, that number climbs to 1.5 billion elderly making up 15% of the total population [13]. Estimated distributions of elderly people can be seen in Figure 1.1. AD is estimated to be the cause of 60-70% of dementia [14, 15].

The development of AD has wide-ranging societal and economic effects. In the

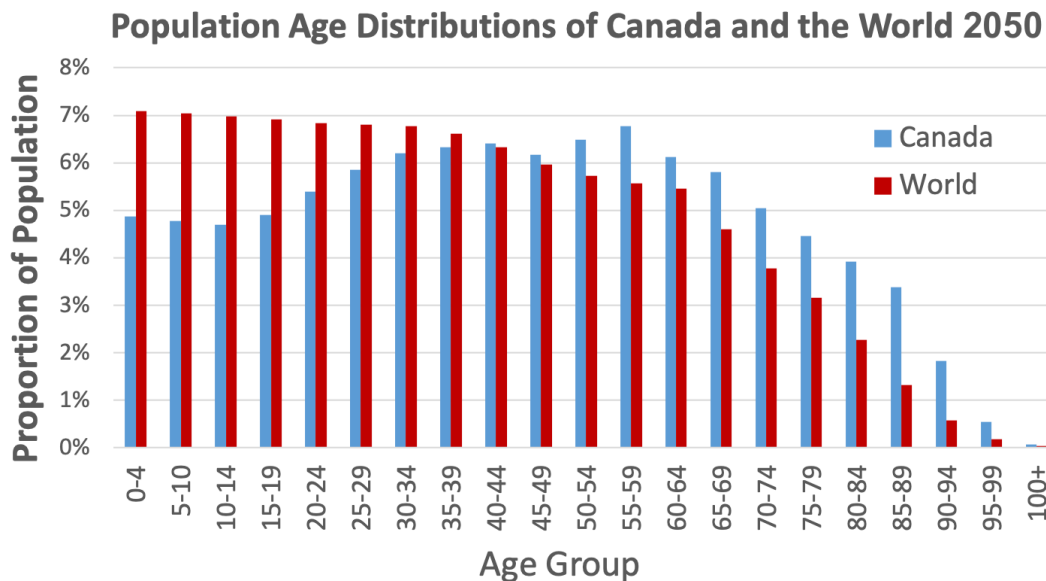


Figure 1.1: Predicted distribution of ages in the populations of Canada and the world in 2050. Data from United Nations Department of Social and Economic Affairs [13].

United States of America, the social costs (both direct expenditure and loss of productivity) are approximately \$100 billion per year [16]. Worldwide estimates of direct costs are about \$160 billion [17] and are expected to rise. Where money for offsite care is not available, there is a large burden placed on family members of those who are afflicted with Alzheimer's Disease. Problematic behaviors associated with AD are varied and can include sleepwalking, behavioral disorders, hallucinations, and social isolation [18]. Caregivers are also at risk of developing mental health issues as a result of the high burden of care in absence of well-developed coping mechanisms [19].

However, the most unfortunate outcome of Alzheimer's disease is that it robs a human being of their memories, independence, sense of self, and diminishes their quality of life. Despite the importance of this disease, it is relatively poorly understood and no cures exist. Accordingly, developing a more robust understanding of Alzheimer's Disease may help to develop therapies to ensure healthy aging.

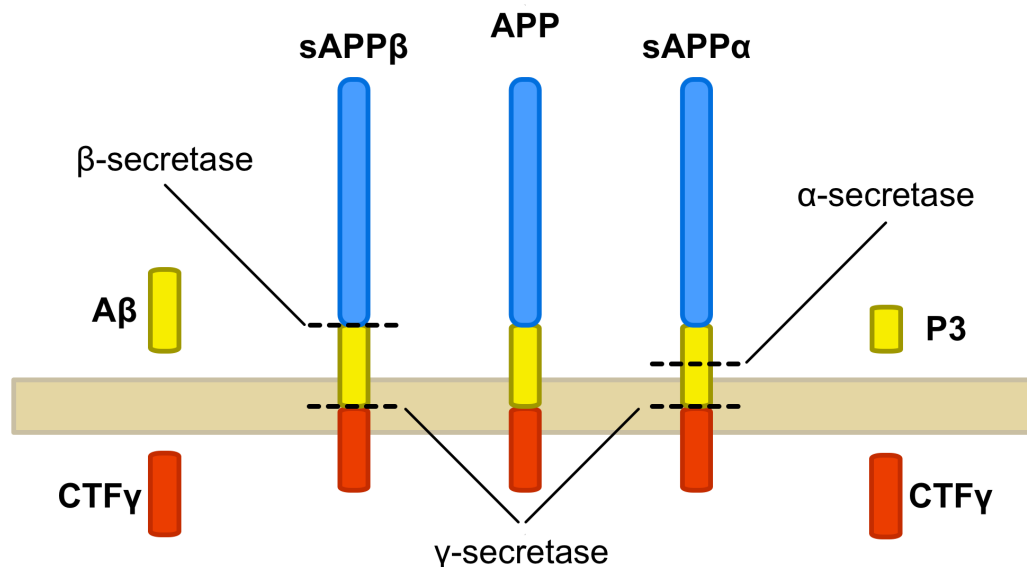


Figure 1.2: Amyloid precursor protein is differentially cleaved by β -secretase and α -secretase. The β -secretase produces the insoluble $A\beta$ fragment which can pathologically oligomerize. Other cleavages produce soluble fragments that do not aggregate. γ -secretase liberates the intracellular C-terminal fragments.

1.2 Alzheimer's Disease Pathogenesis and Aetiology

1.2.1 Amyloid Pathology

Although our current understanding of the disease is inadequate, several theories have been put forward that attempt to explain how Alzheimer's disease begins and how it progresses. Among the top theories for the progression of Alzheimer's disease is the abnormal cleavage of a protein called Amyloid Precursor Protein. (APP) [20]. APP is a membrane-bound protein thought to be involved a variety of cellular processes within neurons though it's function is unknown [21–23]. It undergoes proteolytic cleavage by several secretases and the resulting fragments are thought to have different effects downstream [24, 25]. The amyloidogenic nature of this pathway is dependent on whether of not APP interacts with alpha secretases or beta secretases before fragments are liberated by gamma secretase cleavage [26, 27]. A schematic of this process can be seen in Figure 1.2.

The beta secretase complex cleaves the protein in the transmembrane region and

produces two fragments: $sAPP\beta$ and $A\beta$ [28]. While initially soluble, the $A\beta$ fragments oligomerize and precipitates out of solution after aggregating. Beta-secretase-mediated cleavage can produce fragments that are 40 or 42 amino acids in length: $A\beta_{1-40}$ and $A\beta_{1-42}$. While $A\beta_{1-40}$ is generally regarded as apathogenic or weakly pathogenic, the slightly longer $A\beta_{1-42}$ is supposed to be the root of the disease [29,30]. The ratio of $A\beta_{1-40}$ to $A\beta_{1-42}$ is being investigated as a diagnostic marker for AD [31]. Regardless of the relative contribution of each form of amyloid to the progression of disease, both fragments display the ability to bind to itself and form oligomeric fibrils [32]. These fibrils become highly ordered sheets, and form insoluble aggregates (plaques) on the brain.

The alpha secretases are responsible for the majority of APP cleavage and occurs at an alternative site within the transmembrane region of the protein that prevents the formation of the beta-amyloid fragment [33]. Cutting here produces soluble extracellular fragments: $sAPP\alpha$ and P3 instead of $A\beta$ [33]. Currently, there is little to no evidence to suggest that P3 has negative effects on cellular fitness or to determine a function of this small truncation [34]. Released $sAPP\alpha$ and $sAPP\beta$ perform distinct but unclear roles in the extracellular space [35].

In either case, following transmembrane cleavage gamma secretase liberates the amyloid intracellular domain of the protein which then acts as a transcription factor [36]. This second cleavage is also what liberates the $A\beta$ fragments from the membrane. The complex of gamma secretase is made of PSEN1, APH-1, PEN-2, and nicastrin [37]. PSEN1 is the functional member of the complex responsible for gamma secretase activity towards APP [38]. Mutations in PSEN1 have been shown to increase the risk of developing AD [39,40].

A combination of errors in this pathway may ultimately result in heightened production of the $A\beta_{1-42}$ leading to the formation of plaques. Disappointingly, therapies used to remove the plaques did not ameliorate the effects of disease [41,42]. Accord-

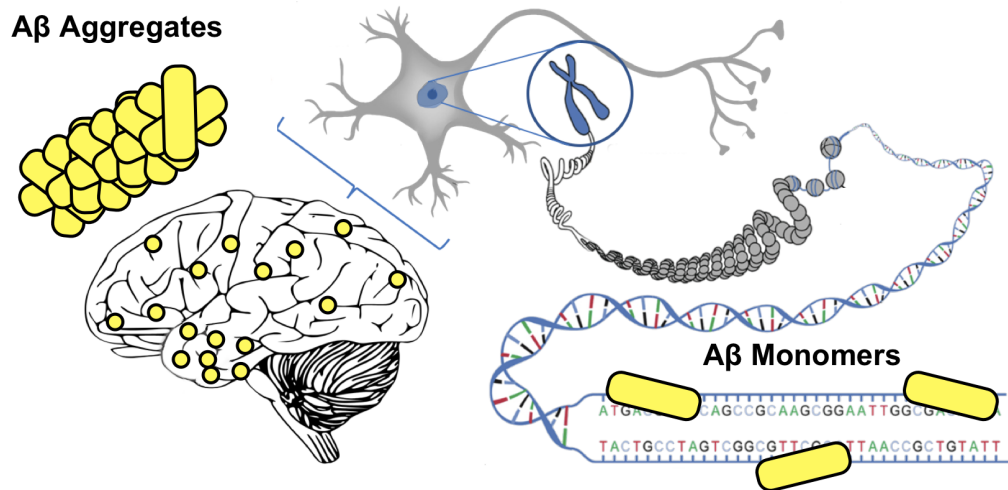


Figure 1.3: The classical hypothesis of the influence of amyloid on the brain. Amyloid plaques consisting of amyloid beta fragments are deposited on the cortex and affect neurons extracellularly. Alternatively, amyloid beta monomers can migrate to the nucleus and affect gene expression. Figure adapted from OpenStax under Creative Commons License 4.0 [43].

ingly, oligomeric $A\beta_{1-42}$ may be the true cause of pathogenicity, either by binding with receptors, or acting as a transcription factor in the nucleus. A proposed mechanism of amyloid beta affecting gene expression is presented in Figure 1.3.

1.2.2 Tau Fibrils

When examining a brain afflicted with AD, in addition to extracellular plaques, one may also observe intracellular tangles [44]. These tangles are composed of another protein found in the brain of AD patients alongside amyloid: microtubule-associated protein tau, or tau for short [45]. Microtubules are analogous to the skeletal structure of the body, but also provide means for cellular cargo to navigate the cytoplasm. Ordinarily, Tau interacts with tubulin in axonic microtubules to stabilize them [46]. The extent to which tau stabilizes microtubules is dependent on the isoform of tau, and how phosphorylated it is [47, 48]. Hyperphosphorylation of tau leads to neurodegenerative processes in AD [49]. Tau is an intrinsically disordered protein like APP and shows a similar ability to aggregate [50]. The accumulation of aggregated tau

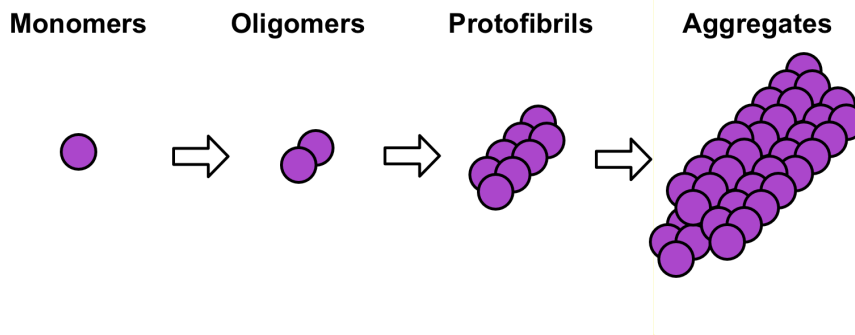


Figure 1.4: A simplified model of insoluble protein aggregation. Monomeric unstructured proteins form structures oligomers, protofibrils, and long tangles or aggregations depending on the protein. Proteins known to aggregate in neurodegenerative disorders include $A\beta$, tau, and α -synuclein

replaces tubulin within the cell body and forms neurofibrillary tangles made predominantly of tau [51]. Generally, aggregation occurs as a result of monomeric proteins adopting higher order structures as they interact with other monomers (Figure 1.4). Tangled fibrils of tau are thought to be able to induce toxicity, though the mechanism is unclear [52, 53]. Interactions with $A\beta$ have been suggested as one method by which toxicity can be induced [54].

1.2.3 Alpha Synuclein

Although the focus of this work is Alzheimer's disease, it is also important to touch on synucleinopathic Lewy-body Dementia (LBD). Like other dementias, LBD impairs cognition, affects sleep, causes visual hallucinations, and affects the autonomic nervous system [55]. LBD is clinically confirmed with histological examination of cortical tissue [56]. Similar to AD, brains with LBD are marred with fibrillar aggregations of proteins—in this case, α -synuclein [57]. α -synuclein is an intrinsically disordered protein found mainly in synaptic terminals [58, 59]. Although the function of α -synuclein is difficult to elucidate, it is thought that the protein is involved in synaptic signalling, Golgi function, and modification of the composition of lipid membranes [60, 61]. Normal α -synuclein resists aggregation, yet is present in Lewy Bodies in high

concentrations [57, 62].

Furthermore, α -synuclein may interact with microtubule structures and associated proteins, like tau, causing them to become phosphorylated and break down [63–65]. α -synuclein has also been shown to interact with amyloid beta, with each disordered protein seeding aggregation of the other [66].

1.2.4 Apolipoprotein E4

Lipids like triglycerides, cholesterol, and phospholipids are necessary for maintaining the functionality of the cell membrane. In order to maintain the necessary lipid composition of membranes throughout the body, cells rely on lipoproteins to package and transport lipids in fatty bubbles all over the body through an aqueous medium like lymph or blood. The lipoproteins are spherical structures with a single-layered phospholipid shell dotted with proteins that protects the hydrophobic triglycerides and cholesterol from the aqueous solution outside the lipoprotein [67].

Apolipoproteins are responsible for maintaining the structure and signalling the identity of the lipoprotein to cells [68]. Apolipoprotein E (APOE) binds low-density lipoprotein receptors on the cell surface to facilitate recognition and uptake of the lipoprotein [69].

APOE protein has several polymorphisms and each allele contributes differently to the relative risk of developing disease [70]. The E4 variant is the strongest predictor of AD [71]. Individuals homozygous for *APOE* ϵ 4 are 20 times more likely to develop AD than others [72]. Although having two copies of the *APOE* ϵ 4 gene greatly increases the risk of developing AD, the mere presence of the gene is not sufficient or necessary to cause AD [73]. Furthermore, the exact role *APOE* ϵ 4 plays in AD is unknown, though some studies link it to the immune response to *A* β and subsequent neuroinflammation [71]. APOE has been shown to enhance proteolytic degradation of amyloid beta, but this function is impaired in the E4 variant [74].

1.2.5 Mitochondrial Deficiency

Mitochondria are intracellular organelles responsible for providing cells with energy necessary for basic functions: they are the powerhouse of the cell. In addition, bidirectional signalling to and from the mitochondria suggests roles in metabolic regulation, cell cycle control, and apoptosis [75]. They achieve this through a series of intense chemical reactions within their cell walls that generates an enormous amount of oxidative stress [76]. Reactive oxygen species (ROS) are necessary for the normal function of the mitochondria, but excess levels of ROS can damage the mitochondria themselves [77]. Cells that use lots of energy, like neurons, astrocytes, and others, will accordingly place greater stress on the mitochondria to fill their energy demands [78]. It follows then that, dysfunction of the mitochondria can have severe neurological effects [79]. Diseases like Parkinson's disease, Huntington's disease, Alzheimer's disease and amyotrophic lateral sclerosis have been linked to various disorders of the mitochondria [79].

Mitochondrial damage is associated with aging, but is significantly increased in mitochondria from AD brain tissue relative to non-AD age-matched control samples [80]. Oxidative damage to the mitochondria is purported to be one of the earliest steps in the progression of the disease [81]. However, energy regulation issues are present throughout the entire progression of AD [82]. It has been proposed that a cascade of events related to the mitochondria are ultimately responsible for the progression of the disease over time, involving $A\beta$, tau, and other proteins [83, 84].

Damaged mitochondria are targeted to lysosomes in a process called mitophagy. Impairment of this process reduces the fitness of cells to recycle mitochondria and hinders proper neural function [85, 86]. Failure of cells to counteract defects within the mitochondria result in pro-apoptotic signals [87, 88]. Autophagy is also able to clear away amyloid plaques from the extracellular space using lysosomes [89]. It is unsurprising then that there is considerable cross-talk between autophagy, apoptosis,

and necrosis [90–92].

The above sections illustrate that AD is a very heterogenous and complex pathology. It is clear that there is no simple solution to preventing the disease or intervening in its progression. Therapies designed to combat the development of symptoms or attenuate their effects will not have the desired effect of halting the multifaceted progression of the disease. Attempts to treat the disease this way indicates that our understanding of the molecular processes underlying AD is wanting. Accordingly, it may make sense to take a step back and examine the problem from a different perspective.

1.3 The Transcriptomic Angle

1.3.1 Stress Response Genes

In order for a cell to respond efficiently to a stimulus, it may be necessary for it to rapidly upregulate or downregulate gene products. Genes that are the first to respond to a stimulus are classified as stress response genes (SRGs) or early response genes and control transcriptional changes. They are activated in various cell types in response to a variety of stimuli—both internal and external—indicating that this is a very general response that utilizes ancient and conserved genes [93,94]. With respect to neurons specifically, SRGs are critical for the formation of memories, synaptic plasticity, and learning [95,96]. Activation of pathways such as RhoA-actin, ERK and p38 MAPK and PI3K can lead to SRG expression [97]. Fos, Jun, and Myc are key SRGs, transcription factors, and among the first SRGs to be discovered [98].

In the case of heat shock, SRGs will attempt to activate chaperones to protect the brain by helping proteins fold correctly [99]. The presence of denatured proteins causes transiently expressed chaperones HSP90 and HSP70 to dissociate from Hsf1 to assist other proteins [100]. This allows Hsf1 to upregulate chaperones and initiate other genetic programming by behaving as a transcription factor and activating heat-

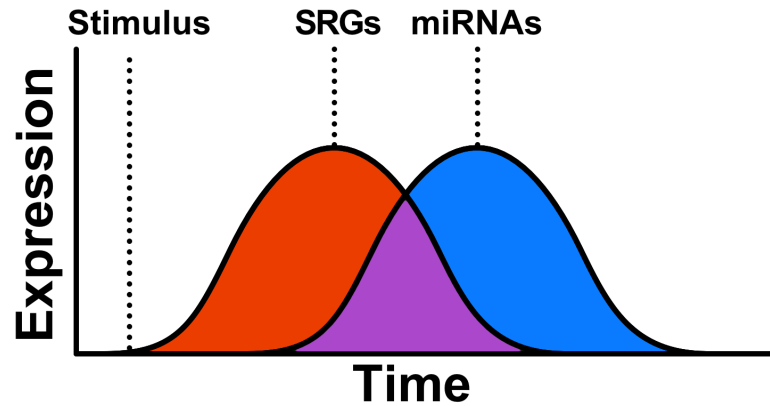


Figure 1.5: Stress response genes are expressed shortly after a stimulus. Levels of SRG expression are followed by miRNA production to abrogate the response and return to homeostasis.

shock responsive elements on the DNA [101]. As a result, the heat-shock response pathway is activated. In order to return the levels of SRGs to basal levels microRNAs are produced that target the 3' UTR of SRGs (Figure 1.5).

The response of SRGs rises within minutes, and subsides after 90 minutes [97,102]. SRGs do not require the production of bespoke regulatory factors after a stimulus to be able to recruit polymerase. Instead, cells are primed for transcription of these genes by preloading and pausing RNA polymerase II in the promoter-proximal region. For example, the Fos promoter is bound by initiated RNA Polymerase II and is primed for elongation despite the absence of an activating signal [103]. Since the polymerase is already initiated, rapid unpausing of the polymerase will result in rapid transcription. The reason for this type of regulation is to allow for the synthesis of secondary products as quickly as possible. During the stress response, housekeeping genes are repressed while cellular energy is diverted to the transcription and translation of genes necessary for survival [104]. The return to homeostasis is helped by a concomitant wave of microRNA expression that targets SRGs [105–107]. The microRNAs produced by SRGs are also able to activate the apoptotic response [108]. If the cell encounters a stimulus or stress that it cannot resolve, the consequences may be dire. Given the

high stakes of the situation, a cell must respond in a rapid, reliable, and measured way.

1.3.2 Non-Coding RNAs

Tight regulation of gene products is critical to normal functioning in the cell. Translation is an energy intensive process, requiring ATP, GTP, multiple initiation factors, elongation factors, and post-transcriptional modification of mRNA itself. Transcription is comparatively less expensive [109]. Accordingly, regulating translation with the products of transcription seems like a sensible investment. It makes sense then that protein-coding regions make up a mere 1% of total human DNA [110]. Despite this fact, 90% of the genome is still transcribed into some other form of RNA [111].

Non-coding RNAs perform many functions. The most well-known of the ncRNAs are the humble tRNAs. Discovered in 1965, the role of the tRNA is to facilitate translation by moving amino acids to the ribosome where it undergoes catalysis by rRNA to form the peptide bond if the tRNA anticodon matches the mRNA codon [112, 113]. 7SK RNA controls positive transcription elongation factor which is responsible for halting polymerase II activity in advance of elongation [114]. The 7SL RNA is a required component of the signal recognition particle, which targets proteins to the endoplasmic reticulum immediately after translation [115].

1.3.3 B2 SINE RNAs

Among the non-coding elements of the genome are several classes of highly repetitive sequences derived from retrotransposons. Retrotransposons are selfish genetic elements that through reverse transcription. This process results in proliferation of the elements throughout the genome and expansion of the genome itself [116]. Repetitive DNA accounts for 50% of the non-coding sequences in the human genome [117]. These retrotransposons can be divided into long terminal repeat (LTR) retrotransposons and

non-LTRs. Replication of LTRs shares many features with retroviruses, but only proliferate in the host genome [118]. Non-LTRs can be subdivided into long interspersed nuclear elements (LINEs) and short interspersed nuclear elements (SINEs). LINEs are autonomous elements and contain all genes to propagate themselves. In contrast, SINEs rely on the transcriptional machinery of LINEs to propagate [118]. SINEs account for approximately 10% of the non-coding genome and are widely distributed throughout the entirety of the human genome [119]. They are thought to contribute to genetic diversity by facilitating genomic rearrangement [120]. Accordingly, SINEs are useful markers for understanding lineage specific changes and speciation [121].

It has been proposed that these repetitive regions (and ncRNAs in general) represent a vast unexplored region of genetic function [122, 123]. The opposite view is also articulated by Palazzo and Lee [124]. They articulate the reasonable position that junk RNA/DNA is entirely permissible within the evolutionary paradigm as we know it, and that the appropriate null hypothesis for any candidate RNA should be first and foremost that it is junk. Increased expression levels, predictable expression profiles, cellular localization, processing, sequence conservation, and causal roles in biological processes, would provide evidence that an RNA is indeed functional.

Alu elements are highly successful SINE elements that are ubiquitous within human DNA; there are one million copies spread throughout the genome [117]. The Alu element is derived from the 7SL RNA and is about 300nt in length [125]. During evolution, 7SL-derived retrotransposons diverged at the rodent primate split. The rodent branch became the B1 RNA and the primate branch became the Alu element [121]. Some suggest that this was helpful in the cognitive development of the human species as the elements allowed for more genetic plasticity [126].

Functionally, the Alu RNA is also involved in adenosine deaminase RNA editing [127], poly-A tailing [128], and splicing [129]. Most importantly however, the Alu element is transcribed by polymerase III has been shown to be able to regulate tran-

scription of polymerase II [130]. During heat shock, the Alu RNA inhibits mRNA production [131]. The Alu RNA can directly bind polymerase II at the promoter region of genes that are downregulated as a result of heat shock [132]. B1 is 140 nucleotides long and is able to bind polymerase II, but does not inhibit transcription [131]. To my knowledge, the B1 RNA has not been shown to have a definitive function.

Conversely, the murine B2 SINE RNA is not related by sequence to the human Alu or murine B1 RNAs. The B2 is instead derived from tRNA [133]. However, it appears to have been functionalized over evolutionary time to perform a similar function as the Alu [134]. Like B1 and Alu, the 200nt-long B2 RNA is upregulated under stress [135]. Jennifer Kugel's group at the University of Colorado Boulder has done extensive research into the B2 RNA. The B2 RNA has been shown to repress polymerase II after heat shock [136]. Contact between both upstream and downstream regions of the TATA box and polymerase II are disrupted by B2, altering the conformation of the complex, and preventing elongation [132]. The RNA achieves this by tightly binding the DNA cleft and active site of the enzyme [137]. With respect to studying how human SINEs influence the response of cells to stress, the B2 RNA appears to be a suitable proxy.

1.4 Hypothesis and Objectives

1.4.1 Rationale

Previous studies by Dr. Zovoilis and others have shown that learning is dependent on active and open chromatin to allow learning associated genes to be transcribed [138]. Histones are involved in regulating the transcription of genes by altering the structure of chromatin. Acetylation of histones is linked to a loosening and unwinding of chromatin which enhances transcription. Methylation compresses chromatin and prevents transcription. Cognitive decline has been linked to deregulation of H4K12

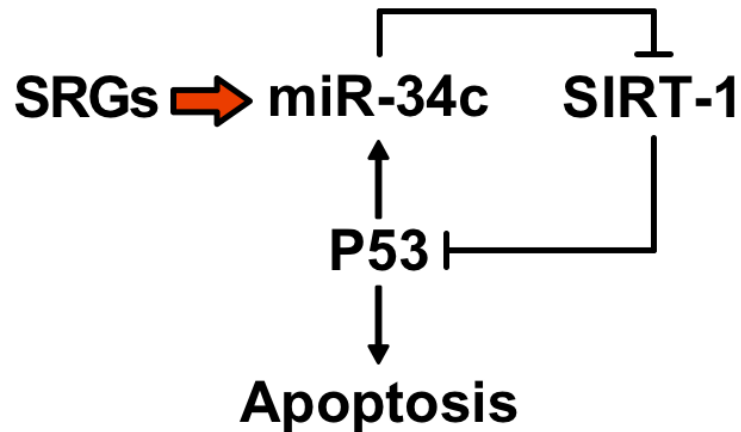


Figure 1.6: The cycle of SRGs increasing production of miR-34c and pro-apoptotic proteins. Abnormal expression of compensatory miRNA expression has been observed in aging and AD-model mice. Repression of SIRT-1 relieves repression of p53. Pathological expression of SRGs may compound and sustain this feedback loop.

[138]. Accordingly, H4K12ac is linked to proper functioning of learning. Genes that are controlled by H4K12 are learning associated genes. Learning associated genes are likely also stress response genes.

As mentioned previously, SRG expression is modulated by the expression of microRNAs. MicroRNAs are able to reduce the expression of proteins by binding mRNAs and targeting them for degradation [139]. An abundance of microRNA complementary to the 3' UTR of a target mRNA means that the mRNA be destroyed and its protein product will be less abundant in the cell [140]. A microRNA called miR-34c is highly enriched in the hippocampus and directly involved in memory [141]. Following transcriptional profiling and behavioral studies, Zovoilis et al. found that excessive amounts of miR-34c resulted in memory impairment in mouse models [141]. This microRNA targets SIRT1, which exerts control over essential processes like apoptosis via the master regulator P53 [142, 143]. The feedback loop between SRGs, miRNAs, and p53 is described in Figure 1.6.

Previous studies by Dr. Zovoilis have also revealed how the B2 RNA is involved in activating the stress response. Polycomb repressive complex 2, more specifically the

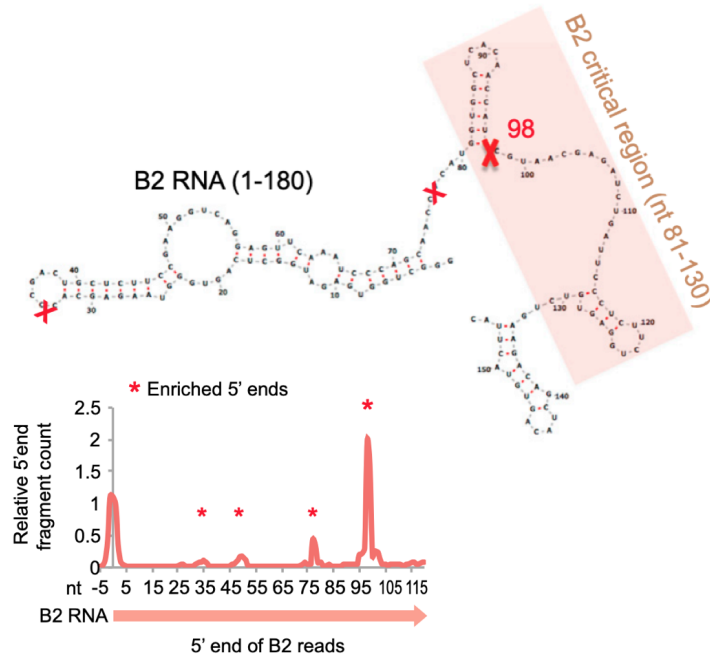


Figure 1.7: Fragments of B2 can be observed at approximately 98 bases downstream of the transcriptional start site. Cleavage in the critical polymerase II binding region of B2 abolishes the ability of the RNA to prevent transcription. Figure is from Zovoilis et al. in *Cell*, 2015 [144] Adapted and reprinted with permission.

catalytic subunit of the complex, EZH2, has been shown to directly bind B2 [144]. Furthermore, this interaction is specific to B2 and results in an irreversible first-order cleavage event. Hydrolysis within the Pol II binding region of B2 abolishes the activity of B2 to prevent transcription (Figure 1.7). Accordingly, B2 cleavage results in activation of the stress response within 15 minutes of stimulus. However, B2 is also upregulated during stress. Generalized increases in expression of B2 causes the RNA to localize to housekeeping genes and causes repression at those loci [144]. It appears that this mechanism functions as a cellular switch to change gene expression patterns from a resting state to a responsive one.

1.4.2 Hypothesis

Our brains are required to respond to an enormous amount of stimulus and demand a tremendous amount of energy to function. The response to these stimuli—heat-

shock, learning, disease, etc.—must be appropriately calibrated or cells will fail. Respond too slowly or too weakly and the challenge will overwhelm the system. Respond too aggressively and for too long and resources will have been exhausted. It is clear that this delicate balance is disturbed in neurodegenerative diseases like Alzheimer’s.

It is also clear that one of the mechanisms that cells rely on to respond quickly to stress is initiation of polymerase at responsive genes, followed by pausing of the complex by non-coding RNA like B2 or Alu, and activation through cleavage of the RNA. Dysregulation of this mechanism may have far-reaching effects on the transcriptome of the cell. Sustained dysfunction likely results in erroneous expression of stress response genes and their microRNA regulators. Ultimately, this cellular runaway train ends at the expiration of the cell via apoptosis or starvation. Taken together, we hypothesize a connection between SINE RNAs, stress response genes or learning associated genes, and the progression of Alzheimer’s Disease. To this end, the aims of this thesis are:

1. Assess levels of SRG expression in AD models
2. Look for changes in SINE processing in AD models
3. Determine if a connection exists between stress-induced B2 activation and AD

A proposed method for the interplay of these elements is elaborated in Figure 1.8.

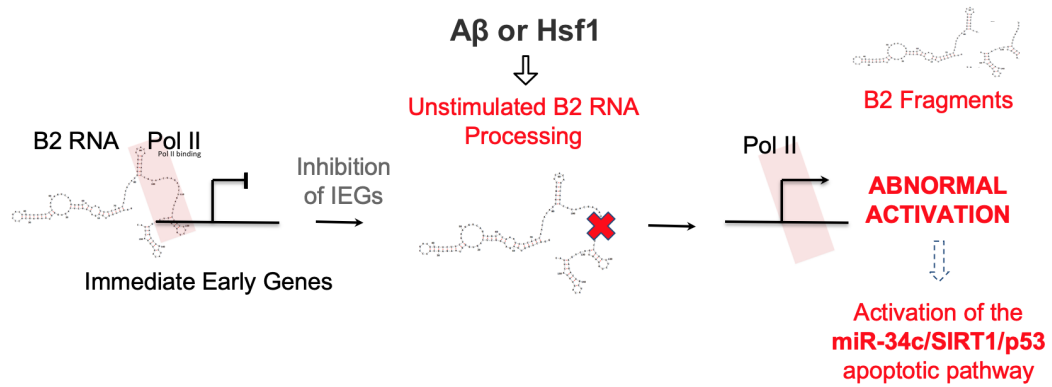


Figure 1.8: A possible model of how the B2 RNA may be influenced by factors like $A\beta$ or Hsf1 to produce the symptoms of Alzheimer's disease. Abnormal processing of B2 activates the stress response and allows for transcription of SRGs. Sustained expression of SRGs overwhelms the ability of the cell to return to homeostasis and accumulation of microRNAs downregulates SIRT-1, ultimately allowing for acetylation of p53 and activation of the apoptotic pathway.

Chapter 2

Methods

2.1 Transgenic Mouse Model

2.1.1 Genetic Background and Age

Brain tissue from humanized Alzheimer’s Disease model transgenic APP_{NL-G-F} mice were acquired from our collaborators at the Mohajerani Lab at the Canadian Centre for Behavioral Neuroscience (CCBN) at the University of Lethbridge. The NL-G-F mutations were in the amyloid precursor protein knocked-in to the WT genome. This allows for expression of APP at normal levels, avoiding issues related to APP overexpression. Each mutation contributes to increase the severity and speed onset of the disease [145] An explanation of the mutations can be found in Table 2.1.

AD and WT mice were of cared for the in CCBN and allowed to mature to different ages. Table 2.2 breaks down the cohort mice by genotype, age, and number of replicates. The combined effect of the APP_{NL-G-F} mutations results in a mouse that experiences rapid onset of Alzheimer’s disease-like symptoms at approximately 6 months. RNA was extracted at different points during the amyloidogenesis as shown

Table 2.1: Effects of introduced Swedish, Arctic, and Iberian familial AD mutations in humanized APP mice.

Symbol	Mutation	Effect
NL	Swedish	Increases total $A\beta$ production
G	Arctic	Increases aggregation and oligomerization of $A\beta$
F	Iberian	Increases the $A\beta_{1-42}/A\beta_{1-40}$ ratio

Table 2.2: Genotypes, ages, and number of sampled mice.

Genotype	Age	Number
APP_{NL-G-F}	3 months	3
APP_{NL-G-F}	6 months	3
APP_{NL-G-F}	12 months	3
C57-Black	3 months	2
C57-Black	6 months	3
C57-Black	12 months	3

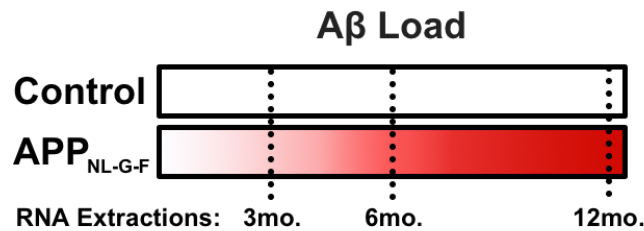


Figure 2.1: Schematic representation of the progression of amyloidogenesis in APP_{NL-G-F} mice. Cognitive decline is rapid and observable at 6 months of age. Total RNA from the hippocampus, prefrontal cortex, and olfactory bulbs was extracted at 3 months, 6 months, and 12 months of age.

in Figure 2.1. Histology of AD and WT mice illustrate the increased plaque density in transgenic mice as seen in Figure 2.2.

2.1.2 Sample Acquisition

Mice were sacrificed in accordance with University of Lethbridge Animal Care Committee guidelines. Whole mice hippocampi were extracted in collaboration with the Mohajerani Lab and stored in Trizol at -80°C in advance of quality check, library preparation, and next-generation sequencing. Sacrifice and dissection was performed by Dr. Jogender Mehla.

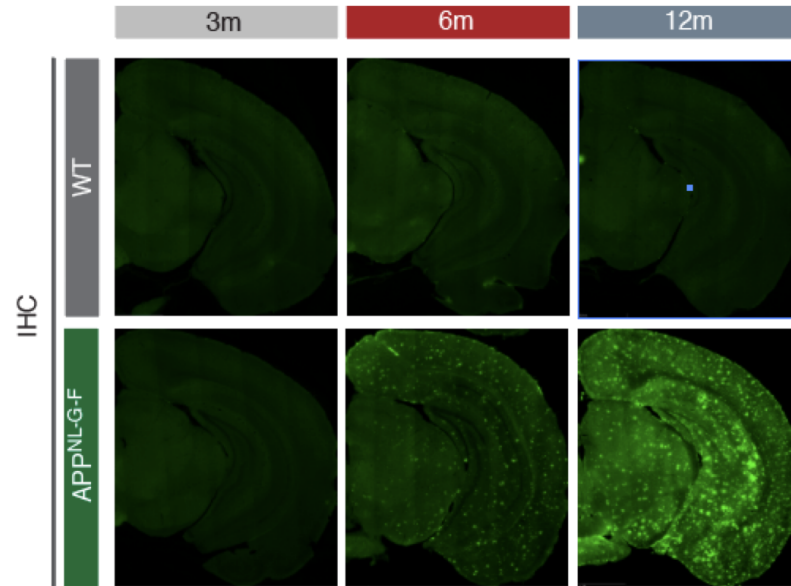


Figure 2.2: Cortical histology shows significantly increased plaque density on aged transgenic mice relative to controls. Histology was performed by Dr. Jogender Mehla and the figure is adapted from his previous work [146] and reprinted with permission.

2.2 Cell Culture

2.2.1 HT22 Cell Line

HT22 mouse hippocampal neuronal cells (Sigma) were cultured in expansion medium consisting of High Glucose Dulbecco's Modified Eagle Medium (Sigma) with 10% Fetal Calf Serum (Sigma), 1% L-Glutamine (Gibco), and 1% Penicillin/Streptomycin (Gibco). Cells were split by removing old media by vacuum, rinsing with sterile phosphate-buffered saline (PBS) (Sigma), and trypsinization with TrypLE Express (Gibco) before removing to fresh flasks to expand the culture. After three passages, enough cells had been prepared to proceed. For freezing, cells were supplemented with 10% dimethyl sulfoxide (DMSO) (Sigma) before flash freezing and storage in liquid nitrogen. Prior to experimentation, cells were removed from liquid nitrogen and warmed to 37°C in a bead bath before centrifuging to facilitate the removal of the DMSO-laden freezing medium. The HT22 cells were then resuspended in expansion medium and allowed to acclimate to a new flask.

2.2.2 Counting Cells

In advance of other experiments, cells were trypsinized, resuspended in 10ml of expansion medium in a 15ml conical centrifuge tube, and a sample of 20 μ l was moved to a bright line hemacytometer from Hausser Scientific. The cells were visualized under a simple light microscope and counted. The average of each quadrant of the hemacytometer was multiplied by ten to estimate the total number of cells per microlitre of media.

2.2.3 Amyloid-Beta Oligomers

One hundred thousand cells were added to 6-well plates and allowed to acclimate at 37°C for 20 hours. Growth medium was removed and cells were washed with PBS after which 800 μ l of expansion medium supplemented with amyloid beta proteins at a concentration of 3M for 1 hour. Amyloid beta monomers were obtained from Sigma-Aldrich via custom synthesis in the following forms: amyloid beta fragments from 1 to 42 amino acids in length ($A\beta_{1-42}$), a truncation of that sequence from amino acids 1 to 40 ($A\beta_{1-40}$), and the reversed peptide from position 42 to position 1 ($A\beta_{rev}$). Prior to experimentation, lyophilized peptides were solubilized by dissolving 2mg of protein in 1mL of 10% ammonium hydroxide. The total volume was split into aliquots before serial dilutions in TAP buffer. All diluted peptides were stored at -80°C.

Plate layouts and control incubation can be seen in Figure 2.3. Subsequently, the cells were challenged by incubation with amyloid beta fragments or transfection with anti-B2 locked nucleic acids (LNAs) (Exiqon/Qiagen) for one hour after which cells were collected in Trizol reagent (ThermoFisher) for RNA extraction and downstream applications.

2.2.4 LNA Transfections

Locked nucleic acid transfection was similarly performed using the HiPerFect reagent (QIAGEN) and 200,000 cells. Working stocks were prepared to a concen-

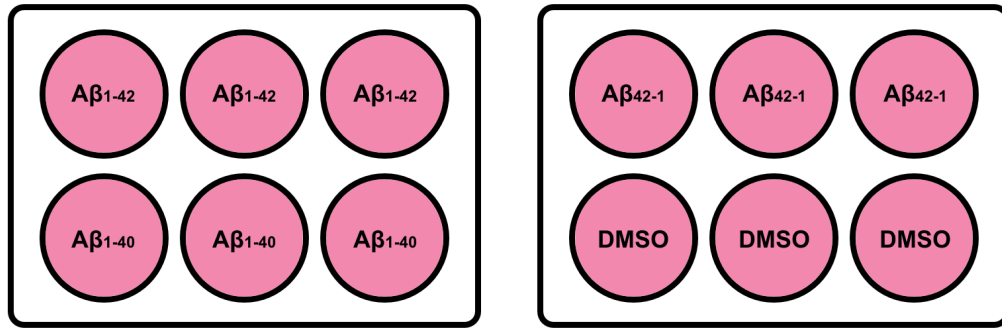


Figure 2.3: Layout of cell culture wells treated with $A\beta$. 100,000 cells were incubated at 37°C with 3M $A\beta$ for 1 hour.

tration of 50 M and $3\mu\text{l}$ were mixed with $30\mu\text{l}$ of sterile H_2O , $4\mu\text{l}$ of HiPerFect before $12.3\mu\text{l}$ of the mixture were added to the cells in their original medium for a final concentration of 0.14M. The sequence of the LNAs used are as follows; Anti-B2: 5'-GTTACGGATGGTTGTG-3', Anti-Hsf1: 5'-CGAAGGATGGAGTCAA-3', and Control: 5'-CCTCAATTTTATCAC-3'. The layout of the plates and combinations of LNA and $A\beta$ can be seen in Figure 2.4 and Figure 2.5 Transfections of Anti-B2 LNA and control LNA were performed with 200,000 cells over 24 hours at 37°C . Additional transfections were performed with a combination of $A\beta$ and Anti-Hsf1 LNAs. 200,000 cells were incubated with LNA at 37°C for 24 hours before 3M $A\beta$ was added for 1 hour. In each case, cells were trypsinized, briefly centrifuged to collect, and immersed in Trizol before RNA extraction for qPCR and RNA-seq.

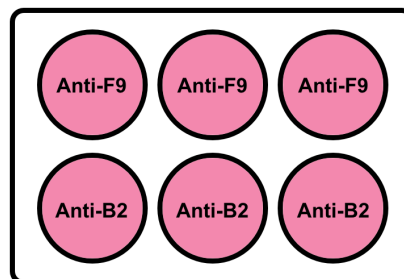


Figure 2.4: Layout of cell culture wells treated with LNA. 200,000 cells were incubated with Anti-B2 LNA or Control LNA at 37°C for 24 hours.

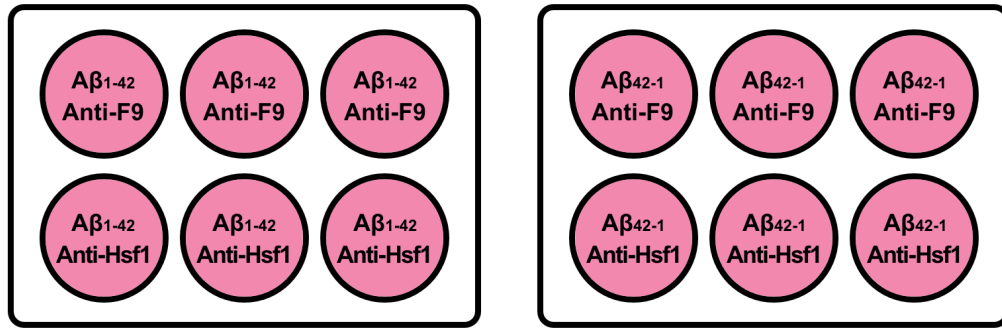


Figure 2.5: Layout of cell culture wells treated with LNA and $A\beta$. 200,000 cells were incubated with LNA at 37°C for 24 hours before 3M $A\beta$ was added for 1 hour.

2.3 In Vitro Methods

2.3.1 B2 RNA In Vitro Transcription

B2 RNA was obtained from in vitro transcription using purified T7 polymerase incubating for 4 hours at 37°C using template of the following sequence (5'-3'):

```
GGGGCTGGTGAGATGGCTCAGTGGGTAAGAGCACCCGACTGC
TCTTCCGAAGGTCCGGAGTTCAAATCCCAGCAACCACATGGTG
GCTCACAACCATCCGTAACGAGATCTGACTCCCTCTTCTGGAG
TGTCTGAAGACAGCTACAGTGTACTTACATATAATAATAAAT
AAATCTTTAAAAAAAAA.
```

Template DNA was produced from PCR amplification of a gBlock (IDT) using a T7 forward primer: 5'-TAATACGACTCACTATAG-3' and B2 reverse primer: 5'-TTTTTTTTTAAAGATTTATTTATTTATTATATGTAAGTACA-3'. RNA was purified with the RNA Clean and Concentrate kit (Zymo Research).

2.3.2 RNA-Protein Incubations

Synthesized $A\beta$, $A\beta_{1-42}$, $A\beta_{1-40}$, $A\beta_{rev}$ peptides were diluted in TAP buffer (50mM Tris (pH 7.5), 5mM $MgCl_2$, 0.2mM EDTA, 0.1% NP-40, 10% Glycerol, 2mM DTT) to concentrations of 2M, 1M, 0.5M, 0.25M, and 0.125M. Phosphorylated human heat-shock factor 1 (Hsf1) was serially diluted to 2M, 1M, and 0.5M in TAP buffer. Prior to incubation, the RNA was folded by heating for 1 minute at 50°C and subsequently

cooling by 1°C every 30 seconds in F2 buffer (250mM HEPES, 1.5M NaCl) and water. 1pmol of RNA was incubated with 500nmol of Amyloid Beta or Hsf1 in TAP buffer at 37°C unless otherwise noted. The processing of the RNA was observed by using 10% Urea PAGE (180V for 50 minutes) stained with SYBR Green II (Invitrogen) for 20 minutes and visualized on a Typhoon Trio imaging system (GE Healthcare Life Sciences) (526SP filter, 532nm laser, 700V). Densitometry was performed using the ImageJ/Fiji software [147]

2.4 Gel Electrophoresis Methods

2.4.1 Agarose Gels

DNA templates for in vitro transcription were analyzed on 2% agarose to ensure adequate separation. Gels were run in a solution of 1X Tris, Boric Acid, and EDTA (TBE) buffer for 60 minutes at 120V. The gels were immediately stained with SYBR 1 (Invitrogen) staining solution for approximately 20 minutes before visualization on the Typhoon imaging system or Amersham Imager 600. Each gel was scanned at high resolution with appropriate wavelengths and filters depending on the apparatus.

2.4.2 Urea PAGE

Quantification of the processing and intrinsic degradation rates of RNA samples were visualized with 10% Urea PAGE. Briefly, a mixture of water, 5X TBE, and 40% acrylamide was supplemented with urea to ensure denaturation of loaded RNA. The gel was polymerized with 10% ammonium persulfate (APS) and N, N, N', N'-tetramethylethylenediamine (TEMED) before samples were loaded and run at 180V for 80 minutes within a buffering solution of 1X TBE. Gels were stained with diluted SYBR II in TBE as recommended before visualization.

2.4.3 Quantification of Processing Rates

Following successful imaging, the digital files were imported into the ImageJ/Fiji software package for densitometric analysis [147]. Equally sized areas of the gel centered on the band of interest were assessed for the average pixel darkness of the area which corresponds to the known addition of the RNA to the well. Following normalization of each area to the initial amount of RNA, rates of degradation can be calculated as the change in density over the time at which the samples were incubated. This technique was similarly applied to calculate the effect of protein concentration on B2 processing.

2.5 Quantitative Polymerase Chain Reaction

2.5.1 Sample Preparation

Synthesis of cDNA was accomplished with the SuperScript III first strand synthesis system (Life Technologies) with standard protocols provided by the manufacturer and 100ng of random primers (Promega). Quantitative real-time PCR was performed with Luna qPCR Master Mix (New England Biolabs) according to the manufacturer's instructions. A full list of primer sequences is included in Appendix A in Table A.1 Reaction conditions were as follows: initial denaturation: 95°C for 3 minutes, followed by 40 cycles of denaturation at 95°C for 15s, annealing at 54°C for 30s, and extension at 66°C for 30s.

2.6 RNA Sequencing

2.6.1 Library Preparation of Hippocampal Samples

Library preparation was performed by and in collaboration with Dr. Babita Gollen at the Zovoilis Lab. Total RNA was extracted from hippocampus of *APP_{NL-G-F}* mice using the Trizol method which is similar to a phenol-chloroform extraction. Then, 1.5 μ g of total RNA was separated into two fractions of short (less than 200bp) and

longer (greater than 200 bp) RNAs using the mirVana separation kit (Invitrogen) with slight modifications: after addition of the lysis/binding buffer and miRNA homogenate additive solution, 1/3 volume of 100% ethanol was added and then mixture was passed through the column. After filtration, the column contained long RNA whereas small RNA was found in the filtrate. To the filtrate, 2/3 volume of 100% ethanol was added. The mixture was passed through a new column to extract short RNAs. Short and long RNAs from each column were eluted as described in the mirVana kit. Short-RNAs were not subjected to the ribosomal depletion while the ribosomal RNA was depleted from long RNA using the NEBNext rRNA depletion kit (Human/Mouse/Rat). Ampure beads were used for eluting the ribosomal depleted long RNA. An RNeasy MinElute Spin Column (QIAGEN) was used to concentrate the ribosomal depleted long RNA and Agilent Bioanalyzer RNA Pico kit was used to test the size and quality of long RNAs.

2.6.2 Long RNA-Seq

NEBNext Ultra II Directional RNA Library Kit was used to prepare the long RNAs libraries with some modifications. RNA was fragmented for 7 minutes at 95°C. First strand synthesis was done for 50 min at 42°C and second strand cDNA synthesis followed by the Mag-Bind total pure NGS beads selection of 1.8x. End Prep of cDNA library was followed by ligation of the adapters using the NEBNext Ultra II Ligation Master Mix and NEBNext Ligation Enhancer. Incubation with the USER enzyme was done for 30 min before the PCR amplification, followed by a double size selection of 0.5x-1.2x. Mag-Bind total pure NGS beads were used at a 0.9x sample-beads ratio for the size selection of final library. Agilent high sensitivity DNA kit (Agilent) was used for evaluating the libraries. RNA-seq libraries were quantified using the NEBNext Library Quant Kit for Illumina (NEB). Library preparations were completed by Dr. Babita Gollen.

2.6.3 Short RNA-Seq

Short RNAs were subjected to PNK phosphorylation for 1 hour at 37°C. RNeasy MinElute Spin columns were used to concentrate the short RNA after the PNK phosphorylation and NEBNext multiplex small RNA library kit (NEB) was used to prepare the short RNA library with some modification. Briefly, 3'SR adaptor was incubated for 2 hours and at the end libraries were subjected to 1.2X size selection instead of double size selection. Library preparations were completed by Dr. Babita Gollen.

2.6.4 Preparation for Cell Culture Samples

The short RNA-seq and long RNA-seq library for HT22 cell lines were prepared as described above for mouse hippocampus with some modification. 300ng of RNA was used as the starting material.

2.7 Bioinformatics Analysis

A full list of software, versions, and links can be found in Table 2.3 and Table 2.4.

Initial exploration of B2 processing in mice was done with publicly available conventional RNA-seq data of AD mice from Daugherty et al., 2017 [148]. Briefly, reads were aligned to UCSC mouse reference genome mm10 (June 2018) and 5' ends of each read were plotted relative to the start of the the B2 element sequence to visualize fragmentation. Each 5' end represents a new cleavage of the RNA, and by totalling the number of fragments per position of the B2 RNA, we can visualize where the most cutting is happening.

Differentially expressed genes were compared between AD, heat-shock, and learning associated gene lists. The gene ontology was performed using DAVID [149] and Panther [150] (January 2020) . Pathways were obtained from KEGG [151] (January 2020). Statistical analysis of SRG transcriptional start site (TSS) plots used the continuous two-sided Mann-Whitney-U test to determine if the differences in the traces

were statistically significant.

Analysis of SRG expression and normalization of B2 RNA processing rates among ages and phenotypes was done by Yubo Cheng. Briefly, FastQC was used to quality-control both short and long RNA-seq reads in fastq form in advance of adaptor trimming with cutadapt to remove standard Illumina adaptor sequences. Short RNA-seq reads were mapped using single-ended BWA ALN with no parameters altered. Reads were mapped to UCSC mouse reference genome mm10 (June 2018). Long RNA-seq reads were mapped to reference genome ensembl GRCm38 (November 2018) primary assembly using hisat2. The assembly was completed with the following options: Report >alignments tailored for transcript assemblers including StringTie, Searches >for at most 1 distinct primary alignments for each read. SAM files were converted to BAM files and then to BED files using samtools and bamToBed from BEDTools respectively.

FPKM (Fragments Per Kilobase of transcript per Million) and TPM (Transcripts Per Million) for genes using long-RNA-seq data were generated using StringTie using the Ensembl GRCm38 (patch 94) gff3 file excluding irregular chromosomes. DEseq was used for differential expression analysis between AD and WT cases and performed by Yubo Cheng in R. Boxplot central lines represent the median value and Student's t-test was performed on indicated groups.

Table 2.3: Bioinformatic software and version numbers used in this research.

Software	Source
FastQC	Babraham Bioinformatics
BWA 0.7.17	Li and Durbin [152]
Hisat2 2.1.0	Kim et al. [153]
samtools 1.6	Li et al. [154]
BEDtools 2.26.0	Quinlan and Hall [155]
Cutadapt 1.18	Martin et al. [156]
DEseq2	Anders and Huber [157]
StringTie-1.3.4d	Petea et al. [158]
PANTHER v14.0	Mi et al. [150]
DAVID 6.8	Huang, Sherman, and Lempicki [149]
KEGG 93.0	Kanehisa and Goto [151]
Draw Venn Diagrams	University of Ghent
Link Below R 3.4.3.	R Studio Inc.
Python 3.7	Python Software Foundation
SciPy 1.4.1	SciPy Developers [159]

Table 2.4: Links to the bioinformatic software used in this thesis.

Software	Link
FastQC	https://www.bioinformatics.babraham.ac.uk/projects/fastqc/
BWA	http://bio-bwa.sourceforge.net/
Hisat2	http://daehwankimlab.github.io/hisat2/
samtools	http://www.htslib.org/
bedtools2	https://github.com/arq5x/bedtools2
Cutadapt	https://cutadapt.readthedocs.io/en/stable/
DEseq2	https://github.com/mikelove/DESeq2
StringTie	https://ccb.jhu.edu/software/stringtie/
PANTHER	http://www.pantherdb.org/
DAVID	https://david.ncifcrf.gov/
KEGG	https://www.genome.jp/kegg/
Draw Venn Diagrams	http://bioinformatics.psb.ugent.be/webtools/Venn/
R	https://www.R-project.org/
Python	https://www.python.org/
SciPy	https://www.scipy.org/

Chapter 3

Results

3.1 Gene Networks Controlled by B2 have Diverse Functions

3.1.1 GO Terms and KEGG Pathways of PreHS B2 Binding Genes

Based on previous work from Zovoilis et al., it is known that the B2 RNA plays a role in the stress response [144]. Genes that were identified by previous B2 CHART (Probe 1) peaks present only in pre-heat shock (Appendix B.1) cells are heat-shock responsive genes that are under control of B2. However, it is unlikely that heat-shock is the only stimulus that B2 is involved in. Accordingly, the unique genes present in the pre-heat shock (preHS) peaks were used in gene ontology analysis using the DAVID 6.8 [149] web platform and the results are seen in Figure 3.1.

From the analysis provided by DAVID 6.8, we determined that several KEGG [151] pathways were enriched in genes from the preHS gene list. The top result of the analysis was “Inflammatory mediator of regulation of TRP channels” which is to be expected given that the function of that pathway is to respond to temperature stimulus. The KEGG pathway diagram representing TRP channels is shown in Figure 3.2.

More interesting however is the presence of neural-specific pathways. Specifically, calcium signalling (Figure 3.3) and glutamatergic synapse pathways contain genes that are expected to be regulated by B2. Within the calcium signalling pathway, membrane-bound proteins, phospholipases, and proteins activated by calmodulin were present within the preHS gene list. At the downstream end of the pathway, adenylate cyclase 1, nitric oxide synthase, and calcium/calmodulin-dependent protein kinase I

3.1. GENE NETWORKS CONTROLLED BY B2 HAVE DIVERSE FUNCTIONS

Term	RT	Genes	Count	%	P-Value	Benjamini
Inflammatory mediator regulation of TRP channels	RT		32	0.0	4.0E-11	1.1E-8
Arachidonic acid metabolism	RT		26	0.0	1.5E-10	2.0E-8
ABC transporters	RT		17	0.0	1.1E-8	9.6E-7
Glutamatergic synapse	RT		25	0.0	2.0E-7	1.3E-5
Serotonergic synapse	RT		27	0.0	2.1E-7	1.1E-5
Retinol metabolism	RT		21	0.0	6.0E-7	2.7E-5
Linoleic acid metabolism	RT		15	0.0	1.9E-6	7.0E-5
Calcium signaling pathway	RT		30	0.0	3.4E-6	1.1E-4
Retrograde endocannabinoid signaling	RT		18	0.0	2.7E-4	7.9E-3
Neuroactive ligand-receptor interaction	RT		35	0.0	3.1E-4	8.2E-3
Axon guidance	RT		20	0.0	5.4E-4	1.3E-2
Chemical carcinogenesis	RT		16	0.0	7.0E-4	1.5E-2

Figure 3.1: KEGG (January 2020) pathways of preHS genes created using DAVID 6.8 (January 2020) gene ontology analysis. Pathways with a false discovery rate as determined by the Benjamini-Hochberg procedure of less than 0.05 were discarded. Enriched pathways broadly relate to channels and transporters, chemical signalling across synapses, and metabolism.

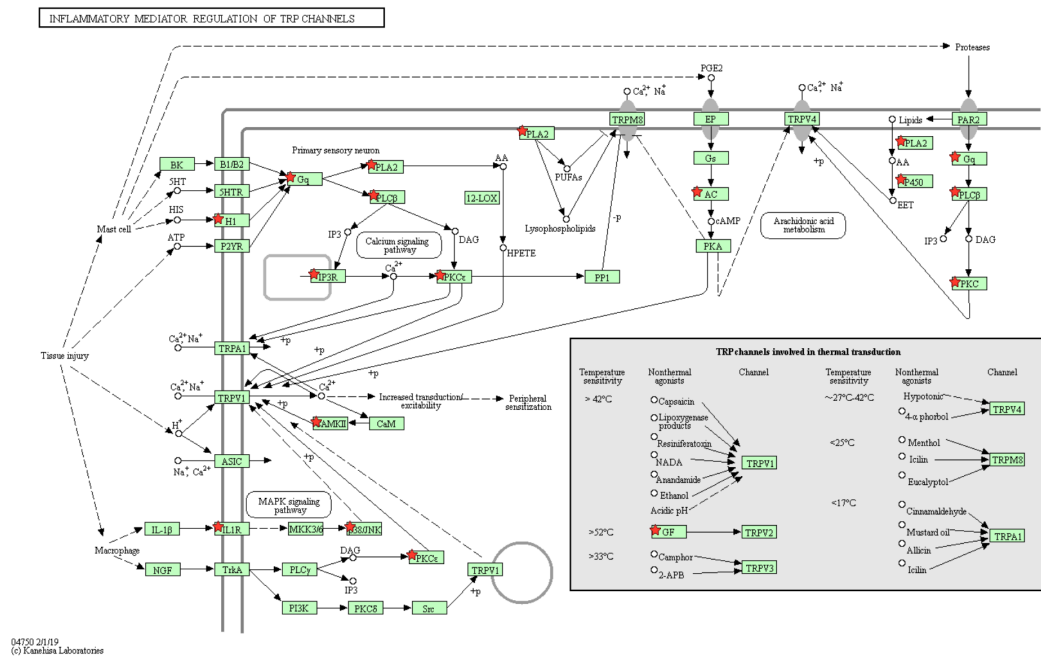


Figure 3.2: Inflammatory mediator regulation of TRP channels KEGG pathway diagram created from DAVID 6.8 gene ontology analysis of preHS genes. Red stars indicate genes from the preHS list that were also present within the pathway. The pathway shows enrichment in genes related to primary sensor neurons and MAPK signalling.

3.1. GENE NETWORKS CONTROLLED BY B2 HAVE DIVERSE FUNCTIONS

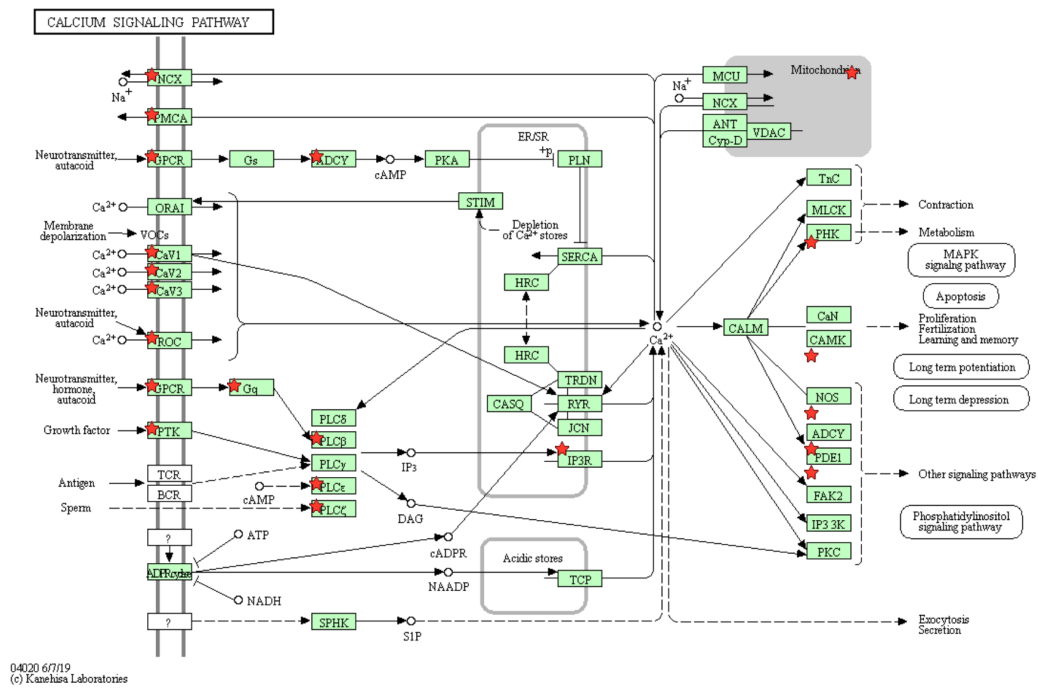


Figure 3.3: KEGG calcium signalling pathway diagram created from DAVID 6.8 gene ontology analysis of preHS genes. Red stars indicate genes from the preHS list that were also present within the pathway. Specifically, genes were enriched that coded for membrane-bound proteins, phospholipases, and proteins activated by calmodulin.

are present.

Within the glutamatergic synapse pathway, preHS genes are found concentrated in the post-synaptic neuron as shown in Figure 3.4. Activation of this network may be related to synaptic plasticity, neuronal excitability, long-term potentiation, or long-term depression of the neuron.

3.1.2 PreHS B2 Binding Genes and Learning-Associated Genes have Overlap

Based on the results of the analysis of the preHS genes, we set out to examine the role that B2 plays in neural pathways. The preHS gene list and learning-associated genes from Zovoilis et al. [138] were compared to each other using the Ghent University bioinformatics website Venn diagram tool (Figure 3.5). Of the 1907 preHS genes and 1130 learning-associated genes, 109 genes were shared between the two lists.

3.1. GENE NETWORKS CONTROLLED BY B2 HAVE DIVERSE FUNCTIONS

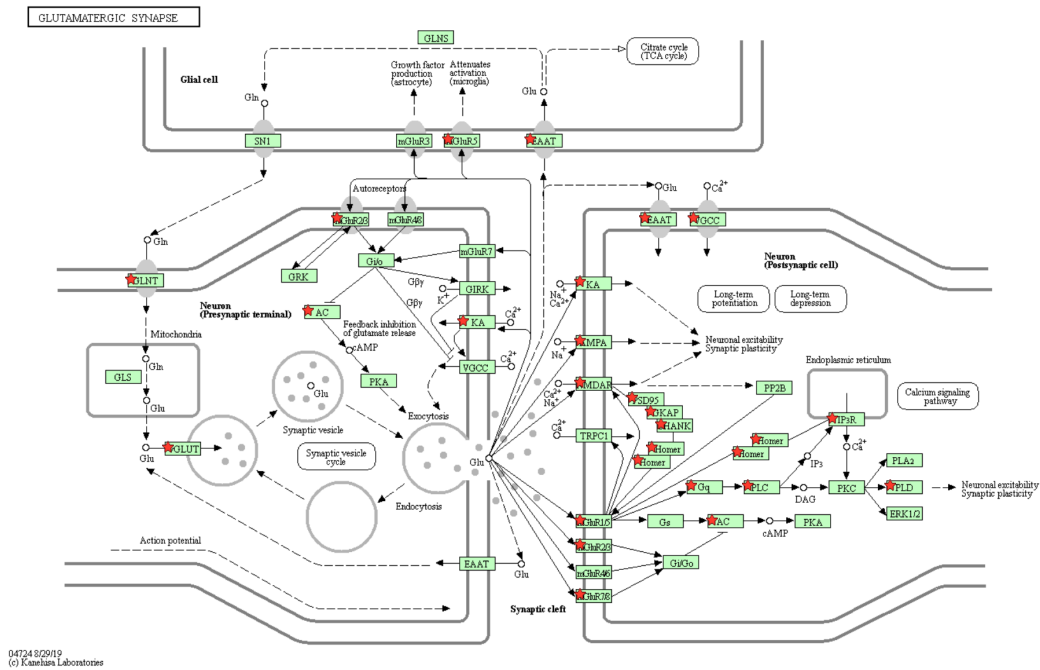


Figure 3.4: KEGG glutamatergic synapse pathway diagram created from DAVID 6.8 gene ontology analysis of preHS genes. Red stars indicate genes from the preHS list that were also present within the pathway. Specifically, genes were enriched in the post-synaptic space and are known to be responsible for responding to sodium, calcium, and glutamine present in the synaptic cleft. Activation of these genes may lead to neuronal excitability, long-term potentiation or depression, and synaptic plasticity.

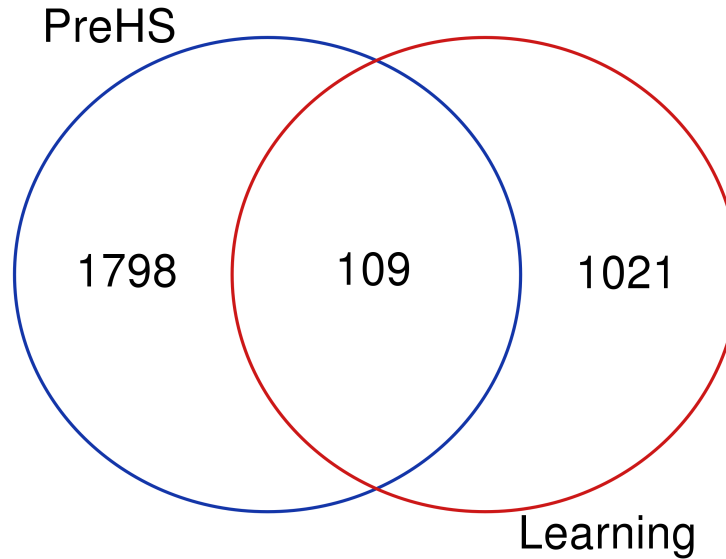


Figure 3.5: Venn diagram representing the number of genes common that were unique or common between preHS genes and learning-associated genes. List unions were computed using the Ghent University bioinformatics website Venn diagram platform. Of the 1907 preHS genes and 1130 learning-associated genes, 109 genes were shared.

The overlap of stress response genes that are controlled by B2 and genes that are associated with learning reveal that there are gene networks responsible for learning that are regulated by B2 processing.

The 109 genes that were common to both pathways are reported in Appendix B. Gene ontology analysis using PANTHER [150] (Figure 3.6) and DAVID 6.8 provide some insights into the roles of these genes. PANTHER reveals that these genes are related to cell-cell interaction, synaptic function, and neural development. Similar ontologies related to neurons, synapses, and calcium signalling were suggested by DAVID 6.8 (Figure 3.7). These findings demonstrate that B2 binding genes may play a role in synaptic excitation and signalling.

3.2. B2 RNA PROCESSING AND SRG ACTIVATION IN RNA-SEQ DATA

	Mus musculus (REF)		upload_1 (▼ Hierarchy, NEW! ?)				
GO biological process complete	#	#	expected	Fold Enrichment	+/-	raw P value	FDR
cell-cell junction assembly	87	7	.41	17.09	+	2.97E-07	9.39E-04
↳ cell junction assembly	132	7	.62	11.26	+	4.17E-06	3.87E-03
↳ cell junction organization	179	7	.84	8.30	+	2.79E-05	1.83E-02
↳ cell-cell junction organization	125	7	.59	11.89	+	2.96E-06	3.12E-03
cell-cell adhesion via plasma-membrane adhesion molecules	184	7	.87	8.08	+	3.30E-05	2.08E-02
↳ cell-cell adhesion	384	10	1.81	5.53	+	1.65E-05	1.19E-02
↳ cell adhesion	787	16	3.71	4.32	+	1.02E-06	1.79E-03
↳ biological adhesion	797	16	3.75	4.26	+	1.20E-06	1.89E-03
synapse organization	282	9	1.33	6.78	+	9.41E-06	7.42E-03
modulation of chemical synaptic transmission	522	14	2.46	5.70	+	2.13E-07	1.68E-03
↳ regulation of trans-synaptic signaling	523	14	2.46	5.68	+	2.17E-07	1.14E-03
↳ regulation of signaling	3212	33	15.13	2.18	+	9.08E-06	7.54E-03
↳ regulation of biological process	11285	74	53.15	1.39	+	4.96E-05	2.79E-02
↳ biological regulation	11902	76	56.05	1.36	+	7.83E-05	3.98E-02
↳ regulation of cell communication	3197	33	15.06	2.19	+	8.45E-06	7.41E-03
trans-synaptic signaling	363	9	1.71	5.26	+	6.45E-05	3.39E-02
regulation of vesicle-mediated transport	594	12	2.80	4.29	+	2.72E-05	1.87E-02
↳ regulation of transport	1954	24	9.20	2.61	+	1.16E-05	8.69E-03
neuron development	836	16	3.94	4.06	+	2.20E-06	2.67E-03
↳ cellular developmental process	3760	35	17.71	1.98	+	3.80E-05	2.31E-02
↳ developmental process	5523	48	26.01	1.85	+	3.76E-06	3.71E-03
↳ anatomical structure development	5169	48	24.34	1.97	+	5.82E-07	1.31E-03
↳ neuron differentiation	1028	18	4.84	3.72	+	1.65E-06	2.36E-03
↳ generation of neurons	1647	24	7.76	3.09	+	6.16E-07	1.21E-03
↳ neurogenesis	1754	24	8.26	2.91	+	1.86E-06	2.44E-03
↳ nervous system development	2241	30	10.55	2.84	+	1.02E-07	1.61E-03
↳ system development	4190	43	19.73	2.18	+	2.23E-07	8.80E-04
↳ multicellular organism development	4792	46	22.57	2.04	+	3.14E-07	8.26E-04
↳ multicellular organismal process	7228	54	34.04	1.59	+	6.10E-05	3.32E-02
cell morphogenesis	729	13	3.43	3.79	+	4.40E-05	2.57E-02
↳ anatomical structure morphogenesis	2189	27	10.31	2.62	+	2.59E-06	2.92E-03

Figure 3.6: PANTHER [150] Overrepresentation Test (January 2020) of 109 genes common to preHS and learning-associated genes using the GO Ontology Database - biological processes complete, reveal enrichment of pathways related to cell-cell interaction, synaptic function, and neural development. Statistical significance was determined by Fisher's Exact Test, and results with a false discovery rate of 0.05 were discarded. The FDR column is the Bonferroni adjusted P-value which accounts for multiple testing. The Expected column represents the amount of genes that would be expected to be found in the category by chance alone.

3.2. B2 RNA PROCESSING AND SRG ACTIVATION IN RNA-SEQ DATA

Category	Term	RT	Genes	Count	%	P-Value	Benjamini
GOTERM_CC_DIRECT	neuron projection	RT	12	0.1	5.2E-6	1.0E-3	
GOTERM_CC_DIRECT	synapse	RT	12	0.1	2.9E-5	2.8E-3	
GOTERM_BP_DIRECT	cell adhesion	RT	12	0.1	3.5E-5	2.3E-2	
GOTERM_CC_DIRECT	dendrite	RT	11	0.1	1.2E-4	7.6E-3	
GOTERM_CC_DIRECT	postsynaptic density	RT	8	0.0	1.5E-4	7.2E-3	
GOTERM_MF_DIRECT	protein binding	RT	36	0.2	4.6E-4	9.4E-2	
GOTERM_CC_DIRECT	cell junction	RT	12	0.1	6.3E-4	2.4E-2	
GOTERM_CC_DIRECT	postsynaptic membrane	RT	7	0.0	6.9E-4	2.2E-2	
GOTERM_CC_DIRECT	neuronal cell body	RT	10	0.1	1.0E-3	2.8E-2	
GOTERM_BP_DIRECT	chemical synaptic transmission	RT	6	0.0	1.9E-3	4.7E-1	
GOTERM_BP_DIRECT	regulation of potassium ion transmembrane transport	RT	3	0.0	2.6E-3	4.4E-1	
GOTERM_CC_DIRECT	membrane	RT	48	0.3	2.8E-3	6.7E-2	
GOTERM_MF_DIRECT	ion channel binding	RT	5	0.0	3.2E-3	2.9E-1	
GOTERM_CC_DIRECT	voltage-gated potassium channel complex	RT	4	0.0	6.4E-3	1.3E-1	
GOTERM_CC_DIRECT	cell projection	RT	10	0.1	7.0E-3	1.3E-1	
GOTERM_MF_DIRECT	calcium ion binding	RT	10	0.1	8.6E-3	4.6E-1	
GOTERM_CC_DIRECT	presynaptic active zone	RT	3	0.0	9.0E-3	1.5E-1	
GOTERM_MF_DIRECT	potassium channel regulator activity	RT	3	0.0	1.3E-2	5.0E-1	
GOTERM_BP_DIRECT	negative regulation of cellular response to oxidative stress	RT	2	0.0	1.5E-2	9.2E-1	
GOTERM_CC_DIRECT	terminal bouton	RT	4	0.0	1.7E-2	2.4E-1	
GOTERM_CC_DIRECT	cytoplasm	RT	43	0.3	1.7E-2	2.3E-1	
GOTERM_BP_DIRECT	adult walking behavior	RT	3	0.0	1.9E-2	9.3E-1	
GOTERM_MF_DIRECT	aryl hydrocarbon receptor binding	RT	2	0.0	2.0E-2	5.8E-1	
GOTERM_MF_DIRECT	metal ion binding	RT	26	0.2	2.4E-2	5.8E-1	
GOTERM_BP_DIRECT	brain development	RT	5	0.0	2.4E-2	9.4E-1	
GOTERM_BP_DIRECT	potassium ion transport	RT	4	0.0	2.7E-2	9.3E-1	
GOTERM_BP_DIRECT	negative regulation of peptidyl-cysteine S-nitrosylation	RT	2	0.0	3.0E-2	9.3E-1	
GOTERM_CC_DIRECT	protein complex	RT	8	0.0	3.1E-2	3.5E-1	
GOTERM_MF_DIRECT	nucleotide binding	RT	17	0.1	3.2E-2	6.3E-1	
GOTERM_BP_DIRECT	positive regulation of neuron projection development	RT	4	0.0	3.3E-2	9.2E-1	
GOTERM_CC_DIRECT	dendritic spine	RT	4	0.0	3.4E-2	3.6E-1	
GOTERM_MF_DIRECT	ATP binding	RT	14	0.1	3.9E-2	6.5E-1	
GOTERM_CC_DIRECT	trans-Golgi network	RT	4	0.0	4.4E-2	4.2E-1	
GOTERM_MF_DIRECT	AP-2 adaptor complex binding	RT	2	0.0	4.5E-2	6.6E-1	
GOTERM_BP_DIRECT	learning	RT	3	0.0	4.5E-2	9.5E-1	
GOTERM_BP_DIRECT	negative regulation of ERK1 and ERK2 cascade	RT	3	0.0	4.5E-2	9.5E-1	
GOTERM_MF_DIRECT	cytoskeletal protein binding	RT	3	0.0	4.6E-2	6.4E-1	
GOTERM_MF_DIRECT	voltage-gated potassium channel activity	RT	3	0.0	4.9E-2	6.2E-1	
GOTERM_CC_DIRECT	presynaptic membrane	RT	3	0.0	5.0E-2	4.4E-1	

Figure 3.7: DAVID 6.8 [149] Functional Annotations (January 2020) of 109 genes common to preHS and learning-associated genes. Annotation of genes by molecular function, biological process, and cellular compartment reveal enrichment of ontologies related to neurons, synapses, and calcium signalling. Statistical significance was determined by Fisher's Exact Test.

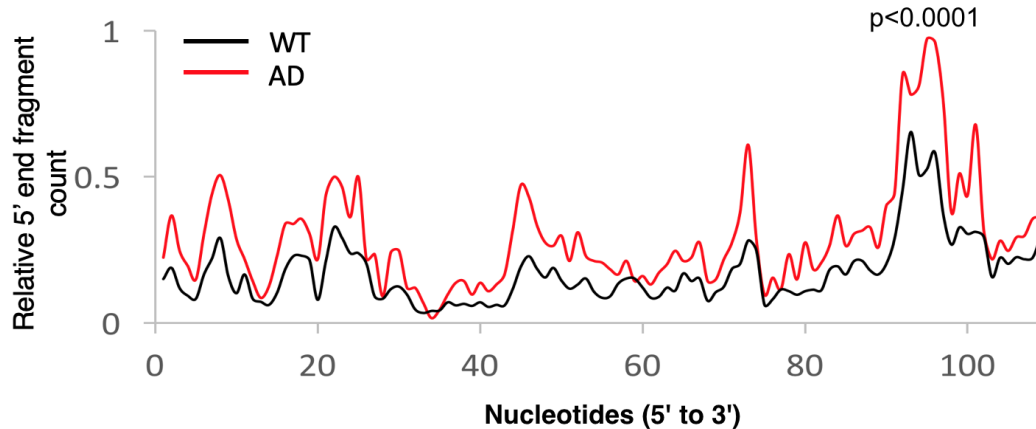


Figure 3.8: TSS plot of RNA reads mapped to the full length B2 RNA from wild-type and Alzheimer model mice. Reads were normalized to position one. Increased values show increased cleavage of the B2 RNA at that point. The plot shows an increase in processing at nucleotide 98, which is characteristic of cleavage of B2. The plot also shows a general increasing the amount of B2 fragments in AD mice relative to wild-type. $p < 0.0001$, Smirnov-Komolgorov test. WT mice: $n=4$, AD mice: $n=3$.

3.2 B2 RNA and SRG Activation Analysis in Standard RNA-Seq Data

3.2.1 B2 RNA Processing is Increased in Mouse Models of AD

Before proceeding to mouse models, cell culture, and short RNA-seq, it was prudent to first examine publicly available data of standard RNA sequencing to determine if signs of B2 cleavage could be observed in AD mouse models. Daugherty et al. [148] used a transgenic mouse model predisposed to develop a pathology similar to Alzheimer's disease with a genotype of $APP_{SWE}/PS1\Delta E9$. Their cortical RNA was prepared for HiSeq 2500 with Illumina TruSeq Stranded mRNA and read in single-ended 51bp reads. Fastq files were aligned to the B2 consensus sequence and a transcriptional start site (TSS) plot was produced for wild-type and AD mice (Figure 3.8).

The plot shows processing similar to Figure 3.9 in that peaks can be observed at approximately 75 and 98 bases and an additional peak near 45 bases. However, the publicly available data was prepared with a method of RNA-seq that fragments

the RNA and creates noise. This makes it challenging to definitely say if the B2 RNA is characteristically fragmented at the 98bp region, or if the library preparation influences cleavage at a region that is naturally unstable. Using a library preparation method developed by Dr. Zovoilis [144] increases the signal to noise ratio of processing to background as seen in Figure 3.9.

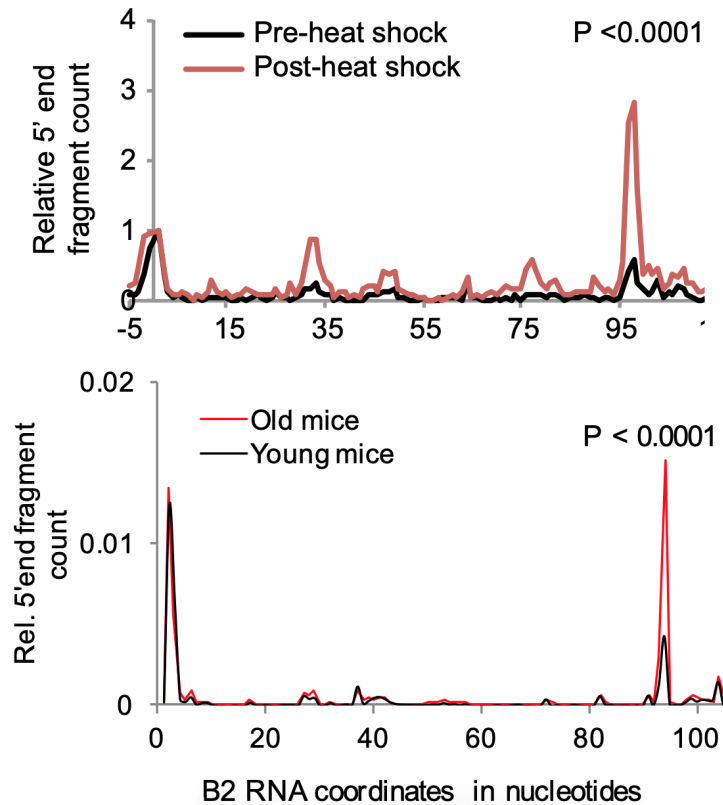


Figure 3.9: Top: B2 RNA is highly processed at 98 bases post-heat shock. Reprinted with permission from Zovoilis et al. in *Cell*, 2015 [144]. Bottom: Increased cleavage of the B2 RNA is observed in the unstimulated hippocampi of aging mice (sequencing data: Zovoilis Lab, unpublished). In each panel, reads that aligned to the B2 element identified and their 5' ends were plotted according to their position. Increasing values represent a higher concentration of fragments at that position. Characteristic cutting is observed at 98 bp consistent with previous work suggesting that B2 is cleaved in age as well as AD and heat shock. $p < 0.0001$ in each case.

The top graph of Figure 3.9 shows B2 processing as a result of a stressful stimulus. In the unstimulated mice no processing was observed. Similarly, young mice that were not presented with a stimulus responded normally and no processing occurred. Old

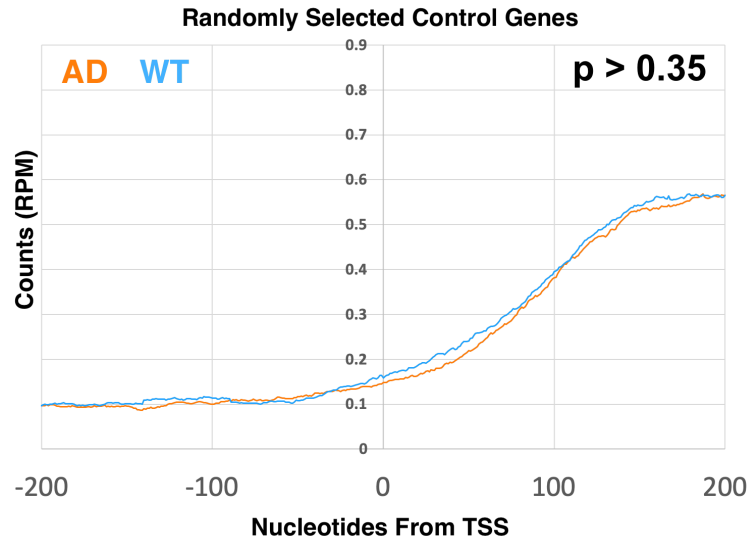


Figure 3.10: TSS plot of randomly selected gene reads in WT and AD mice. Traces show minimal difference in the level of transcription of control genes between AD mice and WT mice. Differences were quantified with Mann-Whitney-U test. $p=0.351$. WT mice: $n=4$, AD mice: $n=3$.

mice exhibited signs of B2 processing despite the absence of a stressor. Accordingly, aging has a negative effect on the stability of the B2 RNA and may cause issues with physiological regulation.

3.2.2 Alzheimer's Disease and Old Age Results in Aberrant Transcription of Stress Response Genes

Even though there are hints that B2 is abnormally processed in Alzheimer's disease mice, we wanted to check whether or not stress related genes were abnormally activated. Reads from the *APP_{SWE}/PS1 Δ E9* and WT mice were aligned to the genome and reads that mapped to stress response genes (Figure 3.11) or randomly selected controls (Figure 3.10) were plotted. For each case, the metagene plot shows the difference in transcription of each class of gene between each mouse genotype. Figure 3.10 shows that there is little to no difference between the AD and WT mice. This indicates that any elevated processing of the B2 RNA does not have an effect on genes outside of those bound by B2 itself.

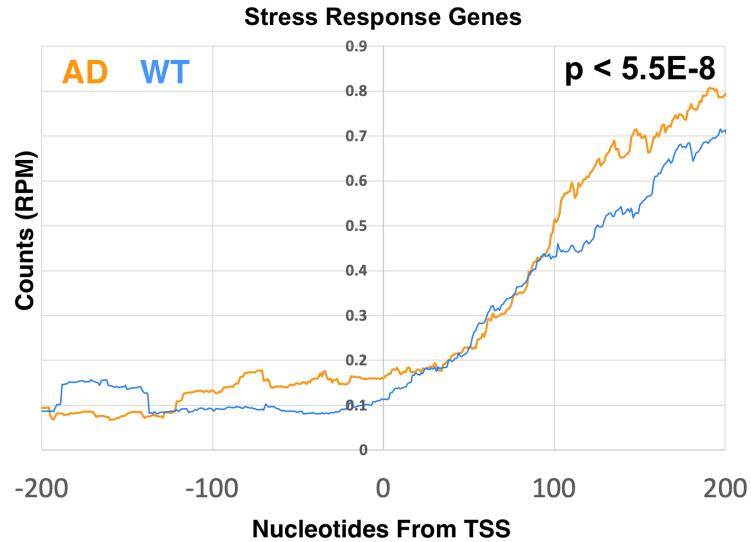


Figure 3.11: TSS plot of stress response gene reads in WT and AD mice. Traces show significant difference in the level of transcription of SRGs between AD mice and WT mice. Differences were quantified with Mann-Whitney-U test. $p < 5 \times 10^{-8}$ WT mice: $n=4$, AD mice: $n=3$.

In Figure 3.11 we see that the level of stress response gene (SRG) 5' fragments remains fairly close for the first 100 bases of the metagene plot. However, after that point we see increased levels of SRG reads from the AD mice. This could suggest that although polymerase is initiated on the DNA and paused proximally to the promoter, B2 is blocking elongation in the WT case. The increase in transcription in AD mice could be the result of increased B2 cleavage releasing repression of the polymerase.

3.2.3 B2 is Colocalized with Transcriptionally Active Regions

It is known that B2 RNA binds initiated Polymerase 2 [160] and stalls it ahead of important stress response genes [144]. CHART-seq data from Zovoilis et al. [138] reveals that there is an enrichment of B2 RNA at regions of active chromatin in the hippocampi of mice. Figure 3.12 shows a concentration of B2 CHART reads clustered around the transcriptional start site of SRGs associated with learning [138].

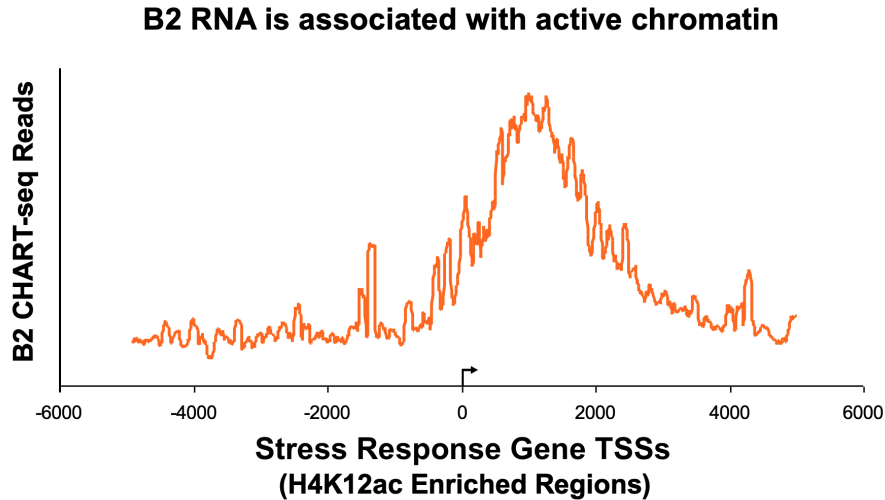


Figure 3.12: CHARTseq data from Zovoilis et al. [138] shows increased B2 reads in H4K12 acetylated regions associated with active chromatin. B2 is localized to actively transcribed genes.

3.3 B2 Processing in APP Mice using Short RNA-seq

Given that there is evidence of the involvement of B2 in Alzheimer’s disease, we began experiments with mouse models in collaboration with the University of Lethbridge’s Canadian Center for Behavioral Neuroscience (CCBN). Mice with the genetic background APP_{NL-G-F} mice and C57-Black mice were raised by our collaborators in the Mohajerani Lab at the CCBN. RNA-seq library prep was performed by Dr. Babita Gollen. Final differential expression analysis and normalization of SINE processing rates were performed by Yubo Cheng.

3.3.1 RNA Sequencing Reveals Increased Processing of the B2 RNA in AD Mice

The utilization of short-RNA-seq library preparation allows for a clearer view of B2 processing. By eschewing the fragmentation of nucleic acids common to library preparations and using magnetic beads to size-select for RNA under 200 bases long, we increase the proportion of reads that potentially map to the B2 RNA, as well as minimize fragmentation not associated with a physiological process. This allowed

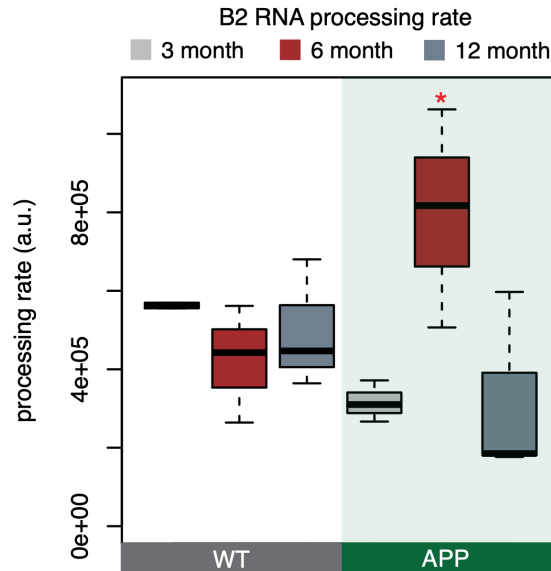


Figure 3.13: Short RNA-seq reveals increased processing of SINE RNAs in 6-month-old AD mice models. Star indicates $p < 0.05$ as determined by Student's t-Test. 3-month-old mice $n=2$. All other groups $n=3$. Data and graphic produced by Yubo Cheng. Figure adapted from Cheng, Y, Gollen B, Saville L, Isaac C, et al., submitted 2020.

us to observe differences in the amount of B2 cleavage between samples without the noise present in other RNA-seq data (Figure 3.9). In Figure 3.13 we do observe a significant increase in SINE processing at 6 months in the AD mice relative to WT. At approximately 6 months of age, these mice begin to develop symptoms of memory and learning impairment. This is consistent with the known progression of Alzheimer's-like symptoms in APP_{NL-G-F} [146]. Taken together, it appears that increased processing of B2 correlates with the progression of amyloid beta pathology, but not necessarily its end state.

3.3.2 RNA Sequencing Reveals Increased Transcription of Hsf1 in AD Mice

In addition to the previous results, Figure 3.14 shows the results of the long-RNA-seq preparation to interrogate changing levels of heat shock factor 1 (Hsf1). Interestingly, the pattern of Hsf1 expression mimics the processing rate of B2 RNA.

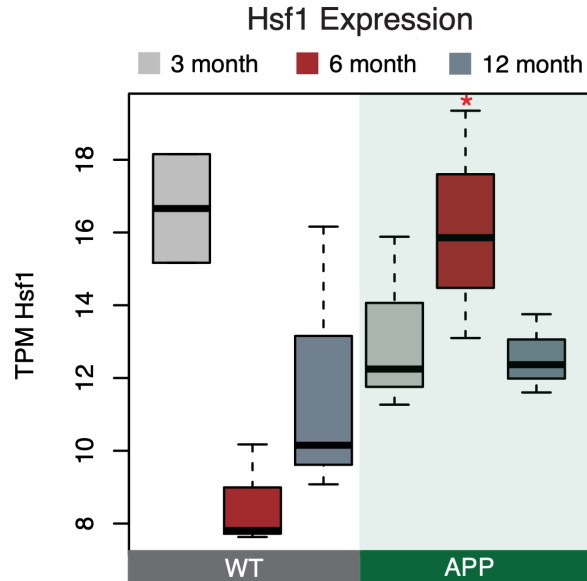


Figure 3.14: Long RNA-seq of mouse brain tissue shows an increase in levels of Hsf1 produced in APP+ 6-month-old mice. Star indicates $p < 0.05$ as determined by Student's t-Test. 3-month-old mice $n=2$. All other groups $n=3$. Data and graphic produced by Yubo Cheng. Figure adapted from Cheng. Y, Gollen B, Saville L, Isaac C, et al., submitted 2020.

At 6 months of age, the levels of Hsf1 in AD mice are significantly higher than in WT mice. It is important to note that although Hsf1 is nominally a transcription factor used in the response to heat-shock, it plays a larger role in responding to stress. Indeed, it may be the case that both EZH2 and Hsf1 are able to cut B2 and activate transcription of SRGs.

3.3.3 AD Causes Abnormally High Expression of SRGs

Continuing the previously established trend, Figure 3.15 shows 6 month-old AD mice are expressing SRGs at significantly higher levels than WT counterparts. This suggests that the cognitive difficulties experienced by AD mice may be related to abnormal activation of stress-related genes.

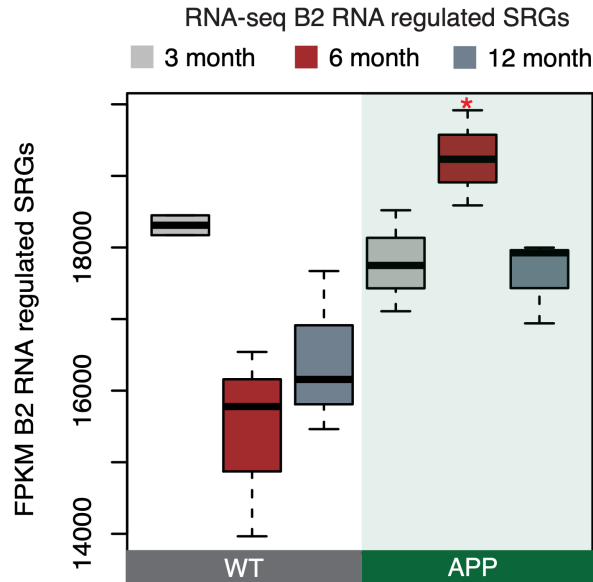


Figure 3.15: Long RNA-seq of mouse brain tissue shows an increase of transcription of stress response genes in 6-month-old APP+ mice. Star indicates $p < 0.05$ as determined by Student's t-Test. 3-month-old mice $n=2$. All other groups $n=3$. Data and graphic produced by Yubo Cheng. Figure adapted from Cheng. Y, Gollen B, Saville L, Isaac C, et al., submitted 2020.

3.3.4 AD Also Causes a Depression in Overall Transcription

Additionally, chronic activation of immediately early genes may have negative effects on cellular health. Figure 3.16 reveals that even though SRGs are abnormally upregulated at 6 months in AD mice, in general, global transcription is down. In heat-shock, transcription is generally downregulated, suggesting that the same response is may be occurring due to the overactivation of the stress-response pathway. Alternatively, heightened transcription of stress-response genes may be exhausting cellular resources to the detriment of the animal. Pathological activation of SRGs can lead to apoptosis and could account for the loss of neurons observed in AD patients.

Taken together, it appears that the 6-month time point is critical for the evolution of Alzheimer's disease-like symptoms in APP_{NL-G-F} . We have seen previously in Figure 3.13 that B2 is aberrantly processed during this time frame. We have also shown that stress response genes are upregulated during this window as well, implying that B2 is being cleaved to activate the stress response. Similarly, increased transcription

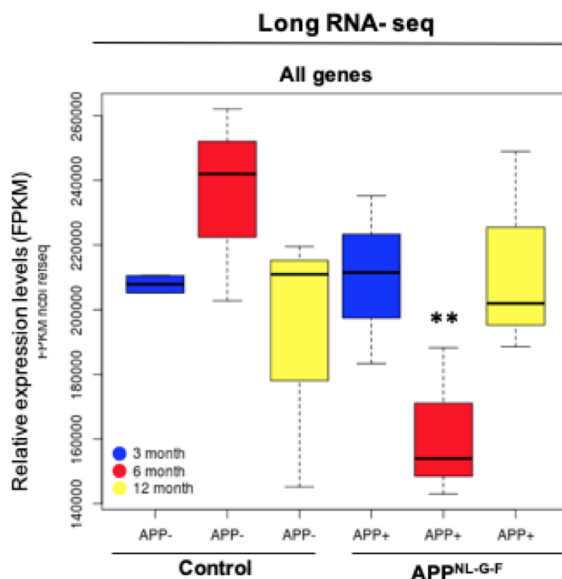


Figure 3.16: Long RNA-seq of mouse brain tissue shows a generalized depression of transcription in 6-month-old APP+ mice. Star indicates $p < 0.05$ as determined by Student's t-Test. 3-month-old mice $n=2$. All other groups $n=3$. (Zovoilis Lab, unpublished).

of Hsf1 during this period may suggest an interaction between B2 and Hsf1 that leads to activation.

3.4 B2 RNA Processing In Vitro

3.4.1 B2 RNA is Not Degraded by Amyloid Beta Fragments

To assess avenues of B2 RNA cleavage in Alzheimer's conditions, it was necessary to investigate which proteins—if any—could directly cause B2 fragmentation. Accordingly, properly folded B2 RNA was incubated with proteins suspected to play a causal role in amyloid-aging pathology. Amyloid precursor protein (APP) cleaved at the beta-secretase site yields an insoluble fragment with the ability to aggregate: $A\beta_{1-42}$. In contrast, $A\beta_{1-40}$ is thought to be non-pathogenic and does not aggregate. $A\beta_{\text{rev}}$ is the reversed sequence of $A\beta_{1-42}$ and is also non-aggregative. Each of these proteins was mixed with the B2 RNA and incubated for a full 24 hours at 37°C in TAP buffer. Both $A\beta_{1-40}$ and $A\beta_{\text{rev}}$ are intended to be negative controls to contrast any

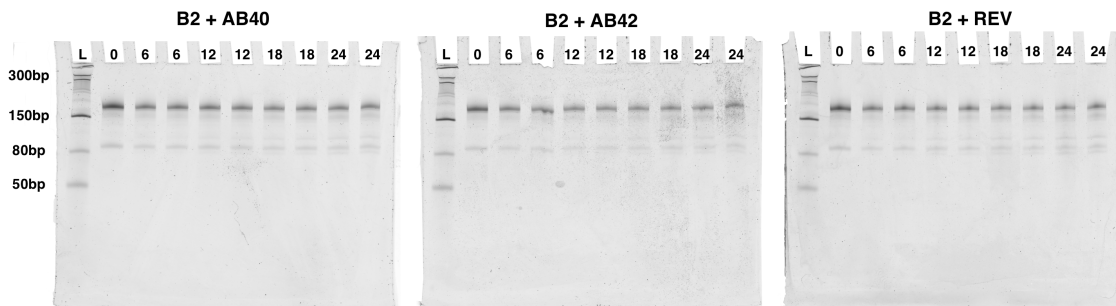


Figure 3.17: SDS-PAGE of B2 RNA processing when incubated with amyloid fragments. Each lane represents 1 picomole of folded B2 RNA was incubated at 37°C for 24 hours in F2 buffer in addition to amyloid proteins in TAP buffer at concentrations of to 0.05 μ M $A\beta_{1-42}$, 0.05 μ M $A\beta_{1-40}$, or 0.05 μ M $A\beta_{rev}$. Lanes labelled with the same times indicate technical replicates. Lanes marked zero have not been incubated and act as a negative control for any processing that might be observed over time in subsequent lanes. No processing of the RNA was observed over time.

processing that might have occurred in the $A\beta_{1-42}$ incubations. However, none of the proteins demonstrated an ability to activate B2 cleavage in vitro (Figure 3.17). This surprising finding indicates that amyloid fragments are not able to induce B2 cleavage on their own. However, since previous evidence suggests that B2 RNA is processed in amyloid-aging pathology, we set out to determine if other proteins beyond $A\beta$ were responsible.

3.4.2 B2 is Degraded by Hsf1 Over Time In Vitro

Knowing that Hsf1 is upregulated at the same time as B2 is undergoing significant processes caused us to suspect that Hsf1 was the protein responsible for cleaving B2. Similar to the previous experiment, Hsf1 was incubated with B2 RNA at 37°C for varying amounts of time. Each time point was performed in duplicate and the samples were visualized via SDS-PAGE. Based on the decreasing intensity of the band representing full-length B2 RNA, and the increasing intensity of lower molecular weight bands, we can see that B2 RNA is indeed fragmented in the presence of Hsf1 (Figure 3.18). Unlike the previous incubations with amyloid, incubation of B2 RNA with Hsf1 showed consistent processing over time. This result suggests that Hsf1 is suffi-

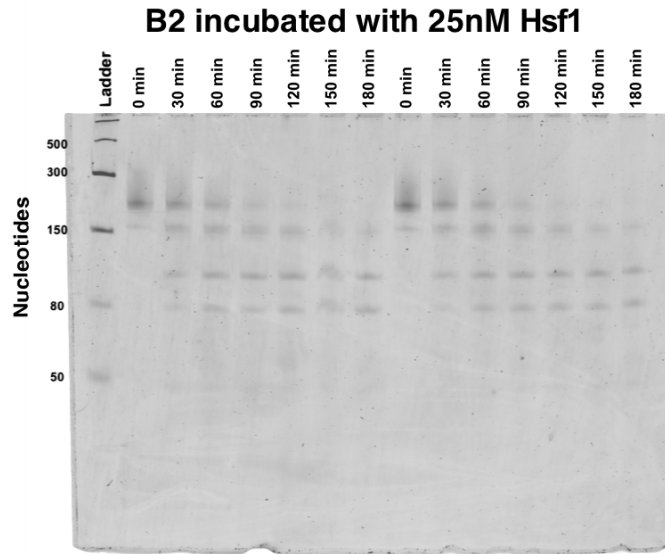


Figure 3.18: SDS-PAGE of B2 RNA incubated with Hsf1 protein over time. Each lane represents folded B2 RNA (1 picomole) which has been incubated in F2 buffer with Hsf1 protein in TAP buffer at a concentration of 25nM for up to 3 hours at 37°C. Lanes labelled with the same times indicate technical replicates. Lanes marked zero have not been incubated and act as a negative control for any processing that might be observed over time in subsequent lanes. Decreasing intensity of the band representing full-length B2 RNA, and the increasing intensity of lower molecular weight bands, shows that B2 RNA is fragmented in the presence of Hsf1.

cient to cleave B2 and may be responsible for activation of the stress response. While amyloid may play a key role in the progression of the disease, it is not responsible for the instability of the B2 RNA.

3.4.3 The Processing Rate of B2 is Dose-Dependent on Hsf1

Since Hsf1 appears to be causally linked to B2 processing, its role was further investigated. Hsf1 was titrated with B2 RNA and incubated over 90 minutes to determine the rate at which Hsf1 processes B2 (Figure 3.19). Each titration was performed in duplicate and each technical replicate was shown on via SDS-PAGE. Each sample of B2 RNA was prepared as previously described, however, we suspect that issues transcribing the RNA resulted in truncated forms of the RNA within the sample. Despite this, the band of interest representing the full-length B2 RNA was

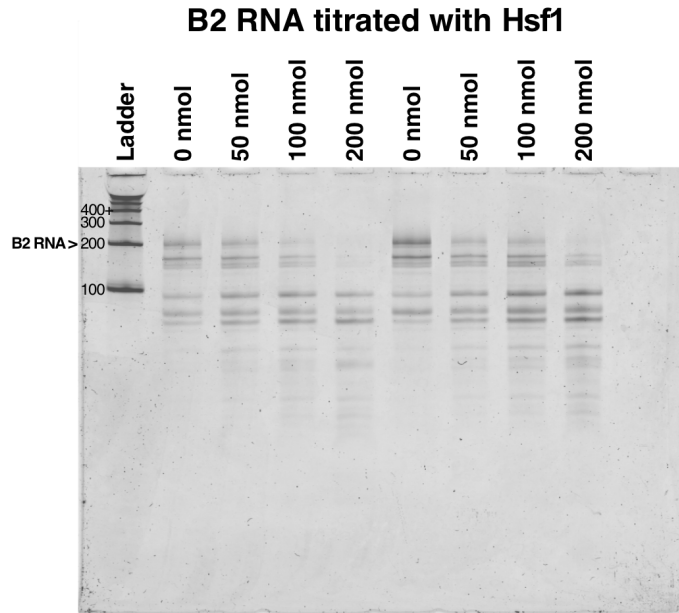


Figure 3.19: SDS-PAGE of B2 RNA incubated with increasing amounts of Hsf1. One picomole of folded B2 RNA was incubated in F2 buffer with increasing amounts of Hsf1 in TAP buffer for 90 minutes at 37°C. Each reaction was performed in duplicate and loaded on the gel. The decreasing intensity of the top band representing full-length B2 RNA indicates increasing degradation based on increasing concentration of Hsf1. Figure from Cheng. Y, Gollen B, Saville L, Isaac C, et al., submitted 2020.

retained. When focussing on the full-length band, we can see that as the concentration of Hsf1 increases, the band fades, indicating cleavage into small fragments.

ImageJ was used to quantify the rate of processing through densitometry and reveals a linear relationship was observed between concentration and degradation (Figure 3.20). The linear relationship suggests first-order reaction between Hsf1 and B2 RNA, indicating that the cleavage event requires only a single Hsf1 molecule per B2 RNA to occur, and is therefore not a cooperative process. Taken together, the incubations of B2 RNA reveal that amyloid beta is not directly involved in the cleavage of B2 RNA. Instead, we see that Hsf1 alone is sufficient to induce the fragmentation of B2 RNA, and though $A\beta$ is not responsible for B2 degradation, it is still likely to be involved earlier on in the activation of the stress response.

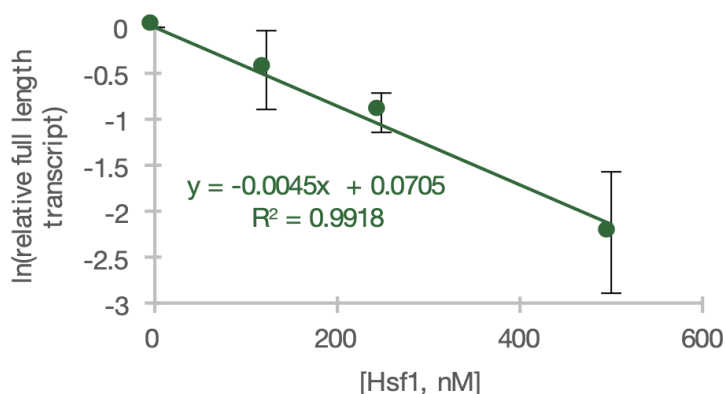


Figure 3.20: Densitometric quantification of remaining B2 RNA show a dose-dependent relationship between the degradation of the RNA and the concentration of Hsf1. The intensity of the top band of the previous gel Figure 3.19 was quantified using ImageJ and the relative reduction in intensity was plotted as a function of the concentration of Hsf1. The plot reveals a linear relationship between B2 processing and Hsf1 concentration, suggesting stoichiometric and direct action of Hsf1 on B2. $R^2 > 0.99$. Error bars represent the standard deviation of the two technical replicates. Figure from Cheng. Y, Gollen B, Saville L, Isaac C, et al., submitted 2020.

3.5 Cell Culture and LNA and Amyloid Challenges

3.5.1 Incubation of Hippocampal Neurons with Amyloid Results in an Increase in FOSB Transcription

In order to corroborate the evidence of SRG activation from RNA-seq data, HT22 mouse hippocampal neurons were incubated with amyloid fragments to investigate the role of $A\beta$ to influence gene expression. After cell cultures were treated for 1 hour with $1\mu\text{M}$ amyloid concentrations, we observed via qPCR that FOSB was highly upregulated after incubation with $A\beta_{1-42}$ (Figure 3.21). FOSB is a stress responsive gene and is related to the pro-apoptotic pathway, but also plays roles in the development of addiction in the brain [161]. However, no upregulation of FOSB was observed in cells treated with $A\beta_{1-40}$, $A\beta_{\text{rev}}$, or DMSO. Instead, a reduction in the expression of FOSB was observed. This makes sense since the expression of FOSB—an SRG—was measured against HPRT—a housekeeping gene—which is ordinarily itself downregulated during stress and more highly expressed than SRGs at rest. The results show

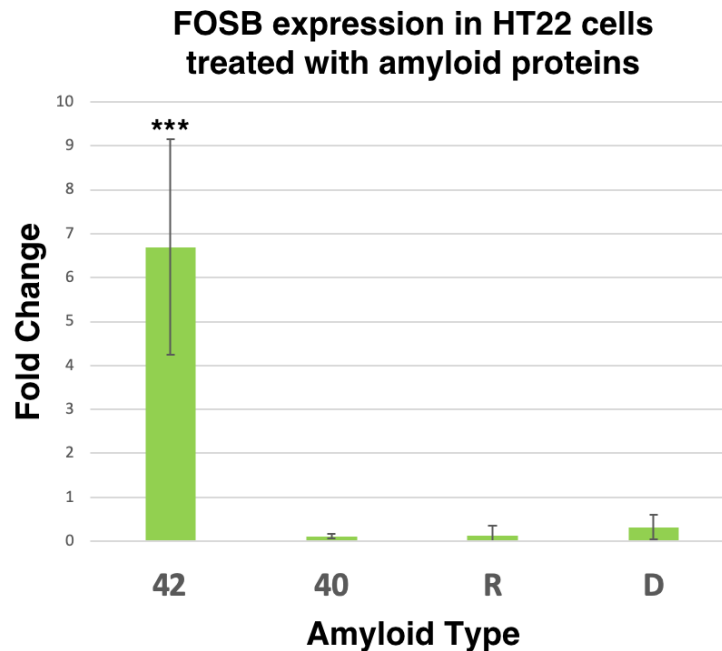


Figure 3.21: HT22 cells treated with amyloid proteins (42: $A\beta_{1-42}$, 40: $A\beta_{1-40}$, R: $A\beta_{\text{rev}}$, and DMSO control) were assessed by qPCR using the relative standard curve method. FOSB is strongly upregulated in HT22 cells in the presence of $A\beta_{1-42}$ after 1 hour of incubation with $1\mu\text{M}$ of protein. $A\beta_{1-40}$, $A\beta_{\text{rev}}$, and DMSO did not upregulate FOSB. Each group represents 3 technical replicates of HT22 cell cultures. Asterisks represent statistically significant differences of $p < 0.05$, as determined by Student's t-Test.

that only $A\beta_{1-42}$ is able to induce the expression of FOSB in HT22 cells, and therefore the stress response at large. Furthermore, we learned that other $A\beta$ fragments do not activate the stress response.

3.5.2 The Downregulation of Hsf1 Limits the Activation of FOSB by Amyloid Beta During Amyloid Toxicity

Since FOSB was shown to be upregulated in amyloid-aging pathology, we wanted to investigate the role of Hsf1 in activating transcription of SRGs. Expression of FOSB was assessed through qPCR following transfection of anti-Hsf1 LNA and incubation with amyloid fragments (Figure 3.22). Locked nucleic acids (LNA) are short segments of non-reactive nucleic acids which actively hybridize to RNA or DNA complimentary

to themselves. Binding of LNA to RNA functionally creates dsRNA, the presence of which causes the cell to downregulate those transcripts. Effectively, LNA transfection significantly reduces the levels of transcripts of a target gene within the cell. Hippocampal neurons were transfected with LNA 24 hours before incubation with amyloid to ensure that Hsf1 transcripts had been eliminated before the experiment.

We observed strong upregulation of FOSB when Hsf1 was present and the cells were incubated with $A\beta_{1-42}$ relative to cells that did not have Hsf1 depleted. The results suggest that FOSB gene expression under $A\beta_{1-42}$ stress is dependent on the availability of Hsf1.

Additional examination of the effects of depleting Hsf1 in cells was achieved by utilizing our short RNA-seq methods. We found that the processing of B2 was abolished when Hsf1 was depleted by the LNA (Figure 3.23). This suggests that Hsf1 is required to process B2 while under amyloid-induced stress and is therefore a key factor in amyloid-aging pathology.

Taken together, our data suggest that Hsf1 is required for upregulation of FOSB in the presence of $A\beta_{1-42}$. When Hsf1 is depleted by the LNA, B2 is not cut, and the cell does not respond to the stimulus. Accordingly, we suggest that during the progression of amyloid-aging pathology, Hsf1 is activated in response to accumulation of $A\beta_{1-42}$ and directly causes the B2 RNA to fragment, thereby releasing SRGs from repression.

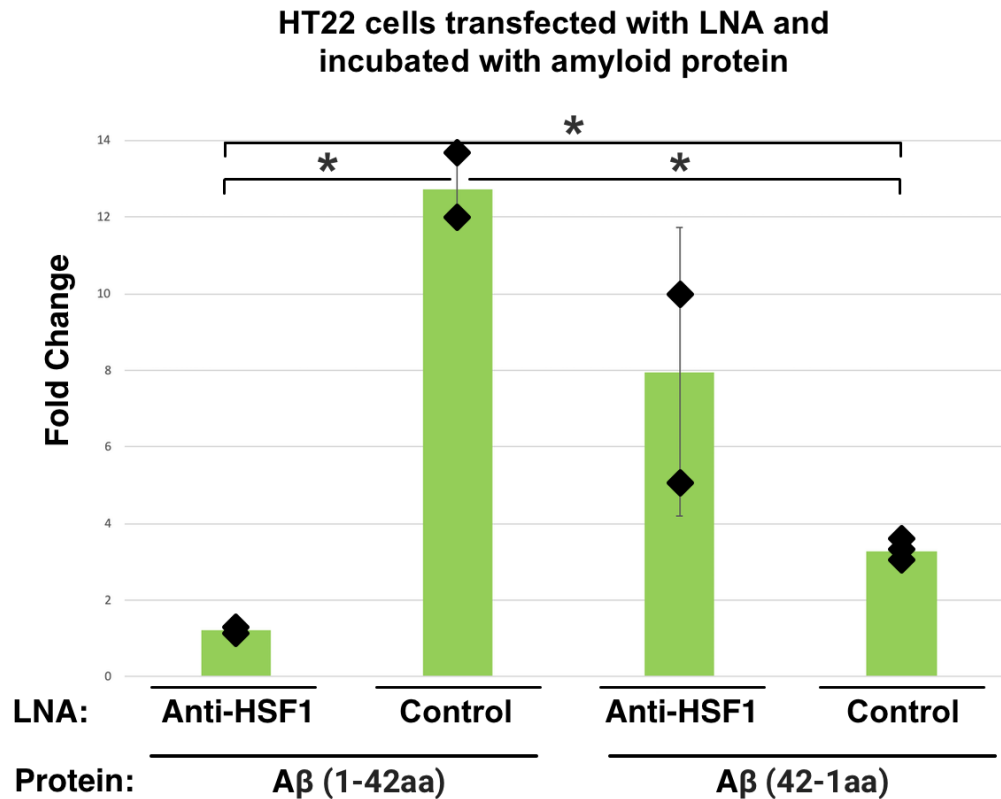


Figure 3.22: Hippocampal neuron gene expression following incubation with amyloid and LNAs. $A\beta_{1-42}$ represents pathogenic $A\beta$ fragments and $A\beta(42-1aa)$ represents the reversed sequence of the peptide. Treatments are further separated into groups treated with Anti-Hsf1 LNA to reduce levels of Hsf1 in the cell or a scrambled control LNA. The results suggest that FOSB gene expression under $A\beta_{1-42}$ stress is dependent on the availability of Hsf1. Gene expression was assessed by relative standard curve against HPRT. Cells were incubated with 50nM LNA for 24h, and then 30 μ M of amyloid for 6 hours. All steps performed at 37°C. Each group consists of three plates of cells. 1 outlier was excluded from each group except $A\beta_{rev}$ and Control LNA. Datapoints are represented as diamonds. The bars represents the mean value of the group. Significant relationships ($p < 0.05$) as determined by Student's t-Test are indicated with a star.

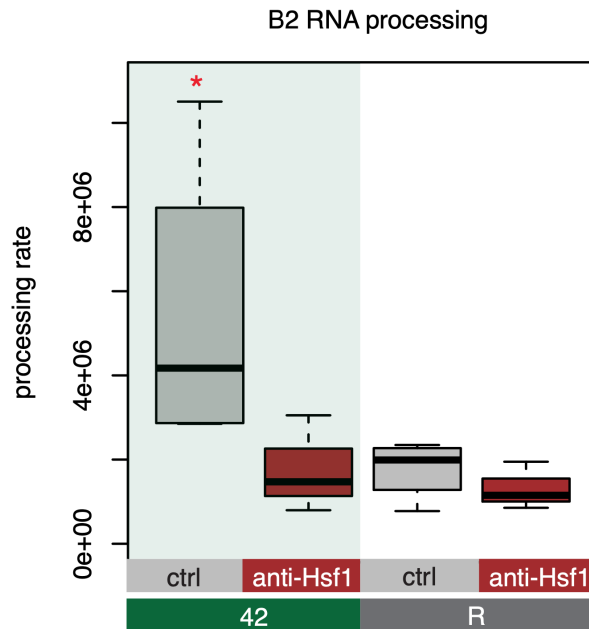


Figure 3.23: B2 processing observed in short RNA-seq of hippocampal cell culture. Each bar represents technical replicates of plates of hippocampal neurons treated with either $A\beta_{1-42}$ (42) or the reversed control peptide, $A\beta_{rev}$ (R). The treatments were further divided between those treated with anti-Hsf1 LNA or a scrambled LNA (ctrl). Short RNA-seq reveals $A\beta_{1-42}$ is sufficient to cause processing of B2 RNA when treated with scrambled LNA but processing was not upregulated with $A\beta_{rev}$. Interestingly, B2 processing is abolished in the absence of Hsf1, indicating that Hsf1 is necessary for B2 processing. Star indicates $p < 0.05$ between 42 and R for cell treated with the control LNA ($n=4/\text{group}$, t-Test). No significant increase was observed between cells treated with anti-Hsf1 LNA ($n=3/\text{group}$). Figure from Cheng. Y, Gollen B, Saville L, Isaac C, et al., submitted 2020.

Chapter 4

Discussion

4.1 The Link Between Learning, Stress, and Memory

The ability of cell to respond to a stimulus is a fundamental quality of life. Given that responding to stress is critical for the survival of the cell, it seems reasonable to speculate that this response may have been the first to evolve. Accordingly, the mechanisms that enable the detection of a signal and the coordination of a response are likely ancient and well-conserved. Indeed, many facets of the response to stress are not stressor-specific [162]. Coordinating an appropriately sensitive response to stress is key to balancing the trade-off between plasticity and rapidity of response with wanton expenditure of cellular resources [163].

It is unsurprising then that genes related to the response to heat-shock are involved in other processes (Figure 3.1). The involvement of multipurpose machinery reduces the burden of cells to maintain extraneous machinery for niche cases. We have seen that a multitude of genes are shared in the response to heat-shock and learning (Figure 3.5) and that these genes are involved in neuronal gene networks (Figure 3.6). Since we already know that B2 regulates the stress response from previous work by Zovoilis et al. [144], the pathways that were identified in the GO analysis are likely also regulated by B2. Furthermore, CHART-seq of H4K12ac revealed that B2 is indeed co-localized to active chromatin (SRGs) related to memory formation (Figure 3.12). Taken together, the highly general mechanism by which B2 regulates gene expression is likely common to many responses to stress.

The pathologies of aging and AD are diverse and may interact with B2 in a variety of ways. Common to both pathologies is the decline of learning, memory, and difficulty adapting to change. Chronic activation of SRGs is likely to exceed the capacity of the cell to respond and will result in cell death and neurodegeneration. Given that B2 appears to be a crucial regulator of transcription, it is sensible to investigate seriously the possibility that abnormal B2 processing plays a significant role in amyloid-aging pathology.

4.2 B2 RNA is Aberrantly Processed in AD

Examination of publicly available RNA-seq data of AD mouse models revealed suggestions that B2 was being aberrantly processed in AD models relative to WT mice (Figure 3.8). However, based on the fragmentation inherent to the library preparation that the authors used, the alignment of reads to the B2 RNA was messy and inconclusive. It is impossible to tell if the region was destabilized by a specific interaction resulting from the AD phenotype, or if the library preparation itself resulted in enriched fragmentation at the characteristic cutting point.

Short RNA-seq developed by Dr. Zovoilis [144] to enrich sequencing for reads under 200 bases in length paints a clearer picture of processing as seen in Figure 3.9. The processing observed in previous work related to heat-shock matches the processing of B2 RNA observed in the brains of mice that had simply aged to 16 months. This suggests that as the mice aged the regulatory network responsible for activating the stress response is deregulated over time. Furthermore, when looking at the difference in the rate of SINE RNA processing in WT and AD mice, we observed that the relatively young 6-month old AD mice exhibited vastly increased rates of processing as compared to their age-matched counterparts (Figure 3.13). This corresponds to the age where cognitive decline is first observed in the transgenic model (Figure 2.1) and indicates pathological activation of the stress response. Interestingly, at 12 months

of age there appears to be an attenuation of processing rate that returns the rate of processing to that of the wild-type mice. This could be an intrinsic factor to the model that has allowed the mice to reduce the effects of APP_{NL-G-F} -mediated B2 processing, but not to recover lost cognitive ability. Alternatively, the decrease in the rate of B2 processing could be explained by the cessation of the stress response following advanced neurodegeneration. Taken together, the results suggest that B2 RNA is processed in both an age-dependent and amyloid-dependent manner which may synergistically impact cognitive decline.

A timeline of B2 processing by $A\beta$ fragments revealed that none of the fragments were able to induce cleavage (Figure 3.17). Conversely, incubation of B2 with Hsf1 over time resulted in marked processing (Figure 3.18). After 12h hours, the B2 RNA was completely degraded. Titration of Hsf1 to B2 suggests that activity of Hsf1 was dose-dependent and appears linear (Figure 3.20). Processing with Hsf1 is consistent with the thought that the B2 response mechanism is broad and affected by a variety of stimuli. Additionally, given the inflammation present in AD, it makes sense for Hsf1 to be upregulated during the disease. Abnormal activity of Hsf1 on B2 may be the proximal cause for chronic pathological SRG activation.

4.3 B2 RNA Processing is Related to Abnormal SRG Activation

While not useful for studying B2 processing, the publicly available data was suitable for studying changes in stress response genes in AD and WT mice. TSS plots of randomly selected control genes (Figure 3.10) showed no significant difference between disease and wild-type phenotypes. Interestingly, the level of transcription of SRGs was drastically different (Figure 3.11). The pattern of transcription suggests proximal pausing of polymerase II within the first 100 bases following the TSS. Following a period of relatively comparable regulation, the number of SRG reads increases in

the AD case indicating increased elongation. This pattern is consistent with what is known about B2 binding the active site of initiated polymerase II and being cleaved to release the polymerase. Upstream of the TSS increased reads in the AD case suggest some amount of abortive transcription as the polymerase attempts to transition from initiation to elongation. It is unclear what role B2 might play in this process.

The APP_{NL-G-F} mouse model also provided unique insights into the regulation of SRGs in AD. Figure 3.15 shows that SRGs are highly upregulated in AD mice at 6 months of age, coincident with the observation of cognitive decline in the transgenic model. There were no significant differences in 3 and 12-month-old mice. Similarly interesting was the global level of transcription of all genes. While there were no significant difference in the 3 and 12-month-old mice, a general depression of total transcription was observed in the 6-month APP_{NL-G-F} mice. Because B2 is a regulator of SRGs in advance of a stress response, cleavage allows for the rapid uptake of cellular resources to the stress response. However, extra B2 transcribed by polymerase III has been shown to preferentially associate with non-SRGs during the response. A sustained stress response and elevated levels of total B2 could contribute to global repression of transcription not relevant to the stressor. The pattern of expression in SRGs in multiple models appears consistent with the behavior of B2 as a regulator of transcription and keystone RNA in the stress response.

4.4 The Role of Hsf1 and FOSB

Levels of Hsf1 were significantly elevated in APP_{NL-G-F} mice at 6 months relative to the control (Figure 3.14). Accordingly, this result suggests that there is a larger role for Hsf1 in Alzheimer's disease. Elevated levels of Hsf1 are not unexpected however, especially given the role of the heat shock response to unfolded protein—caused either by temperature stress or pathological aggregation. Hsf1 acts as a potent transcription factor during stress as other heat-shock proteins release their control and allow

trimerization of Hsf1 which then modulates gene expression. It is possible that Hsf1 possesses intrinsic ability to degrade B2 in order to initiate the response to stress.

When HT22 cells were challenged by incubation with $A\beta_{1-42}$, expression of FOSB—a potent oncogene and SRG—was observed (Figure 3.21). This suggests that the stress caused by the amyloid successfully induced the stress response. When HT22 cells were challenged with a combination of Anti-Hsf1 LNA and $A\beta$, the results were very different. As expected, incubation with $A\beta_{rev}$ did not meaningfully change gene expression in either the Anti-Hsf1 or control LNA cases. Conversely, incubation with $A\beta_{1-42}$ greatly increased expression of FOSB in the control LNA treatment. Most interestingly however, knockdown of Hsf1 in the cells abolished the ability of cells to respond to the stressor. This suggests that Hsf1 is critical to initiating of the stress response to Alzheimer’s disease, specifically for its role in cutting B2. Alternatively, a combinatorial effect of $A\beta$ and Hsf1 may be a mechanism by which neurons are overwhelmed in AD and committed to apoptosis.

In summary, we know that as AD-model mice age and accumulate amyloid over time. We have also seen that at approximately six months of age, AD mice begin to show symptoms of cognitive decline. During this period, we have also observed a decrease in general transcription, an increase in processing of B2 RNA, and an increase in transcription of stress response genes. Furthermore, we also see that Hsf1 is upregulated during this period and have shown that Hsf1 is capable of causing the B2 RNA to fragment. As a result of abnormal B2 RNA processing, we would expect chronic expression of SRGs over and above what would be required for a normal stress response. The chronic activation of stress response genes likely leads to cellular apoptosis within neural tissue, resulting in neurodegeneration. Since the hippocampal neurons are required for memory, apoptosis in this region could explain the cognitive decline observed in the mice. Overall, it appears that as the amyloid-aging pathology progresses, increasing amounts of amyloid chronically and pathologically activate the

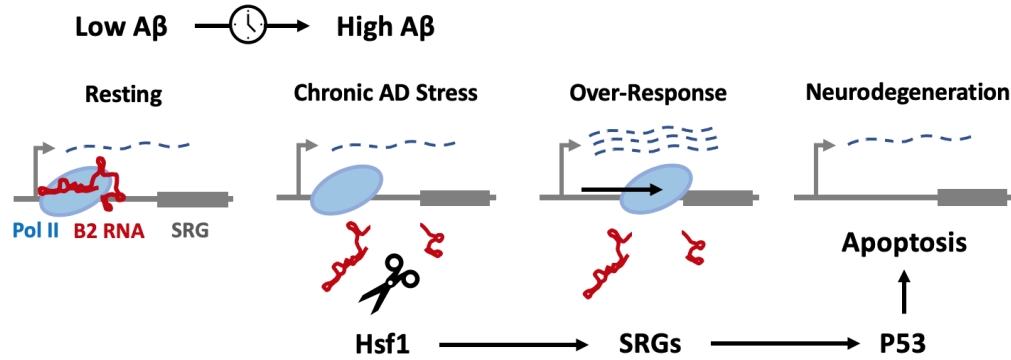


Figure 4.1: Summary figure of the role that B2 plays in the progression of amyloid-aging pathology in mice. As amyloid burden increases over time, the stress response becomes chronically activated, promoting the activation of Hsf1. In turn, Hsf1 cleaves B2 and upregulates stress response genes. Chronic activation of SRGs ultimately activates pro-apoptotic pathways leading to cell death and neurodegeneration, marked by memory impairment and cognitive decline.

stress response, resulting in increases transcription and activation of Hsf1. As the amount of Hsf1 increases in the nucleus, B2 is unable to control the expression of SRGs, leading to the activation of pro-apoptotic pathways, neurodegeneration, and memory impairment commonly associated with Alzheimer’s disease. A summary of this hypothesis can be found in Figure 4.1.

4.5 Future Directions

Overall, it appears that B2 and Hsf1 are together essential components of the stress response. The dysregulation of one or both may be key events in the progression of AD. Intervention in this pathway may prove to be a promising avenue for the development of anti-neurodegenerative therapies. However, more research needs to be conducted to conclusively understand the interplay of these factors in AD.

First of all, the mechanism by which Hsf1 cleaves B2 needs to be understood. Additionally, the effect of B2 dysregulation on the expression of other SRGs needs to be confirmed by qPCR and other quantitative methods. A comprehensive look at neurological genes conclusively regulated by B2 will be invaluable for assessing

the effects of future therapies. Furthermore, the levels of pro-apoptotic proteins and microRNAs should be quantified to conclusively determine the contribution of this pathways to cellular apoptosis and neural death in neurodegenerative disorders. Based on the evidence presented here, and the differences in neurodegeneration between mice and humans, further research should be done to determine how Alu elements and other SINEs contribute to the progression and pathology of Alzheimer's disease in humans.

In examining the applicability of this research to humans, one must consider the multiple roles that amyloid, SINE RNAs, and Hsf1 may all play in the cell. While the role of APP in the cell is not yet known, all tested therapies against amyloid have failed. Accordingly, it seems like an impractical target. Similarly, while Hsf1 is a promising druggable target being investigated as potential target during cancer therapies, inhibiting Hsf1 itself is likely to be far more disruptive than other strategies. The Alu element is a human SINE RNA with a similar function as the B2 RNA. However, the Alu RNA family is far more divergent than the B2 RNA and makes up a sizeable fraction of the genome.

In investigating the Alu RNA as a target for anti-AD therapies, one must first examine at the highly divergent families of all Alu within the genome, and determine which of them—if any—are aberrantly processed in AD. Depending on if there are classes of Alu that are more or less involved with AD, one could attempt large-scale genome editing to replace overactive Alus with more neuroprotective variants. In the same way, increasing the activity of Polymerase III to transcribe additional Alu RNA could build a buffer of RNA and delay the onset of SRG hyperactivation and apoptosis. Alternatively, if the processing of Alu RNA in general is associated with the progress to AD, it may be more effective to design a small molecule that can protect the RNA from attack by Hsf1 as This small molecule could take the form of a protective nucleic acid which binds the Alu and interferes with Hsf1 (or other proteins) as they attempt to cleave the RNA. However, whichever therapeutic option

is more effective must be started before the neurodegeneration becomes advanced. While it may in theory be possible to halt or delay the progression of Alzheimer's disease, it remains challenging to regenerate brain tissue and impossible to recover memories from deceased neurons.

Chapter 5

Conclusion

In conclusion, this work demonstrated a connection between heightened processing of B2 RNA by Hsf1 in response to amyloidopathic stress and abnormal activation of stress response genes.

From previous work we know hippocampus-specific changes of gene expression of SRGs correlates to learning [138]. We also know that SRGs involved in responding to a variety of stimuli are regulated by B2 RNA [144]. Since the SRGs are also targets of pro-apoptotic microRNA, hyper-expression of SRGs has the potential to lead to apoptosis, promoting neural death and learning impairment in amyloid-ageing pathology [141].

In this work we have shown that B2 is abnormally processed as a result of old age and AD in publicly available data, mouse models, and in vitro experiments. We have also demonstrated that increased processing of B2 correlates to a specific increase in transcription of SRGs, and a global decrease in total transcription in a mouse model of AD. Furthermore, we suggest that Hsf1 is the causal agent involved in cutting B2 to activate the stress response in AD. Lastly, we show that Hsf1 is necessary but not sufficient to induce changes in gene expression caused by amyloidopathic stress. We hope that these findings will invogorate research in the role of SINE RNAs in Alzheimer's disease and help develop novel therapies for the disease.

Bibliography

- [1] Nicole C Berchtold and Carl W Cotman. Evolution in the conceptualization of dementia and alzheimer's disease: Greco-roman period to the 1960s. *Neurobiology of aging*, 19(3):173–189, 1998.
- [2] Hans Förstl and Alexander Kurz. Clinical features of alzheimer's disease. *European archives of psychiatry and clinical neuroscience*, 249(6):288–290, 1999.
- [3] Konrad Maurer, Stephan Volk, and Hector Gerbaldo. Auguste d and alzheimer's disease. *The Lancet*, 349(9064):1546–1549, 1997.
- [4] Lars M Ittner and Jürgen Götz. Amyloid- β and tau—a toxic pas de deux in alzheimer's disease. *Nature Reviews Neuroscience*, 12(2):67, 2011.
- [5] Gabriele Cipriani, Cristina Dolciotti, Lucia Picchi, and Ubaldo Bonuccelli. Alzheimer and his disease: a brief history. *Neurological Sciences*, 32(2):275–279, 2011.
- [6] Guy M McKhann, David S Knopman, Howard Chertkow, Bradley T Hyman, Clifford R Jack Jr, Claudia H Kawas, William E Klunk, Walter J Koroshetz, Jennifer J Manly, Richard Mayeux, et al. The diagnosis of dementia due to alzheimer's disease: Recommendations from the national institute on aging-alzheimer's association workgroups on diagnostic guidelines for alzheimer's disease. *Alzheimer's & dementia*, 7(3):263–269, 2011.
- [7] American Psychiatric Association. *Diagnostic criteria from dsM-iV-tr*. American Psychiatric Pub, 2000.
- [8] George T Grossberg. Diagnosis and treatment of alzheimer's disease. *The Journal of clinical psychiatry*, 64:3–6, 2003.
- [9] Deborah Blacker, Marilyn S Albert, Susan S Bassett, Rodney CP Go, Lindy E Harrell, and Marshai F Folstein. Reliability and validity of nincds-adrda criteria for alzheimer's disease: the national institute of mental health genetics initiative. *Archives of neurology*, 51(12):1198–1204, 1994.
- [10] Kaj Blennow and Henrik Zetterberg. Biomarkers for alzheimer's disease: current status and prospects for the future. *Journal of internal medicine*, 284(6):643–663, 2018.
- [11] Joan Lindsay, Danielle Laurin, René Verreault, Réjean Hébert, Barbara Helliwell, Gerry B Hill, and Ian McDowell. Risk factors for alzheimer's disease: a

- prospective analysis from the canadian study of health and aging. *American journal of epidemiology*, 156(5):445–453, 2002.
- [12] Louis A Profenno, Anton P Porsteinsson, and Stephen V Faraone. Meta-analysis of alzheimer’s disease risk with obesity, diabetes, and related disorders. *Biological psychiatry*, 67(6):505–512, 2010.
- [13] United Nations Department of Economic and Social Affairs. United nations department of economic and social affairs, population division. world population prospects: The 2019 revision, key findings and advance tables. In *Technical Report*. Working Paper, 2019.
- [14] Laura Fratiglioni and Walter A Rocca. Epidemiology of dementia. *Handbook of neuropsychology*, 6:193–216, 2001.
- [15] Laura Fratiglioni, Diana De Ronchi, and Hedda Agüero-Torres. Worldwide prevalence and incidence of dementia. *Drugs & aging*, 15(5):365–375, 1999.
- [16] Patrick D Meek, E Kristin McKeithan, and Glen T Schumock. Economic considerations in alzheimer’s disease. *Pharmacotherapy: The Journal of Human Pharmacology and Drug Therapy*, 18(2P2):68–73, 1998.
- [17] Anders Wimo, Linus Jonsson, and Bengt Winblad. An estimate of the worldwide prevalence and direct costs of dementia in 2003. *Dementia and geriatric cognitive disorders*, 21(3):175–181, 2006.
- [18] Linda Teri. Behavior and caregiver burden: Behavioral problems in patients with alzheimer disease and its association with caregiver distress. *Alzheimer Disease and Associated Disorders*, 1997.
- [19] Carl A Thompson, Karen Spilbury, Jill Hall, Yvonne Birks, Colin Barnes, and Joy Adamson. Systematic review of information and support interventions for caregivers of people with dementia. *BMC geriatrics*, 7(1):18, 2007.
- [20] Toshifumi Matsui, Martin Ingelsson, Hiroaki Fukumoto, Karunya Ramasamy, Hisatomo Kowa, Matthew P Frosch, Michael C Irizarry, and Bradley T Hyman. Expression of APP pathway mRNAs and proteins in alzheimer’s disease. *Brain research*, 1161:116–123, 2007.
- [21] Christina Priller, Thomas Bauer, Gerda Mitteregger, Bjarne Krebs, Hans A Kretschmar, and Jochen Herms. Synapse formation and function is modulated by the amyloid precursor protein. *Journal of Neuroscience*, 26(27):7212–7221, 2006.
- [22] Bart De Strooper and Wim Annaert. Proteolytic processing and cell biological functions of the amyloid precursor protein. *Journal of cell science*, 113(11):1857–1870, 2000.

- [23] Gopal Thinakaran and Edward H Koo. Amyloid precursor protein trafficking, processing, and function. *Journal of Biological Chemistry*, 283(44):29615–29619, 2008.
- [24] Gerhard Multhaup, Otmar Huber, Luc Buée, and Marie-Christine Galas. Amyloid precursor protein (APP) metabolites APP intracellular fragment (AICD), A β 42, and tau in nuclear roles. *Journal of Biological Chemistry*, 290(39):23515–23522, 2015.
- [25] Xinwei Cao and Thomas C Südhof. Dissection of amyloid- β precursor protein-dependent transcriptional transactivation. *Journal of Biological Chemistry*, 279(23):24601–24611, 2004.
- [26] Robert Vassar, Brian D Bennett, Safura Babu-Khan, Steve Kahn, Elizabeth A Mendiaz, Paul Denis, David B Teplow, Sandra Ross, Patricia Amarante, Richard Loeloff, et al. β -secretase cleavage of alzheimer’s amyloid precursor protein by the transmembrane aspartic protease BACE. *science*, 286(5440):735–741, 1999.
- [27] Peer-Hendrik Kuhn, Huanhuan Wang, Bastian Dislich, Alessio Colombo, Ulrike Zeitschel, Joachim W Ellwart, Elisabeth Kremmer, Steffen Roßner, and Stefan F Lichtenthaler. ADAM10 is the physiologically relevant, constitutive α -secretase of the amyloid precursor protein in primary neurons. *The EMBO journal*, 29(17):3020–3032, 2010.
- [28] Janelle Nunan and David H Small. Regulation of APP cleavage by α -, β - and γ -secretases. *FEBS letters*, 483(1):6–10, 2000.
- [29] Omar MA El-Agnaf, Devinder S Mahil, Bhroma P Patel, and Brian M Austen. Oligomerization and toxicity of β -amyloid-42 implicated in alzheimer’s disease. *Biochemical and biophysical research communications*, 273(3):1003–1007, 2000.
- [30] Martin Citron, Thekla S Diehl, Grace Gordon, Anja Leona Biere, Peter Seubert, and Dennis J Selkoe. Evidence that the 42- and 40-amino acid forms of amyloid β protein are generated from the β -amyloid precursor protein by different protease activities. *Proceedings of the National Academy of Sciences*, 93(23):13170–13175, 1996.
- [31] Jens Wiltfang, Hermann Esselmann, Mirko Bibl, Michael Hüll, Harald Hampel, Holger Kessler, Lutz Frölich, Johannes Schröder, Oliver Peters, Frank Jessen, et al. Amyloid β peptide ratio 42/40 but not A β 42 correlates with phospho-tau in patients with low- and high-CSF A β 40 load. *Journal of neurochemistry*, 101(4):1053–1059, 2007.
- [32] Matthias Schmidt, Carsten Sachse, Walter Richter, Chen Xu, Marcus Fändrich, and Nikolaus Grigorieff. Comparison of alzheimer A β (1–40) and A β (1–42) amyloid fibrils reveals similar protofilament structures. *Proceedings of the National Academy of Sciences*, 106(47):19813–19818, 2009.

- [33] Elżbieta Kojro and Falk Fahrenholz. The non-amyloidogenic pathway: structure and function of α -secretases. In *Alzheimer's disease*, pages 105–127. Springer, 2005.
- [34] Fabienne Dulin, Frédéric Léveillé, Javier Becerril Ortega, Jean-Paul Mornon, Alain Buisson, Isabelle Callebaut, and Nathalie Colloc'h. p3 peptide, a truncated form of $A\beta$ devoid of synaptotoxic effect, does not assemble into soluble oligomers. *FEBS letters*, 582(13):1865–1870, 2008.
- [35] Max C Richter, Susann Ludewig, Alex Winschel, Tobias Abel, Charlotte Bold, Leonie R Salzburger, Susanne Klein, Kang Han, Sascha W Weyer, Ann-Kristina Fritz, et al. Distinct in vivo roles of secreted APP ectodomain variants APPs α and APPs β in regulation of spine density, synaptic plasticity, and cognition. *The EMBO journal*, 37(11), 2018.
- [36] Yuehua Gao and Sanjay W Pimplikar. The γ -secretase-cleaved c-terminal fragment of amyloid precursor protein mediates signaling to the nucleus. *Proceedings of the National Academy of Sciences*, 98(26):14979–14984, 2001.
- [37] W Taylor Kimberly, Matthew J LaVoie, Beth L Ostaszewski, Wenjuan Ye, Michael S Wolfe, and Dennis J Selkoe. γ -secretase is a membrane protein complex comprised of presenilin, nicastrin, aph-1, and pen-2. *Proceedings of the National Academy of Sciences*, 100(11):6382–6387, 2003.
- [38] Kwangwook Ahn, Christopher C Shelton, Yuan Tian, Xulun Zhang, M Lane Gilchrist, Sangram S Sisodia, and Yue-Ming Li. Activation and intrinsic γ -secretase activity of presenilin 1. *Proceedings of the National Academy of Sciences*, 107(50):21435–21440, 2010.
- [39] Christiane Reitz, Carol Brayne, and Richard Mayeux. Epidemiology of alzheimer disease. *Nature Reviews Neurology*, 7(3):137, 2011.
- [40] Karen Duff, Chris Eckman, Cindy Zehr, Xin Yu, Cristian-Mihail Prada, Jordi Perez-Tur, Mike Hutton, Luc Buee, Yasuo Harigaya, Debra Yager, et al. Increased amyloid- β 42 (43) in brains of mice expressing mutant presenilin 1. *Nature*, 383(6602):710–713, 1996.
- [41] Michael A Castello, John David Jeppson, and Salvador Soriano. Moving beyond anti-amyloid therapy for the prevention and treatment of alzheimer's disease. *BMC neurology*, 14(1):169, 2014.
- [42] Haythum O Tayeb, Evan D Murray, Bruce H Price, and Frank I Tarazi. Bapineuzumab and solanezumab for alzheimer's disease: is the 'amyloid cascade hypothesis' still alive? *Expert opinion on biological therapy*, 13(7):1075–1084, 2013.
- [43] OpenStax. Anatomy and physiology, 2016.

- [44] C Bancher, C Brunner, H Lassmann, H Budka, K Jellinger, G Wiche, F Seitelberger, I Grundke-Iqbal, K Iqbal, and HM Wisniewski. Accumulation of abnormally phosphorylated τ precedes the formation of neurofibrillary tangles in alzheimer's disease. *Brain research*, 477(1-2):90–99, 1989.
- [45] M Goedert, MG Spillantini, R Jakes, D Rutherford, and RA Crowther. Multiple isoforms of human microtubule-associated protein tau: sequences and localization in neurofibrillary tangles of alzheimer's disease. *Neuron*, 3(4):519–526, 1989.
- [46] Mark M Black, Theresa Slaughter, Simon Moshich, Maria Obrocka, and Itzhak Fischer. Tau is enriched on dynamic microtubules in the distal region of growing axons. *Journal of Neuroscience*, 16(11):3601–3619, 1996.
- [47] E-M Mandelkow, J Biernat, G Drewes, N Gustke, B Trinczek, and E Mandelkow. Tau domains, phosphorylation, and interactions with microtubules. *Neurobiology of aging*, 16(3):355–362, 1995.
- [48] Michel Goedert, MG Spillantini, NJ Cairns, and RA Crowther. Tau proteins of alzheimer paired helical filaments: abnormal phosphorylation of all six brain isoforms. *Neuron*, 8(1):159–168, 1992.
- [49] Alejandra del C Alonso, Inge Grundke-Iqbal, Héctor S Barra, and Khalid Iqbal. Abnormal phosphorylation of tau and the mechanism of alzheimer neurofibrillary degeneration: sequestration of microtubule-associated proteins 1 and 2 and the disassembly of microtubules by the abnormal tau. *Proceedings of the National Academy of Sciences*, 94(1):298–303, 1997.
- [50] Don W Cleveland, Shu-Ying Hwo, and Marc W Kirschner. Physical and chemical properties of purified tau factor and the role of tau in microtubule assembly. *Journal of molecular biology*, 116(2):227–247, 1977.
- [51] Bess Frost, Rachel L Jacks, and Marc I Diamond. Propagation of tau misfolding from the outside to the inside of a cell. *Journal of Biological Chemistry*, 284(19):12845–12852, 2009.
- [52] Alejandra del C Alonso, Ben Li, Inge Grundke-Iqbal, and Khalid Iqbal. Mechanism of tau-induced neurodegeneration in alzheimer disease and related tauopathies. *Current Alzheimer Research*, 5(4):375–384, 2008.
- [53] Nichole E LaPointe, Gerardo Morfini, Gustavo Pigino, Irina N Gaisina, Alan P Kozikowski, Lester I Binder, and Scott T Brady. The amino terminus of tau inhibits kinesin-dependent axonal transport: implications for filament toxicity. *Journal of neuroscience research*, 87(2):440–451, 2009.
- [54] Koichi Iijima, Anthony Gatt, and Kanae Iijima-Ando. Tau ser262 phosphorylation is critical for $A\beta$ 42-induced tau toxicity in a transgenic drosophila model of alzheimer's disease. *Human molecular genetics*, 19(15):2947–2957, 2010.

- [55] Ian G McKeith, Bradley F Boeve, Dennis W Dickson, Glenda Halliday, John-Paul Taylor, Daniel Weintraub, Dag Aarsland, James Galvin, Johannes Attems, Clive G Ballard, et al. Diagnosis and management of dementia with lewy bodies: Fourth consensus report of the DLB consortium. *Neurology*, 89(1):88–100, 2017.
- [56] Ursula Hohl, Pietro Tiraboschi, Lawrence A Hansen, Leon J Thal, and Jody Corey-Bloom. Diagnostic accuracy of dementia with lewy bodies. *Archives of Neurology*, 57(3):347–351, 2000.
- [57] Maria Grazia Spillantini, Marie Luise Schmidt, Virginia M-Y Lee, John Q Trojanowski, Ross Jakes, and Michel Goedert. α -synuclein in lewy bodies. *Nature*, 388(6645):839–840, 1997.
- [58] Paul H Weinreb, Weiguo Zhen, Anna W Poon, Kelly A Conway, and Peter T Lansbury. NACP, a protein implicated in alzheimer’s disease and learning, is natively unfolded. *Biochemistry*, 35(43):13709–13715, 1996.
- [59] Doris L Fortin, Venu M Nemani, Susan M Voglmaier, Malcolm D Anthony, Timothy A Ryan, and Robert H Edwards. Neural activity controls the synaptic accumulation of α -synuclein. *Journal of Neuroscience*, 25(47):10913–10921, 2005.
- [60] Antony A Cooper, Aaron D Gitler, Anil Cashikar, Cole M Haynes, Kathryn J Hill, Bhupinder Bhullar, Kangning Liu, Kexiang Xu, Katherine E Strathearn, Fang Liu, et al. α -synuclein blocks er-golgi traffic and rab1 rescues neuron loss in parkinson’s models. *Science*, 313(5785):324–328, 2006.
- [61] Jobin Varkey and Ralf Langen. Membrane remodeling by amyloidogenic and non-amyloidogenic proteins studied by EPR. *Journal of Magnetic Resonance*, 280:127–139, 2017.
- [62] Ulf Dettmer, Andrew J Newman, Eric S Luth, Tim Bartels, and Dennis Selkoe. In vivo cross-linking reveals principally oligomeric forms of α -synuclein and β -synuclein in neurons and non-neural cells. *Journal of Biological Chemistry*, 288(9):6371–6385, 2013.
- [63] Poul Henning Jensen, Henrik Hager, Morten S Nielsen, Peter Højrup, Jørgen Gliemann, and Ross Jakes. α -synuclein binds to tau and stimulates the protein kinase a-catalyzed tau phosphorylation of serine residues 262 and 356. *Journal of Biological Chemistry*, 274(36):25481–25489, 1999.
- [64] Benoit I Giasson, Virginia MY Lee, and John Q Trojanowski. Interactions of amyloidogenic proteins. *Neuromolecular medicine*, 4(1-2):49–58, 2003.
- [65] PG Galloway, P Mulvihill, and G Perry. Filaments of lewy bodies contain insoluble cytoskeletal elements. *The American journal of pathology*, 140(4):809, 1992.

- [66] Kenjiro Ono, Ryoichi Takahashi, Tokuhei Ikeda, and Masahito Yamada. Cross-seeding effects of amyloid β -protein and α -synuclein. *Journal of neurochemistry*, 122(5):883–890, 2012.
- [67] Shlomo Eisenberg and Robert I Levy. Lipoprotein metabolism. In *Advances in lipid research*, volume 13, pages 1–89. Elsevier, 1975.
- [68] Josep Ribalta, Joan-Carles Vallve, Josefa Girona, and Lluís Masana. Apolipoprotein and apolipoprotein receptor genes, blood lipids and disease. *Current Opinion in Clinical Nutrition & Metabolic Care*, 6(2):177–187, 2003.
- [69] Karl H Weisgraber. Apolipoprotein E: structure-function relationships. In *Advances in protein chemistry*, volume 45, pages 249–302. Elsevier, 1994.
- [70] Jean Davignon, Richard E Gregg, and Charles F Sing. Apolipoprotein e polymorphism and atherosclerosis. *Arteriosclerosis: An Official Journal of the American Heart Association, Inc.*, 8(1):1–21, 1988.
- [71] Jungsu Kim, Jacob M Basak, and David M Holtzman. The role of apolipoprotein e in alzheimer’s disease. *Neuron*, 63(3):287–303, 2009.
- [72] Paul S Hauser and Robert O Ryan. Impact of apolipoprotein e on alzheimer’s disease. *Current Alzheimer Research*, 10(8):809–817, 2013.
- [73] Miia Kivipelto, Eeva-Liisa Helkala, Mikko P Laakso, Tuomo Hänninen, Merja Hallikainen, Kari Alhainen, Susan Iivonen, Arto Mannermaa, Jaakko Tuomilehto, Aulikki Nissinen, et al. Apolipoprotein e4 allele, elevated midlife total cholesterol level, and high midlife systolic blood pressure are independent risk factors for late-life alzheimer disease. *Annals of internal medicine*, 137(3):149–155, 2002.
- [74] Qingguang Jiang, CY Daniel Lee, Shweta Mandrekar, Brandy Wilkinson, Paige Cramer, Noam Zelcer, Karen Mann, Bruce Lamb, Timothy M Willson, Jon L Collins, et al. Apoe promotes the proteolytic degradation of A β . *Neuron*, 58(5):681–693, 2008.
- [75] Heidi M McBride, Margaret Neuspiel, and Sylwia Wasiak. Mitochondria: more than just a powerhouse. *Current biology*, 16(14):R551–R560, 2006.
- [76] Saverio Marchi, Carlotta Giorgi, Jan M Suski, Chiara Agnoletto, Angela Bononi, Massimo Bonora, Elena De Marchi, Sonia Missiroli, Simone Patergnani, Federica Poletti, et al. Mitochondria-ROS crosstalk in the control of cell death and aging. *Journal of signal transduction*, 2012, 2012.
- [77] Alicia J Kowaltowski and Anibal E Vercesi. Mitochondrial damage induced by conditions of oxidative stress. *Free Radical Biology and Medicine*, 26(3-4):463–471, 1999.

- [78] Daniel Garcia and Reuben J Shaw. AMPK: mechanisms of cellular energy sensing and restoration of metabolic balance. *Molecular cell*, 66(6):789–800, 2017.
- [79] Rajnish K Chaturvedi and M Flint Beal. Mitochondrial diseases of the brain. *Free Radical Biology and Medicine*, 63:1–29, 2013.
- [80] Patrizia Mecocci, Usha MacGarvey, and M Flint Beal. Oxidative damage to mitochondrial DNA is increased in alzheimer’s disease. *Annals of Neurology: Official Journal of the American Neurological Association and the Child Neurology Society*, 36(5):747–751, 1994.
- [81] Akihiko Nunomura, George Perry, Gjurmakch Aliev, Keisuke Hirai, Atsushi Takeda, Elizabeth K Balraj, Paul K Jones, Hossein Ghanbari, Takafumi Wataya, Shun Shimohama, et al. Oxidative damage is the earliest event in alzheimer disease. *Journal of Neuropathology & Experimental Neurology*, 60(8):759–767, 2001.
- [82] Yan Zhao and Baolu Zhao. Oxidative stress and the pathogenesis of alzheimer’s disease. *Oxidative medicine and cellular longevity*, 2013, 2013.
- [83] Russell H Swerdlow and Shaharyar M Khan. A “mitochondrial cascade hypothesis” for sporadic alzheimer’s disease. *Medical hypotheses*, 63(1):8–20, 2004.
- [84] Yun-An Lim, Virginie Rhein, Ginette Baysang, Fides Meier, Anne Poljak, Mark J. Raftery, Michael Guilhaus, Lars M Ittner, Anne Eckert, and Jürgen Götz. A β and human amylin share a common toxicity pathway via mitochondrial dysfunction. *Proteomics*, 10(8):1621–1633, 2010.
- [85] Hsiuchen Chen and David C Chan. Mitochondrial dynamics—fusion, fission, movement, and mitophagy—in neurodegenerative diseases. *Human molecular genetics*, 18(R2):R169–R176, 2009.
- [86] Dalibor Mijaljica, Mark Prescott, and Rodney J Devenish. Mitophagy and mitoptosis in disease processes. In *Protein Misfolding and Cellular Stress in Disease and Aging*, pages 93–106. Springer, 2010.
- [87] John J Lemasters, Anna-Liisa Nieminen, Ting Qian, Lawrence C Trost, Steven P Elmore, Yoshiya Nishimura, Ruth A Crowe, Wayne E Cascio, Cynthia A Bradham, David A Brenner, et al. The mitochondrial permeability transition in cell death: a common mechanism in necrosis, apoptosis and autophagy. *Biochimica et biophysica acta (BBA)-bioenergetics*, 1366(1-2):177–196, 1998.
- [88] John J Lemasters, Ting Qian, Lihua He, Jae-Sung Kim, Steven P Elmore, Wayne E Cascio, and David A Brenner. Role of mitochondrial inner membrane permeabilization in necrotic cell death, apoptosis, and autophagy. *Antioxidants and Redox Signaling*, 4(5):769–781, 2002.

- [89] Mi-Hyang Cho, Kwangmin Cho, Hoe-Jin Kang, Eun-Young Jeon, Hun-Sik Kim, Hyung-Joon Kwon, Hong-Mi Kim, Dong-Hou Kim, and Seung-Yong Yoon. Autophagy in microglia degrades extracellular β -amyloid fibrils and regulates the NLRP3 inflammasome. *Autophagy*, 10(10):1761–1775, 2014.
- [90] Jorge Moscat and Maria T Diaz-Meco. p62 at the crossroads of autophagy, apoptosis, and cancer. *Cell*, 137(6):1001–1004, 2009.
- [91] Wiem Chaabane, Sirma D User, Mohamed El-Gazzah, Roman Jaksik, Elaheh Sajjadi, Joanna Rzeszowska-Wolny, and Marek J Los. Autophagy, apoptosis, mitoptosis and necrosis: interdependence between those pathways and effects on cancer. *Archivum immunologiae et therapias experimentalis*, 61(1):43–58, 2013.
- [92] Vassiliki Nikolettou, Maria Markaki, Konstantinos Palikaras, and Nektarios Tavernarakis. Crosstalk between apoptosis, necrosis and autophagy. *Biochimica et Biophysica Acta (BBA)-Molecular Cell Research*, 1833(12):3448–3459, 2013.
- [93] Trent Fowler, Ranjan Sen, and Ananda L Roy. Regulation of primary response genes. *Molecular cell*, 44(3):348–360, 2011.
- [94] Megan A Maxwell and George EO Muscat. The nr4a subgroup: immediate early response genes with pleiotropic physiological roles. *Nuclear receptor signaling*, 4(1):nrs-04002, 2006.
- [95] M Dragunow. A role for immediate-early transcription factors in learning and memory. *Behavior genetics*, 26(3):293–299, 1996.
- [96] Niels Plath, Ora Ohana, Björn Dammermann, Mick L Errington, Dietmar Schmitz, Christina Gross, Xiaosong Mao, Arne Engelsberg, Claudia Mahlke, Hans Welzl, et al. Arc/arg3.1 is essential for the consolidation of synaptic plasticity and memories. *Neuron*, 52(3):437–444, 2006.
- [97] Shahram Bahrami and Finn Drabløs. Gene regulation in the immediate-early response process. *Advances in biological regulation*, 62:37–49, 2016.
- [98] Amanda O’Donnell, Zaneta Odrowaz, and Andrew D Sharrocks. Immediate-early gene activation by the mapk pathways: what do and don’t we know?, 2012.
- [99] JY Kim and M Yenari. Heat shock proteins and the stress response. In *Primer on Cerebrovascular Diseases*, pages 273–275. Elsevier, 2017.
- [100] Xu Zheng, Joanna Krakowiak, Nikit Patel, Ali Beyzavi, Jidefor Ezike, Ahmad S Khalil, and David Pincus. Dynamic control of Hsf1 during heat shock by a chaperone switch and phosphorylation. *elife*, 5:e18638, 2016.

- [101] Ruben Baler, Gerhard Dahl, and Richard Voellmy. Activation of human heat shock genes is accompanied by oligomerization, modification, and rapid translocation of heat shock transcription factor HSF1. *Molecular and cellular biology*, 13(4):2486–2496, 1993.
- [102] Michael E Greenberg and Edward B Ziff. Stimulation of 3t3 cells induces transcription of the c-fos proto-oncogene. *Nature*, 311(5985):433–438, 1984.
- [103] Ram Madabhushi, Fan Gao, Andreas R Pfenning, Ling Pan, Satoko Yamakawa, Jinsoo Seo, Richard Rueda, Trongha X Phan, Hidekuni Yamakawa, Ping-Chieh Pao, et al. Activity-induced DNA breaks govern the expression of neuronal early-response genes. *Cell*, 161(7):1592–1605, 2015.
- [104] NM Derks, M Müller, B Gaszner, DTWM Tilburg-Ouwens, EW Roubos, and LT Kozicz. Housekeeping genes revisited: different expressions depending on gender, brain area and stressor. *Neuroscience*, 156(2):305–309, 2008.
- [105] Marcus J Tindall and Angela Clerk. Modelling negative feedback networks for activating transcription factor 3 predicts a dominant role for miRNAs in immediate early gene regulation. *PLoS computational biology*, 10(5), 2014.
- [106] Roi Avraham, Aldema Sas-Chen, Ohad Manor, Israel Steinfeld, Reut Shalgi, Gabi Tarcic, Noa Bossel, Amit Zeisel, Ido Amit, Yaara Zwang, et al. EGF decreases the abundance of microRNAs that restrain oncogenic transcription factors. *Science signaling*, 3(124):ra43–ra43, 2010.
- [107] Stuart Aitken, Shigeyuki Magi, Ahmad MN Alhendi, Masayoshi Itoh, Hideya Kawaji, Timo Lassmann, Carsten O Daub, Erik Arner, Piero Carninci, Alistair RR Forrest, et al. Transcriptional dynamics reveal critical roles for non-coding RNAs in the immediate-early response. *PLoS computational biology*, 11(4), 2015.
- [108] Kenneth S Kosik. The neuronal microRNA system. *Nature Reviews Neuroscience*, 7(12):911–920, 2006.
- [109] Donald Voet and Judith G Voet. Biochemistry, 4-th edition. *NewYork: John Wiley& SonsInc*, 492, 2011.
- [110] ENCODE Project Consortium et al. The ENCODE (ENCyclopedia of DNA elements) project. *Science*, 306(5696):636–640, 2004.
- [111] Mihaela Pertea. The human transcriptome: an unfinished story. *Genes*, 3(3):344–360, 2012.
- [112] Robert W Holley, Jean Apgar, George A Everett, James T Madison, Mark Marquisee, Susan H Merrill, John Robert Penswick, and Ada Zamir. Structure of a ribonucleic acid. *Science*, pages 1462–1465, 1965.

-
- [113] Norbert Polacek and Alexander S Mankin. The ribosomal peptidyl transferase center: structure, function, evolution, inhibition. *Critical reviews in biochemistry and molecular biology*, 40(5):285–311, 2005.
- [114] B Matija Peterlin, John E Brogie, and David H Price. 7SK snRNA: a noncoding RNA that plays a major role in regulating eukaryotic transcription. *Wiley Interdisciplinary Reviews: RNA*, 3(1):92–103, 2012.
- [115] David Akopian, Kuang Shen, Xin Zhang, and Shu-ou Shan. Signal recognition particle: an essential protein-targeting machine. *Annual review of biochemistry*, 82:693–721, 2013.
- [116] Dominic Schmidt, Petra C Schwalie, Michael D Wilson, Benoit Ballester, Ângela Gonçalves, Claudia Kutter, Gordon D Brown, Aileen Marshall, Paul Flicek, and Duncan T Odom. Waves of retrotransposon expansion remodel genome organization and CTCF binding in multiple mammalian lineages. *Cell*, 148(1-2):335–348, 2012.
- [117] Eric S Lander, Lauren M Linton, Bruce Birren, Chad Nusbaum, Michael C Zody, Jennifer Baldwin, Keri Devon, Ken Dewar, Michael Doyle, William FitzHugh, et al. Initial sequencing and analysis of the human genome. 2001.
- [118] Thomas Wicker, François Sabot, Aurélie Hua-Van, Jeffrey L Bennetzen, Pierre Capy, Boulos Chalhoub, Andrew Flavell, Philippe Leroy, Michele Morgante, Olivier Panaud, et al. A unified classification system for eukaryotic transposable elements. *Nature Reviews Genetics*, 8(12):973–982, 2007.
- [119] Prescott L Deininger and Mark A Batzer. Mammalian retroelements. *Genome research*, 12(10):1455–1465, 2002.
- [120] Astrid Böhne, Frédéric Brunet, Delphine Galiana-Arnoux, Christina Schultheis, and Jean-Nicolas Volff. Transposable elements as drivers of genomic and biological diversity in vertebrates. *Chromosome Research*, 16(1):203–215, 2008.
- [121] Jan Ole Kriegs, Gennady Churakov, Jerzy Jurka, Jürgen Brosius, and Jürgen Schmitz. Evolutionary history of 7SL RNA-derived SINEs in supraprimates. *Trends in Genetics*, 23(4):158–161, 2007.
- [122] C Richard Boland. Non-coding RNA: it’s not junk, 2017.
- [123] Mathew W Wright and Elspeth A Bruford. Naming ‘junk’: human non-protein coding RNA (ncRNA) gene nomenclature. *Human genomics*, 5(2):90, 2011.
- [124] Alexander F Palazzo and Eliza S Lee. Non-coding RNA: what is functional and what is junk? *Frontiers in genetics*, 6:2, 2015.
- [125] Feng-Jie Sun, Sophie Fleurdépine, Cécile Bousquet-Antonelli, Gustavo Caetano-Anollés, and Jean-Marc Deragon. Common evolutionary trends for SINE RNA structures. *TRENDS in Genetics*, 23(1):26–33, 2007.

-
- [126] Wojciech Makalowski. Genomic scrap yard: how genomes utilize all that junk. *Gene*, 259(1-2):61–67, 2000.
- [127] Ling-Ling Chen, Joshua N DeCerbo, and Gordon G Carmichael. Alu element-mediated gene silencing. *The EMBO journal*, 27(12):1694–1705, 2008.
- [128] Chongjian Chen, Takeshi Ara, and Daniel Gautheret. Using alu elements as polyadenylation sites: A case of retroposon exaptation. *Molecular biology and evolution*, 26(2):327–334, 2009.
- [129] Noa Sela, Britta Mersch, Agnes Hotz-Wagenblatt, and Gil Ast. Characteristics of transposable element exonization within human and mouse. *PLoS One*, 5(6), 2010.
- [130] Dimitri A Kramerov and Nikita S Vassetzky. Short retroposons in eukaryotic genomes. *International review of cytology*, 247:165–221, 2005.
- [131] Peter D Mariner, Ryan D Walters, Celso A Espinoza, Linda F Drullinger, Stacey D Wagner, Jennifer F Kugel, and James A Goodrich. Human alu RNA is a modular transacting repressor of mRNA transcription during heat shock. *Molecular cell*, 29(4):499–509, 2008.
- [132] Petro Yakovchuk, James A Goodrich, and Jennifer F Kugel. B2 RNA and alu RNA repress transcription by disrupting contacts between RNA polymerase ii and promoter DNA within assembled complexes. *Proceedings of the National Academy of Sciences*, 106(14):5569–5574, 2009.
- [133] Gary R Daniels and Prescott L Deininger. Repeat sequence families derived from mammalian tRNA genes. *Nature*, 317(6040):819–822, 1985.
- [134] Alfredo J Hernandez, Athanasios Zovoilis, Catherine Cifuentes-Rojas, Lu Han, Bojan Bujisic, and Jeannie T Lee. B2 and ALU retrotransposons are self-cleaving ribozymes whose activity is enhanced by EZH2. *Proceedings of the National Academy of Sciences*, 117(1):415–425, 2020.
- [135] Tzu-Huey Li, Jimmy Spearow, Carol M Rubin, and Carl W Schmid. Physiological stresses increase mouse short interspersed element (sine) RNA expression in vivo. *Gene*, 239(2):367–372, 1999.
- [136] Tiffany A Allen, Sandra Von Kaenel, James A Goodrich, and Jennifer F Kugel. The SINE-encoded mouse B2 RNA represses mRNA transcription in response to heat shock. *Nature structural & molecular biology*, 11(9):816–821, 2004.
- [137] Steven L Ponicsan, Stephane Houel, William M Old, Natalie G Ahn, James A Goodrich, and Jennifer F Kugel. The non-coding B2 RNA binds to the DNA cleft and active-site region of RNA polymerase ii. *Journal of molecular biology*, 425(19):3625–3638, 2013.

- [138] Shahaf Peleg, Farahnaz Sananbenesi, Athanasios Zovoilis, Susanne Burkhardt, Sanaz Bahari-Javan, Roberto Carlos Agis-Balboa, Perla Cota, Jessica Lee Wittnam, Andreas Gogol-Doering, Lennart Opitz, et al. Altered histone acetylation is associated with age-dependent memory impairment in mice. *science*, 328(5979):753–756, 2010.
- [139] Donald E Kuhn, Mickey M Martin, David S Feldman, Alvin V Terry Jr, Gerard J Nuovo, and Terry S Elton. Experimental validation of miRNA targets. *Methods*, 44(1):47–54, 2008.
- [140] Pranidhi Sood, Azra Krek, Mihaela Zavolan, Giuseppe Macino, and Nikolaus Rajewsky. Cell-type-specific signatures of microRNAs on target mRNA expression. *Proceedings of the National Academy of Sciences*, 103(8):2746–2751, 2006.
- [141] Athanasios Zovoilis, Hope Y Agbemenyah, Roberto C Agis-Balboa, Roman M Stilling, Dieter Edbauer, Pooja Rao, Laurent Farinelli, Ivana Delalle, Andrea Schmitt, Peter Falkai, et al. microRNA-34c is a novel target to treat dementias. *The EMBO journal*, 30(20):4299–4308, 2011.
- [142] Munekazu Yamakuchi and Charles J Lowenstein. MiR-34, SIRT1, and p53: the feedback loop. *Cell cycle*, 8(5):712–715, 2009.
- [143] Francisco Navarro and Judy Lieberman. mir-34 and p53: new insights into a complex functional relationship. *PloS one*, 10(7), 2015.
- [144] Athanasios Zovoilis, Catherine Cifuentes-Rojas, Hsueh-Ping Chu, Alfredo J Hernandez, and Jeannie T Lee. Destabilization of B2 RNA by ezh2 activates the stress response. *Cell*, 167(7):1788–1802, 2016.
- [145] Takashi Saito, Yukio Matsuba, Naomi Mihira, Jiro Takano, Per Nilsson, Shigeyoshi Itohara, Nobuhisa Iwata, and Takaomi C Saido. Single app knock-in mouse models of alzheimer’s disease. *Nature neuroscience*, 17(5):661–663, 2014.
- [146] Jogender Mehla, Sean G Lacoursiere, Valerie Lapointe, Bruce L McNaughton, Robert J Sutherland, Robert J McDonald, and Majid H Mohajerani. Age-dependent behavioral and biochemical characterization of single APP knock-in mouse (APPNL-GF/NL-GF) model of alzheimer’s disease. *Neurobiology of aging*, 75:25–37, 2019.
- [147] Johannes Schindelin, Ignacio Arganda-Carreras, Erwin Frise, Verena Kaynig, Mark Longair, Tobias Pietzsch, Stephan Preibisch, Curtis Rueden, Stephan Saalfeld, Benjamin Schmid, et al. Fiji: an open-source platform for biological-image analysis. *Nature methods*, 9(7):676–682, 2012.
- [148] Daniel Daugherty, Joshua Goldberg, Wolfgang Fischer, Richard Dargusch, Pamela Maher, and David Schubert. A novel alzheimer’s disease drug candidate targeting inflammation and fatty acid metabolism. *Alzheimer’s research & therapy*, 9(1):50, 2017.

-
- [149] Brad T Sherman, Richard A Lempicki, et al. Systematic and integrative analysis of large gene lists using DAVID bioinformatics resources. *Nature protocols*, 4(1):44, 2009.
- [150] Huaiyu Mi, Anushya Muruganujan, Xiaosong Huang, Dustin Ebert, Caitlin Mills, Xinyu Guo, and Paul D Thomas. Protocol update for large-scale genome and gene function analysis with the PANTHER classification system (v. 14.0). *Nature protocols*, 14(3):703–721, 2019.
- [151] Minoru Kanehisa and Susumu Goto. KEGG: kyoto encyclopedia of genes and genomes. *Nucleic acids research*, 28(1):27–30, 2000.
- [152] Heng Li and Richard Durbin. Fast and accurate short read alignment with burrows–wheeler transform. *bioinformatics*, 25(14):1754–1760, 2009.
- [153] Daehwan Kim, Joseph M Paggi, Chanhee Park, Christopher Bennett, and Steven L Salzberg. Graph-based genome alignment and genotyping with HISAT2 and HISAT-genotype. *Nature biotechnology*, 37(8):907–915, 2019.
- [154] Heng Li, Bob Handsaker, Alec Wysoker, Tim Fennell, Jue Ruan, Nils Homer, Gabor Marth, Goncalo Abecasis, and Richard Durbin. The sequence alignment/map format and SAMtools. *Bioinformatics*, 25(16):2078–2079, 2009.
- [155] Aaron R Quinlan and Ira M Hall. BEDTools: a flexible suite of utilities for comparing genomic features. *Bioinformatics*, 26(6):841–842, 2010.
- [156] Marcel Martin. Cutadapt removes adapter sequences from high-throughput sequencing reads. *EMBnet. journal*, 17(1):10–12, 2011.
- [157] Simon Anders and Wolfgang Huber. Differential expression analysis for sequence count data. *Nature Precedings*, pages 1–1, 2010.
- [158] Mihaela Pertea, Geo M Pertea, Corina M Antonescu, Tsung-Cheng Chang, Joshua T Mendell, and Steven L Salzberg. Stringtie enables improved reconstruction of a transcriptome from RNA-seq reads. *Nature biotechnology*, 33(3):290, 2015.
- [159] Pauli Virtanen, Ralf Gommers, Travis E. Oliphant, Matt Haberland, Tyler Reddy, David Cournapeau, Evgeni Burovski, Pearu Peterson, Warren Weckesser, Jonathan Bright, Stéfan J. van der Walt, Matthew Brett, Joshua Wilson, K. Jarrod Millman, Nikolay Mayorov, Andrew R. J. Nelson, Eric Jones, Robert Kern, Eric Larson, CJ Carey, İlhan Polat, Yu Feng, Eric W. Moore, Jake VanderPlas, Denis Laxalde, Josef Perktold, Robert Cimrman, Ian Henriksen, E. A. Quintero, Charles R Harris, Anne M. Archibald, Antônio H. Ribeiro, Fabian Pedregosa, Paul van Mulbregt, and SciPy 1.0 Contributors. SciPy 1.0: Fundamental Algorithms for Scientific Computing in Python. *Nature Methods*, 2020.

- [160] Celso A Espinoza, Tiffany A Allen, Aaron R Hieb, Jennifer F Kugel, and James A Goodrich. B2 RNA binds directly to RNA polymerase ii to repress transcript synthesis. *Nature structural & molecular biology*, 11(9):822–829, 2004.
- [161] James K Ruffle. Molecular neurobiology of addiction: what’s all the (δ) fosb about? *The American journal of drug and alcohol abuse*, 40(6):428–437, 2014.
- [162] Dietmar Kùltz. Molecular and evolutionary basis of the cellular stress response. *Annu. Rev. Physiol.*, 67:225–257, 2005.
- [163] Markus Arnoldini, Rafal Mostowy, Sebastian Bonhoeffer, and Martin Ackermann. Evolution of stress response in the face of unreliable environmental signals. *PLoS computational biology*, 8(8), 2012.

Appendix A

Reagents

Cell culture methods are provided in Section 2.2.1.

Table A.1: Forward primer sequences used in this study for qPCR.

Transcript	Forward (5'-3')
Fosb-201	AGGAACCAGCTACTCAACCC
Jak2-202	GGTGTCTGTGTCTGTGGAGA
Mapk10-201	CTCAGCAGACCCTTCCAGAA
Osmr-201	TTTCGTCACTCCGTACACCA
Trp53-206	AAACGCTTCGAGATGTTCCG
Ptk2-201	TTCAGCCCCAGGAAATCAGC
Rgma-201	GGTCGCTACTGAGTCCGCT
Sgk1-204	AGAATGAGGGGAATGGTAGCG
Egr1-201	ACCACAGAGTCCTTTTCTGACA
Med1-203	CGTGAAAGGTTTTCTGCGGG
Hsf1-201	GGATACCCCTTTGTCCCCAA

Table A.2: Reverse primer sequences used in this study for qPCR.

Transcript	Reverse (5'-3')
Fosb-201	AAGTCGATCTGTCAGCTCCC
Jak2-202	CCCCGTTCTCCTGTCTTCTT
Mapk10-201	GCGTCCATCAGTTCCATCAC
Osmr-201	GCTGCTCTTGTACGGATTGG
Trp53-206	GTAGACTGGCCCTTCTTGGT
Ptk2-201	CAGGCCAACTTCCTTCACCA
Rgma-201	GTTACCACTAGCCTCTCCCTTG
Sgk1-204	TTGAGAGGGACTTGGCGGA
Egr1-201	TGAAAAGGGGTTTCAGGCCAC
Med1-203	TCTTCTCCATTACTIONGACGCACA
Hsf1-201	TGGCATCCAGGTGATCACTT

Table A.3: Locked nucleic acid sequences used in cell culture experiments.

Gene	Sequence (5'-3')
Anti-B2	GTTACGGATGGTTGTG
Anti-Hsf1	CGAAGGATGGAGTCAA
Scramble Control	CCTCAATTTTATCAC

Table A.4: Protein sequences of $A\beta$ fragments.

Protein	Sequence
$A\beta_{1-42}$	DAEFRHDSGYEVHHQKLVFFAEDVGSNKGAIIGLMVGGVVIA
$A\beta_{1-40}$	DAEFRHDSGYEVHHQKLVFFAEDVGSNKGAIIGLMVGGVV
$A\beta_{\text{rev}}$	AIVVGGVMLGIIAGKNSGVDEAFFVLKQHHVEYGSDFRFEAD

Table A.5: Nucleic acid reagents for in vitro transcription of B2 RNA.

Reagent	Sequence
T7 Forward	TAATACGACTCACTATAG
B2 Reverse	TTTTTTTTTAAAGATTTATTTATTTATTATATGTAAG TACA
B2 Template	GGGGCTGAGATGGCTCAGTGGGTAAGAGCACCCGAC TGCTCTTCCGAAGGTCCGAGTTCAAATCCCAGCAAC CACATGGTGGCTCACAACCATCCGTAACGAGATCTGA CTCCCTCTTCTGGAGTGTCTGAAGACAGCTACAGTGT ACTTACATATAATAAATAAATAAATCTTTAAAAAAAAA A

Appendix B

Gene Lists

B.1 Pre-Heatshock Genes

Pre-Heatshock Genes are from work previously published in Cell by Zovoilis et al. These genes are regulated by B2 RNA and are released in the event of heat-shock.

0610040F04Rik, 1110002E22Rik, 1110012J17Rik, 1110019D14Rik, 1110020G09Rik, 1110032F04Rik, 1110038D17Rik, 1500009C09Rik, 1500017E21Rik, 1700001F09Rik, 1700007B14Rik, 1700007G11Rik, 1700008F21Rik, 1700011L22Rik, 1700013N06Rik, 1700019A02Rik, 1700024B05Rik, 1700025F22Rik, 1700025G04Rik, 1700030G06Rik, 1700034O15Rik, 1700040L02Rik, 1700049E17Rik2, 1700057H15Rik, 1700060C16Rik, 1700082M22Rik, 1700106N22Rik, 1700112E06Rik, 1700113H08Rik, 1700128F08Rik, 1810048J11Rik, 2010001E11Rik, 2010002M12Rik, 2010012P19Rik, 2210408F21Rik, 2210408I21Rik, 2310002L09Rik, 2310035C23Rik, 2310057J18Rik, 2410089E03Rik, 2610034B18Rik, 2610034M16Rik, 2610035D17Rik, 2610037D02Rik, 2610203C22Rik, 2610305D13Rik, 2610316D01Rik, 2810008M24Rik, 2810046L04Rik, 2900079G21Rik, 2900092C05Rik, 3110007F17Rik, 3110047P20Rik, 3110082D06Rik, 4632419I22Rik, 4833424O15Rik, 4921539E11Rik, 4930433N12Rik, 4930440I19Rik, 4930456L15Rik, 4930457A20Rik, 4930467K11Rik, 4930469K13Rik, 4930471C06Rik, 4930471M23Rik, 4930473A06Rik, 4930485B16Rik, 4930506M07Rik, 4930522L14Rik, 4930524B15Rik, 4930529M08Rik, 4930552P12Rik, 4930554G24Rik, 4930554H23Rik, 4930558K02Rik, 4931408C20Rik, 4931428L18Rik, 4932438A13Rik, 4932441J04Rik, 4933405D12Rik, 4933411K20Rik, 5033411D12Rik, 5033414D02Rik, 5730419I09Rik, 5730522E02Rik, 7SK, 8030451A03Rik, 9030224M15Rik, 9130014G24Rik, 9130019P16Rik, 9130401M01Rik, 9230106D20Rik, 9230107M04Rik, 9330158H04Rik, 9330182L06Rik, 9430031J16Rik, 9430076C15Rik, 9530026P05Rik, 9530036O11Rik, 9930013L23Rik, 9930014A18Rik, A1cf, A230004M16Rik, A330008L17Rik, A330021E22Rik, A430010J10Rik, A430107O13Rik, A730037C10Rik, A830018L16Rik, A930011G23Rik, A930038C07Rik, AC110374.1, AC115121.2, AC122210.1, AC122448.1, AC124807.1, AC133509.1, AC134552.1, AC157822.1, AC166252.2, AC188608.1, AI314180, AI838599, AL833773.1, AW554918, AY512915, Abca12, Abca13, Abca16, Abca3, Abca4, Abca6, Abca7, Abca8b, Abcb1a, Abcb8, Abcc12, Abcc2, Abcc5, Abcc8, Abcd2, Abcg1, Abcg2, Abhd16a, Ablim2, Abtb1, Accn1, Ace3, Acn9, Acnat2, Acss3, Acvrl1, Adad1, Adam26a, Adam34, Adamts12, Adamts20, Adamts3, Adamts6, Adamts9, Adamtsl1, Adarb1, Adarb2, Adcy8, Adcyap1, Adcyap1r1, Add3, Adk, Adrbk2, Agbl1, Agbl3, Agbl4, Agmo, Agpat1, Agpat3, Ahi1, Ahr, Aig1, Aim2, Ak5, Akap6, Akap9, Alb, Aldh1a7, Alg6, Alk,

Alox5, Als2cr12, Alx1, Amy1, Angpt1, Ank1, Ank2, Ankrd22, Ankrd36, Anks1b, Ano10, Ano2, Ano4, Antxr2, Anubl1, Anxa13, Aoah, Aox1, Apaf1, Apba2, Aplf, Apoh, Apol10b, Apol11a, Arap2, Argef1, Arfip1, Arhgap18, Arhgap26, Arhgap27, Arhgap28, Arhgap29, Arhgap39, Arhgef10, Arhgef5, Arid1b, Arid2, Arid3a, Arid5b, Arl4a, Armc2, Arnt2, Arntl, Arpm1, Arsj, Arvcf, Asap1, Asb15, Asb3, Asb5, Ascc3, Astn2, Astx4a, Astx4d, Astx6, Asxl3, Asz1, Atad2b, Atg7, Atp10b, Atp11c, Atp13a5, Atp2b1, Atp2b2, Atp6v1b1, Atrn1, Atxn11, Atxn711, B230104C08Rik, B3gat2, B930007M17Rik, BB287469, BC005561, BC017158, BC021891, BC024659, BC042782, BC057079, BC067068, Bai1, Bai2, Bai3, Baiap2l2, Bank1, Basp1, Bbs7, Bcas3, Bckdha, Bcl11a, Bclaf1, Best3, Bet3l, Bicc1, Bicc1, Birc5, Blnk, Bmpr1b, Bnc1, Bnc2, Brd1, Brd2, Brd4, Brpf3, Bst2, Btbd11, Btbd9, Btrc, Bves, C030046E11Rik, C030047K22Rik, C130026I21Rik, C130060K24Rik, C1qtnf3, C1qtnf7, C1s, C230029F24Rik, C6, C7, C8a, C9, CN725425, Cabin1, Cacna1c, Cacna1e, Cacna1g, Cacna2d1, Cacna2d4, Caeng2, Caeng5, Cadps2, Calcr, Caln1, Camk2b, Capsl, Car10, Carf, Casd1, Casp12, Catsperb, Cbara1, Cbln1, Ccdc109a, Ccdc110, Ccdc129, Ccdc132, Ccdc152, Ccdc34, Ccdc46, Ccdc50, Ccdc60, Ccdc79, Ccdc80, Ccdc86, Ccdc91, Cd1d1, Cd200r2, Cd36, Cd46, Cdc14a, Cdc40, Cdep1, Cdh10, Cdh11, Cdh12, Cdh13, Cdh18, Cdh20, Cdh23, Cdh4, Cdh6, Cdh8, Cdh9, Cdk14, Cdk17, Cdk5rap2, Cdk8, Cdyl2, Celsr1, Celsr2, Cenpo, Cenpt, Cenpw, Cep290, Ces1g, Cfhr3, Cftr, Cgn, Chchd3, Chchd6, Chi3l3, Chl1, Chn1, Chn2, Chrm2, Chst11, Chst9, Cilp2, Clca3, Clca5, Clcn7, Cldn22, Clec16a, Clec1a, Clec4a2, Clec4a4, Clec4b1, Clec4b2, Clec4d, Clec4e, Clec4n, Clip4, Clnk, Clvs2, Cmc1, Cnksr3, Cnot2, Cnot6, Cnot6l, Cntln, Cntn1, Cntn3, Cntn4, Cntn5, Cntn6, Cntnap2, Cntnap3, Cntnap4, Cntnap5a, Cntnap5b, Cntnap5c, Col11a1, Col14a1, Col19a1, Col22a1, Col23a1, Col24a1, Col28a1, Col2a1, Col6a1, Colec10, Cope, Copg2, Cops5, Corin, Cox7b2, Cpa1, Cpa5, Cpa6, Cpeb1, Cpeb3, Cpne8, Cpsf3l, Cpvl, Cpxcr1, Crim1, Cript, Crisp3, Crispld1, Crls1, Cry1, Csf2rb2, Csgalnact1, Csmd1, Csmd2, Csmd3, Csn1s1, Csnk2a2, Cthrc1, Ctif, Ctnna2, Ctnna3, Ctnnd2, Ctps2, Cttncp2, Cxcl13, Cxcl15, Cyp2b10, Cyp2b9, Cyp2c29, Cyp2c37, Cyp2c38, Cyp2c39, Cyp2c40, Cyp2c55, Cyp2c66, Cyp2c67, Cyp2c68, Cyp2c69, Cyp2d12, Cyp2j11, Cyp2j12, Cyp2j13, Cyp2j5, Cyp2j6, Cyp2j8, Cyp4a10, Cyp4a12a, Cyp4a12b, Cyp4a14, Cyp4a31, Cyp4a32, Cyp4f15, Cyp4f16, Cyp4f40, Cyth4, D10Bwg1379e, D15Erttd621e, D19Erttd386e, D5Erttd577e, D630013G24Rik, D630037F22Rik, D6Erttd527e, D830044D21Rik, Dab1, Dab2, Dagla, Dao, Dapl1, Dbc1, Dbx2, Dcaf6, Dcaf7, Dclk1, Ddah2, Ddo, Ddr1, Ddx24, Defa17, Defb38, Defb50, Deptor, Dgkb, Dgki, Dhcr24, Diap2, Dip2a, Dkk2, Dlc1, Dlg1, Dlg2, Dlg4, Dlg5, Dlgap1, Dlgap2, Dlx6os1, Dmd, Dnahc5, Dnahc7b, Dnahc9, Dnajc21, Dnajc6, Dner, Dnm3, Dock2, Dock4, Dock8, Dok6, Dpp10, Dpp6, Dppa2, Dpyd, Dpys, Drosha, Dtnb, Dusp10, Dync1i1, Dynlrb2, Dysf, E030010A14Rik, E130114P18Rik, E130309D14Rik, E130309F12Rik, E230016K23Rik, E330009J07Rik, E330010L02Rik, Ebag9, Ebf1, Ech1, Echdc1, Edem1, Eea1, Eepd1, Efcab6, Efna5, Efr3a, Eftud1, Egfem1, Egflam, Egfr, Ehbp1, Ehbp1l1, Eif2c2, Eif2c3, Elac2, Elavl2, Elavl4, Eltd1, Eml6, Emr1, Emr4, Emx2, Enpp1, Enpp3, Enthd1, Epb4.1l2, Epb4.1l3, Epb4.1l4b, Epha5, Epm2a, Epyc, Erbb4, Erc1, Ergic1, Esr1, Esrra, Etnk1, Etv3, Etv6, Evc, Evc2, Exoc4, Exoc6, Exoc6b, Ext1, Eya1, Eya4, F13a1, Faf1, Fam105a, Fam110b,

Fam113b, Fam134b, Fam135b, Fam13c, Fam154a, Fam155a, Fam160b1, Fam162b, Fam176a, Fam184a, Fam190a, Fam19a1, Fam19a2, Fam19a4, Fam19a5, Fam49a, Fam5c, Fam82a1, Fam83a, Fam83f, Fam84b, Fam98a, Fasn, Fbln2, Fbxl17, Fbxl7, Fbxo18, Fbxo21, Fbxo32, Fbxo4, Fbxo5, Fer, Fer115, Fer116, Fgd6, Fgf12, Fgf14, Fgfr2, Fggy, Fhad1, Fhl3, Fig4, Flcn, Flg, Flrt2, Flt4, Fndc1, Fndc3b, Fosb, Foxd2, Foxd3, Foxi3, Foxn3, Foxo3, Foxp1, Foxp2, Foxp4, Fpr-rs4, Fpr3, Fras1, Frem1, Frk, Frmd3, Frmd4a, Frmd4b, Fsd11, Fshr, Fstl5, Fto, Ftsjd2, Fuca2, Fzd6, G930045G22Rik, Gabra2, Gabra4, Gabrb1, Gabrb3, Gabrg3, Galnt14, Galnt16, Gas2l1, Gbp1, Gbp5, Gc, Gcn111, Ghr, Gimap3, Gliplr1, Glis3, Glp1r, Glra3, Gltscr2, Gm10033, Gm10068, Gm10212, Gm10283, Gm10327, Gm10339, Gm10373, Gm10384, Gm10406, Gm10570, Gm106, Gm10649, Gm10696, Gm10715, Gm10963, Gm11161, Gm11217, Gm11228, Gm11240, Gm11261, Gm11376, Gm11751, Gm11757, Gm11758, Gm11762, Gm11823, Gm11867, Gm11884, Gm12023, Gm12068, Gm12132, Gm12296, Gm12474, Gm12478, Gm12519, Gm12532, Gm12600, Gm12602, Gm12637, Gm12648, Gm12649, Gm12666, Gm12668, Gm12680, Gm12695, Gm12708, Gm12724, Gm12811, Gm12824, Gm12841, Gm12886, Gm13235, Gm13251, Gm13272, Gm13327, Gm13847, Gm13849, Gm13974, Gm14061, Gm14271, Gm14643, Gm14697, Gm15104, Gm15137, Gm15155, Gm15404, Gm15494, Gm15581, Gm15631, Gm15668, Gm15723, Gm15825, Gm15834, Gm15939, Gm16029, Gm16039, Gm1604A, Gm1604b, Gm16070, Gm16156, Gm16268, Gm16365, Gm16430, Gm16513, Gm16537, Gm16609, Gm16615, Gm16629, Gm16630, Gm16705, Gm16724, Gm16736, Gm16742, Gm16760, Gm16889, Gm16896, Gm16899, Gm16901, Gm16936, Gm16950, Gm16988, Gm17033, Gm17067, Gm17265, Gm17340, Gm17412, Gm17452, Gm17473, Gm17480, Gm17609, Gm17683, Gm1993, Gm20388, Gm20429, Gm2078, Gm2128, Gm2244, Gm2464, Gm2694, Gm2790, Gm2800, Gm2824, Gm2832, Gm2864, Gm2895, Gm3072, Gm3149, Gm3164, Gm3222, Gm3264, Gm3404, Gm3408, Gm3558, Gm3629, Gm3636, Gm3676, Gm3739, Gm4219, Gm4301, Gm4788, Gm4794, Gm4876, Gm4952, Gm4981, Gm5045, Gm5105, Gm5127, Gm5150, Gm5420, Gm5494, Gm5506, Gm5559, Gm5567, Gm5570, Gm5622, Gm5623, Gm5796, Gm5852, Gm5860, Gm5934, Gm597, Gm628, Gm6288, Gm6685, Gm6741, Gm7334, Gm765, Gm766, Gm7714, Gm7732, Gm7782, Gm7792, Gm7822, Gm7954, Gm7995, Gm8082, Gm8369, Gm8374, Gm8882, Gm8897, Gm8975, Gm9008, Gm960, Gm9740, Gm9750, Gm9766, Gm9992, Gna14, Gnaq, Golga7, Golga7b, Gp1ba, Gp49a, Gpa33, Gpc5, Gpc6, Gpha2, Gphn, Gpm6a, Gpr108, Gpr110, Gpr115, Gpr125, Gpr126, Gpr132, Gpr158, Gprin3, Gpx3, Grb10, Grhl2, Gria4, Grid1, Grid2, Grik2, Grik3, Grin2a, Grin2b, Grina, Grip1, Grm1, Grm3, Grm5, Grm7, Grm8, Grxcr1, Gsdmcl1, Gsta3, Gstcd, Gstm5, Gucy1b3, Gulp1, H2-M2, H60b, Habp2, Hace1, Hbs11, Hdac9, Hdcc2, Heatr6, Heca, Herc3, Hhat, Hibadh, Hipk2, Hirip3, Hivep2, Hivep3, Hk1, Hmcn1, Hmg20a, Hmga2, Hnf4g, Homer2, Hook1, Hpse2, Hrh1, Hs3st1, Hs3st2, Hs3st5, Hs6st3, Hsf2, Hsf2bp, Htr7, Htt, Hus1, Hyal4, Ica1, Ifit2, Ifltd1, Ifna4, Ift27, Igf1, Igf2bp3, Ighv1-19, Ighv1-24, Ighv1-84, Ighv11-2, Ighv8-9, Igkv18-36, Igkv4-78, Igkv6-25, Igkv8-18, Igsf3, Ikbkap, Il1rap, Il1rapl1, Il2rb, Il31ra, Immp11, Inadl, Inpp4b, Ints1, Ipo13, Iqej, Iqsec1, Iqsec3, Irak3, Irs1, Ispd, Itgb4, Itgbl1, Itpr1, Itpr2, Jak2, Jakmip1, Jazf1, Jph1, Kank1, Kbtbd11, Kcnab1, Kenb2, Kcnc1, Kcnc2, Kend2, Kcnh1, Kcnh3, Kcnh5, Kcnh6, Kcnh8, Kenip1, Kenip4, Kcnk10, Kcnk9,

Kenmb2, Kcnq3, Kcnq5, Kent2, Kctd8, Kdm4b, Kdm4c, Kdr, Khdrbs2, Khdrbs3, Kif21a, Kifap3, Klc2, Klf10, Klf15, Klk1b1, Klra9, Ksr2, L3mbtl3, L3mbtl4, Lama1, Lama2, Lama4, Large, Larp6, Lbh, Lclat1, Ldb2, Lemd3, Leprel1, Lgr5, Lhcgr, Lifr, Limch1, Lin28b, Lin7a, Lingo2, Lipa, Lipm, Lipn, Lipo1, Lmbrd1, Lmbrd2, Lmed1, Lmo3, Lphn3, Lpp, Lrba, Lrfn2, Lrfn5, Lrp1, Lrp12, Lrp1b, Lrpprc, Lrrc42, Lrrc4c, Lrrc61, Lrrc68, Lrrc7, Lrriq1, Lrrk2, Lrrn1, Lrrtm4, Lsamp, Ltbp1, Luzp2, Lyst, Macf1, MacroD2, Magi1, Magi2, Mamdc2, Map2k2, Map3k4, Map3k5, Mapk10, Mapkap1, Mast4, Matk, Matn2, Matn3, Mb, Mcm5, Mcm9, Mcoln3, Mctp1, Mdfic, Mdga1, Mdga2, Mecom, Med12l, Med13l, Mef2a, Megf9, Mei4, Meis1, Men1, Meox2, Met, Mex3a, Mfap5, Mgam, Mgat4c, Mgst1, Mical3, Mitf, Mkl1, Mkl2, Mllt3, Mllt4, Mllt6, Mmp16, Mmrn1, Mocs1, Morc1, Mpdz, Mpp6, Mpped1, Mrap2, Mrpl13, Ms4a14, Ms4a4c, Ms4a4d, Ms4a7, Msl2, Msrb3, Mtap, Mtap7, Mterfd3, Mthfd11, Mthfd2l, Mtss1, Muc16, Muc19, Muc20, Mug1, Mug2, Mup15, Mup16, Mup2, Myb, Myh13, Myh2, Myo16, Myo18a, Myo1d, Myo3b, Myt1l, Nalcn, Nat2, Nav3, Nbea, Nbeal1, Ncald, Ncdn, Ncf4, Ncoa7, Ncor2, Nde1, NdrG1, Ndufs8, Nebl, Negr1, Nell1, Nell2, Neto1, Neurl1a, Neurl1b, Neurod6, Nf2, Nfe2, Nfia, Nfib, Nfic, Nfya, Nhlrc3, Nhsl1, Nipal2, Nkain2, Nkain3, Nkx2-5, Nlgn1, Nlrp4e, Nlrp9c, Nms, Nos1, Nos2, Npas3, Npffr2, Npr3, Npy1r, Nr2c1, Nrbp2, Nrg1, NrXn1, NrXn2, NrXn3, Nsfl1c, Nt5dc1, Nt5dc3, Ntf3, Ntm, Ntng1, Ntrk3, Nuak1, Nubpl, Nudcd1, Nuf2, Numbl, Nxph1, Obox3, Oc90, Oca2, Odz1, Odz2, Odz3, Oit3, Olfm3, Olfml2b, Olfr101, Olfr107, Olfr113, Olfr115, Olfr118, Olfr125, Olfr129, Olfr1294, Olfr1431, Olfr1491, Olfr1497, Olfr1500, Olfr308, Olfr339, Olfr38, Olfr398, Olfr403, Olfr448, Olfr460, Olfr76, Olfr810, Opcml, Opn3, Opn5, Oprk1, Oprm1, Osbp2, Osbpl6, Osbpl9, Osmr, Otolg, Otud7a, Oxct1, Oxr1, Pabpc1, Pabpc4l, Pacrg, Pacsin2, Pag1, Palld, Palm2, Palmd, Pam, Papd4, Pappa, Pappa2, Park2, Pax2, Pcbp3, Pcdh15, Pcdh18, Pcdh7, Pcdh9, Pcdha11, Pclo, Pcmt1, Pcnxl2, Pcnxl3, Pcsk5, Pcx, Pde10a, Pde1a, Pde1c, Pde4b, Pde5a, Pde7b, Pdzd2, PdZrn3, PdZrn4, Peg3, PfkM, Pgap1, PgcP, Pgk1, Phc2, Phf14, Phf21b, Phkb, Phox2b, Phyhipl, Pid1, Pigk, Pik3ap1, Pik3c2g, Pisd, Pja2, Pkd1, Pkdec, Pkhd1, Pkib, Pla2g6, Plagl1, Plcb4, Plce1, Plch1, Plcl2, Plcx3, Plcz1, Pld1, Pld5, Plec, Plekhg1, Plekhh2, Plscr3, Plxdc2, Plxna4, Plxnc1, Pofut2, Poli, Polr3b, Polrmt, Pon2, Postn, Ppfia2, Ppfibp1, Ppm1h, Ppm1k, Ppp1r10, Ppp1r14c, Ppp1r3a, Ppp1r9a, Ppp4r4, Ppp6r3, Prdm1, Prdm5, Prep, Prex2, Prh1, Prickle2, Prim2, Prima1, Prkag2, Prkar2b, Prkce, Prkd1, Prkg1, Prlr, Prmt8, Prodh, Prpf38b, Prr5, Prune2, Psd3, Psg28, Psme4, Ptbp1, Ptk2, Ptn, Ptpn3, Ptprcap, Ptprd, Ptprf, Ptprk, Ptprm, Ptprq, Ptprr, Ptprs, Ptprz1, Purg, Pvt1, Qk, RNasePnuc, RP23-405M24.1, RP24-345H5.2, Rab11fip4, Rab30, Rab31, Rabgap1l, Rad51l1, Rai1, Rai14, Raly1, Ranbp17, Rap1gds1, Rapgef5, Rasef, Rassf3, Rassf8, Raver2, Rb1cc1, Rbfox1, Rbfox2, Rbfox3, Rbm14, Rbm20, Rcan2, Rdh16, Rdh19, Reg3g, Rell1, Reln, Ret, Rftn1, Rfx3, Rgma, Rgs20, Rgs22, Rgs6, Rgs7, Rhag, Rhbdd1, Rhobtb1, Rhoj, Rhpn1, Rictor, Rims1, Rims2, Rims3, Rmst, Rnf144a, Rnf152, Rnf220, Rnls, Robo1, Robo2, Ror1, Rorb, Rorc, Ros1, Rp1, Rpn1, Rrp1, Rspo2, Rsrc1, Rtdr1, Rtn1, Runx2, SNORA17, SNORA48, SNORA67, SNORA71, SNORA72, SNORD115, SNORD116, SNORD95, Safb2, Samd12, Samd3, Samsn1, Satb1, Scaf8, Sclt1, Scmh1, Sdk1, Sec22c, Sema3c, Sema3d, Sema3e, Sema5a, Sema6b, Sema6d, Serpina1f, Serpina3i, Serpinb3b, Sesn1,

Sfxn5, Sgcd, Sgce, Sgcz, Sgip1, Sgk1, Sgms1, Sgsm3, Sh2d1b1, Sh3bp1, Sh3gl2, Sh3rf1, Shank3, Shisa6, Shisa9, Shpk, Shq1, Sim1, Sirpb1a, Six3os1, Skap2, Skint11, Skint5, Skint8, Skp2, Slamf6, Slc10a7, Slc13a4, Slc16a10, Slc16a7, Slc17a8, Slc18a1, Slc1a1, Slc1a3, Slc22a1, Slc22a22, Slc22a26, Slc22a27, Slc22a28, Slc22a29, Slc22a30, Slc24a2, Slc24a3, Slc25a13, Slc25a21, Slc25a26, Slc29a3, Slc2a12, Slc2a13, Slc2a9, Slc30a4, Slc35d1, Slc35f1, Slc35f3, Slc37a1, Slc38a1, Slc38a4, Slc44a5, Slc4a4, Slc4a8, Slc5a4a, Slc6a1, Slc6a11, Slc6a12, Slc6a9, Slc8a1, Slc9a4, Slco1a5, Slco1b2, Slco1c1, Slco5a1, Smap1, Smarca2, Smarcad1, Smchd1, Smg5, Smgc, Smndc1, Smoc1, Smoc2, Smr2, Smyd3, Snapc3, Snca, Sncaip, Snd1, Snip1, snoR38, Snrpn, Sntb1, Sntg1, Sntg2, Snx10, Snx13, Snx25, Snx29, Sobp, Sorbs1, Sorbs2, Sorcs1, Sorcs2, Sorcs3, Sox2ot, Sox5, Spag16, Spag17, Spata16, Spata17, Spata22, Spata5, Spata6, Specc11, Speer2, Speer4e, Spef2, Spock3, Spon1, Srdb1, Srgap3, Srrm4, Srrt, St18, St3gal3, St6galnac3, St7, St8sia1, Stambpl1, Stau2, Stk3, Stk31, Stk32b, Stk38l, Ston2, Stx3, Stxbp4, Stxbp5, Stxbp6, Styk1, Sufu, Sulf1, Sult1b1, Sult1c1, Sult2a4, Sult2a5, Sult2a6, Supt3h, Susd1, Svep1, Sybu, Syn2, Syn3, Syne1, Synj2bp, Syt1, Syt10, Syt7, Taar6, Tab1, Tanc2, Tas2r106, Tas2r107, Tatdn2, Tbc1d22a, Tbc1d5, Tbx15, Tbx19, Tbxas1, Tcf20, Tcl1b2, Tcl1b5, Tcte1, Tcte2, Tdrd9, Tecrl, Tff2, Tg, Thada, Themis, Thsd7a, Thsd7b, Tiam2, Tigd2, Tjp3, Tle1, Tle2, Tle4, Tll2, Tlr4, Tm7sf4, Tm9sf3, Tmc1, Tmcc1, Tmcc3, Tmem117, Tmem132c, Tmem132d, Tmem135, Tmem178, Tmem184b, Tmem2, Tmem200a, Tmem207, Tmem232, Tmem26, Tmem71, Tmem9, Tmprss11a, Tmprss11d, Tmprss11f, Tmprss15, Tmprss3, Tmtc2, Tmtc3, Tnc, Tnfsf14, Tnip3, Tnrc6b, Tns3, Tph2, Tpk1, Tprg, Tpte, Traf3ip2, Trappc9, Trdn, Trerf1, Trhde, Trhr, Trim62, Trmt11, Trmt12, Trmt2a, Trp63, Trpm1, Trpm3, Trpm6, Trps1, Tsga10, Tsga14, Tshz2, Tshz3, Tspan11, Tspan12, Tspan9, Ttc23l, Ttc27, Ttc28, Ttc35, Tuba8, Txlnb, Txnrd3, Tyms, U1, U2, U6, U7, Ube3b, Ubr5, Uchl5, Ugt1a10, Ugt2a3, Ugt3a1, Ugt3a2, Unc45b, Unc5c, Unc5d, Unc79, Ush2a, Usp15, Usp19, Usp24, Ust, Utrn, Vac14, Vat1l, Vav3, Vcam1, Vdr, Vep1, Vezt, Vip, Vit, Vmn1r179, Vmn1r183, Vmn1r184, Vmn1r185, Vmn1r28, Vmn1r3, Vmn1r31, Vmn1r42, Vmn1r43, Vmn1r79, Vmn2r-ps100, Vmn2r-ps54, Vmn2r100, Vmn2r102, Vmn2r103, Vmn2r104, Vmn2r105, Vmn2r106, Vmn2r108, Vmn2r109, Vmn2r110, Vmn2r13, Vmn2r18, Vmn2r21, Vmn2r23, Vmn2r24, Vmn2r25, Vmn2r26, Vmn2r4, Vmn2r48, Vmn2r58, Vmn2r60, Vmn2r61, Vmn2r62, Vmn2r63, Vmn2r65, Vmn2r7, Vmn2r70, Vmn2r72-ps, Vmn2r75, Vmn2r78, Vmn2r80, Vmn2r82, Vmn2r87, Vmn2r91, Vmn2r92, Vmn2r93, Vmn2r95, Vmn2r96, Vmn2r97, Vmn2r98, Vmn2r99, Vnn1, Vps13a, Vps13b, Vsnl1, Vta1, Vtila, Vwde, Wdpcp, Wdr25, Wdr27, Wdr63, Wdr96, Wisp1, Wnt2, Wrn, Wscd2, Wwox, Xab2, Xdh, Xkr4, Xpnpep1, Xylt1, Y-RNA, Yif1a, Ypel2, Zbbx, Zbtb4, Zc3h3, Zc3h7a, Zdhhc14, Zdhhc17, Zdhhc6, Zeb1, Zfa, Zfand3, Zfat, Zfhx4, Zfml, Zfp160, Zfp207, Zfp248, Zfp423, Zfp438, Zfp442, Zfp534, Zfp618, Zfp804b, Zfp81, Zfp850, Zfp943, Zfp944, Zfp946, Zfp947, Zfp959, Zfp964, Zfpm2, Zhx2, Zkscan17, Zmat4, Zmpste24, Zmym4, Zwint

B.2 Learning Associated Genes

Learning associated genes are from work previously published in Science by Zovoilis et al. These genes are activated in the event of a learning stimulus.

0610011L14Rik, 1110012J17Rik, 1110018G07Rik, 1110032A04Rik,
 1110049F12Rik, 1190005F20Rik, 1500003O03Rik, 1700001E04Rik, 1700012B15Rik,
 1700025F22Rik, 1700037H04Rik, 1700066M21Rik, 1700081L11Rik, 1810041L15Rik,
 1810074P20Rik, 2010007H12Rik, 2310014H01Rik, 2310035C23Rik, 2510009E07Rik,
 2610019F03Rik, 2610028A01Rik, 2610036D13Rik, 2610110G12Rik, 2700081O15Rik,
 2900092E17Rik, 3110002H16Rik, 3110043O21Rik, 3110048L19Rik, 3110052M02Rik,
 4732471D19Rik, 4930506M07Rik, 4930555G01Rik, 5330417C22Rik, 5430417L22Rik,
 5730410E15Rik, 6330503K22Rik, 6330578E17Rik, 6430704M03Rik, 8430419L09Rik,
 9530068E07Rik, 9930013L23Rik, 9930021J03Rik, A430033K04Rik, A630089N07Rik,
 AI593442, AI987944, AU040829, AW551984, Aatf, Abca2, Abcc5, Abcd3, Abcf1,
 Abhd13, Abi1, Acadsb, Acbd5, Accn1, Ache, Acly, Acox1, Acsl6, Actc1, Actl6b,
 Actr3b, Acvr1, Acvr2a, Adam11, Adam15, Adamts19, Adamts2, Adcy3, Adcy5,
 Add2, Adnp, Adra2a, Adra2c, Adrbk1, Aes, Aggf1, Agpat1, Agpat6, Ahi1, Aifm1,
 Ak3l1, Ak5, Akap1, Akap8, Akt2, Akt3, Aldh18a1, Aldh4a1, Alg2, Aloxe3, Amd1,
 Anapc4, Ank3, Ankrd10, Ankrd40, Ankrd6, Anln, Anxa11, Ap1g1, Ap1g2, Ap2a1,
 Ap2m1, Ap3m1, Apaf1, Apba2, Aplp2, Araf, Arf2, Arf6, Arfgef2, Arhgap21, Arhgef2,
 Arhgef3, Arhgef4, Arid1a, Arid4b, Arih1, Arl4d, Arl5a, Arl8b, Arnt2, Arntl, Arsb,
 Asb8, Asph, Asxl1, Atad1, Atf2, Atg4b, Atg4c, Atp1b2, Atp2a1, Atp2a2, Atp6v0d1,
 Atp6v1b2, Atp6v1g2, Atrx, Atxn2l, Aut2, Avp, Axl, Azi2, B230312A22Rik,
 B3gat1, B4galnt1, B4galnt4, B4galt7, BC011426, BC018242, BC024479, BC024659,
 BC027072, BC031441, BC032203, BC049349, Bai1, Bai3, Baiap3, Bat2, Bcl2l1,
 Bcl9, Bmi1, Bmp2k, Bmpr1b, Bnip3l, Brap, Brms1l, Brwd2, Btaf1, Btbd10, Btrc,
 C030002C11Rik, C030046I01Rik, C230055K05Rik, C230096C10Rik, C330007P06Rik,
 C80913, Cacna1d, Cacna1g, Cacnb2, Cacng3, Cacng8, Cadm4, Cadps, Calm1, Calu,
 Camk1, Camk2d, Camkk2, Camta2, Canx, Capn2, Capzb, Cbfa2t2, Cbln2, Cbx5,
 Ccdc117, Ccdc127, Ccdc49, Ccdc67, Ccni, Ccnl2, Cct2, Cd8b1, Cdc37l1, Cdc42bpb,
 Cdh11, Cdh12, Cdh2, Cdh9, Cdk4, Cdk8, Cdkn2aip, Cecr6, Cenpb, Cep110,
 Cep164, Cfh, Cfl1, Cggbp1, Chfr, Chordc1, Chrna4, Chrn2, Chst2, Cited2, Clasp2,
 Cldn11, Clint1, Clip2, Clip3, Clk2, Clpx, Cltb, Cltc, Cnksr2, Cnksr3, Cnot1, Cnot3,
 Cnot7, Cnot8, Cntn1, Cntn6, Colla1, Col4a1, Col4a2, Col6a1, Coro1b, Coro2b,
 Cpeb4, Cplx1, Crk, Crot, Csdc2, Csde1, Csell, Csn3, Csnk1d, Csnk2a1, Cspg5,
 Cstf2, Ctbp2, Ctnnb1, Ctnnd1, Ctnnd2, Cttm, Cttmnp2, Ctxn1, Cugbp2, Cul2,
 Cyb5r4, Cyfip2, Cyp3a11, D030016E14Rik, D0H4S114, D15Ertd621e, D15Wsu169e,
 D230025D16Rik, D4Bwg0951e, D6Wsu116e, D9Ertd402e, Dab1, Delk3, Ddx18,
 Ddx19a, Ddx50, Dedd2, Dennd4c, Dgcr8, Dgkb, Dgkh, Dgkq, Dgkz, Dhcr7, Diap1,
 Dlat, Dlg1, Dlg5, Dmtf1, Dmwd, Dmxi1, Dnaja3, Dnajb5, Dnajc13, Dnajc14,
 Dnajc16, Dnajc5, Dnm1, Dnm1l, Dnm2, Doc2b, Dock7, Dock9, Donson, Dopey1,
 Dpy19l1, Dsp, Dtx3, Dtx4, Dvl1, Dynlt3, Dyrk1a, E130201H02Rik, E430028B21Rik,
 Edc3, Eef1a1, Eef1a2, Eef2, Efna3, Egl1, Eid1, Eif4b, Eif4enif1, Eif4g2, Eif5a,
 Elmod1, Enoph1, Ensa, Epb4.1l1, Epb4.1l3, Epb4.9, Epdr1, Epn1, Epn3, Eps15,
 Eps8, Erbb2ip, Erc2, Erlin2, Ero1l, Exoc2, Exoc5, Fads1, Faim2, Faneg, Fastkd2,
 Fbxl19, Fbxl3, Fbxl5, Fbxo11, Fbxo28, Fbxo3, Fcho2, Fem1c, Fezf2, Fgd1, Fgf1,
 Fgf13, Fgfr1, Fgl1, Fip1l1, Fkbp14, Fkbp15, Fkbp5, Flot2, Flywch1, Fmn2, Fmnl1,
 Fndc3a, Fndc4, Fntb, Foxk2, Foxn2, Fscn1, Fubp1, Fut8, Fzd10, Gabbr2, Gabra1,
 Gabra3, Gabrb2, Gabrb3, Gad1, Galc, Galnt1, Gas1, Gas7, Gatad2a, Gbx2, Gclm,

Gdap1, Gdi1, Gdi2, Gfap, Ggcx, Git1, Gjb6, Gltp, Gm672, Gmeb2, Gna11, Gna12, Gnai1, Gnao1, Gnas, Gnb5, Gng7, Gnptab, Golga5, Gpc1, Gpd1l, Gps2, Gpt2, Gria4, Grin1, Grit, Grm7, Gsk3a, Gspt1, Gstm1, Gtdc1, Gtpbp2, Gucy1b3, Gzfl, H1fx, Hap1, Hapln4, Hdac2, Hdac4, Hdgfrp3, Heatr3, Heca, Hectd2, Herc2, Hiat1, Hipk2, Hisppd1, Hivep1, Hivep2, Hmgcr, Homer1, Hpcal4, Hps3, Hs3st2, Hs6st2, Hsd17b11, Hsf1, Hsp90ab1, Htr1a, Iars, Ick, Ifit1, Ikzf5, Ilf3, Ilkap, Ina, Ing2, Inha, Inpp4b, Inpp5b, Inpp5e, Ints10, Ints6, Ipo11, Ipo9, Ireb2, Irf2bp1, Isca1, Itga7, Itgam, Jam2, Josd1, Jph4, Kbtbd7, Kcnab1, Kcnab2, Kcnc1, Kenip2, Kcnip3, Kcnip4, Kenj4, Kenj6, Kcnk2, Kenn2, Kcns2, Kent2, Kctd12, Kctd13, Kdelr2, Khdrbs1, Kif21a, Kif21b, Kif3a, Kirrel3, Klc2, Klhdc5, Klhl21, Klhl23, Klhl28, Klhl5, Kpna4, L1cam, L3mbtl2, Lace1, Large, Larp1, Lass2, Lats2, Ldb2, Lemd3, Leng8, Lgi1, Lhfpl3, Lingo1, Lix1, Lmbr1, Lmo3, Lnp, Lonrf2, Lphn1, Lpl, Lrch2, Lrp1b, Lrrc41, Lrrc42, Lrrc4b, Lrrc57, Lrrc59, Lrrc7, Lrrn3, Lsm14b, Lynx1, Mafg, Magee1, Maml1, Maml2, Man1a, Man1c1, Map2k1, Map2k5, Map2k7, Map3k12, Map3k5, Mapk1, Mapk6, Mapk8ip2, March6, March9, Marcksl1, Matr3, Mbd1, Mccc2, Mcf2l, Mcl1, Mdm1, Me2, Med12, Mesdc1, Mfap3, Mfap3l, Mfsd11, Mgat5b, Mical2, Minpp1, Mitf, Mkks, Mlf2, Mll5, Mlxip, Mon2, Morc2a, Mpdz, Mphosph9, Mrpl3, Mt3, Mta1, Mtap6, Mtap7, Mtmr1, Mtmr14, Mtmr2, Mtpn, Mxra7, Myadm, Myh10, Mylip, Mynn, Myo18a, Myst4, Nab1, Narf, Nars2, Nbr1, Ncapd2, Ncdn, Nckap1, Ncoa2, Ncoa4, Ncoa7, Ndel1, Ndn, Ndst1, Nefh, Nelf, Neurod1, Neurod2, Neurog3, Nexn, Nfx1, Nkx2-2, Nln, Nnat, Nol11, Nol4, Nol6, Nosip, Nov, Npy2r, Nras, Nrcam, Nrd1, Nrf1, Nrg3, Nsdhl, Ntng1, Nuak1, Nxph1, Obfc2b, Ogdh, Ogt, Olfm2, Olfm3, Olig1, Orc5l, Osbp, Osbpl11, Osbpl3, Otud4, Otud5, Otud6b, Oxr1, P4ha1, Pacs1, Pacsin2, Pafah1b2, Paics, Pak1, Palm, Parp1, Parp6, Pbrm1, Pcdh8, Pcdhb5, Pcdhga7, Pcgf6, Pcid2, Pclo, Pcsk7, Pcyt1b, Pdcl, Pea15a, Peli1, Pex3, Pex5, Pgbd5, Pgm1, Phc1, Phf12, Phf2, Phf20l1, Phf23, Phkb, Picalm, Pigq, Pik3ca, Pik3r3, Pim2, Pisd, Pja1, Pkia, Pkn2, Pkp4, Pla2g7, Plat, Plcg1, Pldn, Plekhh2, Plekhf2, Plekhg1, Plxna1, Pnkd, Pnpla8, Pnrc1, Polr3e, Pou3f3, Pou6f1, Ppfia1, Ppm1b, Ppm1e, Ppme1, Ppp1cc, Ppp1r2, Ppp1r3c, Ppp1r8, Ppp1r9b, Ppp2r1a, Ppp2r2a, Ppp2r2b, Ppp2r5a, Ppp2r5c, Ppp3r1, Prei4, Prkar1a, Prkar1b, Prkca, Prkcc, Prkcd, Prkci, Prpf8, Prr12, Prune, Psm2, Psm29, Pten, Ptk2b, Ptp4a1, Ptpn12, Ptpn5, Ptprg, Ptpn, Ptpro, Ptpns, Pum1, Pum2, Pus1, Pvrl1, Pygb, Qk, Rab1, Rab11b, Rab11fp2, Rab11fp4, Rab1b, Rab31, Rab37, Rab39b, Rab4a, Rab5a, Rab6, Rab8b, Rabep1, Rabgef1, Rad21, Ralgps1, Ranbp6, Rap1b, Rap1gap, Rapgef4, Rapgef1, Rasa3, Rasgrf1, Rasgrp1, Rasl11a, Rassf5, Raver2, Rbak, Rbbp5, Rbl2, Rbm12b, Rbm22, Rbm8a, Rbms3, Rbmx, Rcbtb1, Rdh12, Rdh13, Rem2, Reps1, Rftn1, Rfxap, Rgs16, Rgs19, Rgs4, Rhob, Ric8b, Rims2, Ring1, Riok3, Rlf, Rmnd5a, Rnf103, Rnf4, Rnf41, Rnmt, Rogdi, Rpl10a, Rps6ka4, Rps6ka5, Rqcd1, Rragb, Rragc, Rreb1, Rsc1a1, Rtf1, Sacm1l, Sacs, Samm50, Sap130, Sap25, Saps3, Sbf1, Sbk1, Scg2, Schip1, Scn1b, Scn3b, Scn8a, Scrn3, Sert1, Sdc4, Sdccag3, Sdf4, Sdha, Sec14l1, Sec23a, Sec23ip, Sec61a2, Sec63, Sel1l, Senp2, Sepn1, Sept11, Sept5, Sept6, Sept9, Serac1, Serpina3n, Sesn1, Setdb1, Sfi1, Sfpq, Sfrs1, Sfrs2, Sfrs4, Sgpl1, Sh2b1, Sh3bgrl, Sh3bp4, Sh3bp5, Sh3gl2, Shank3, Sipa1l3, Sirpa, Sirt2, Slain1, Slc12a6, Slc22a17, Slc25a16, Slc25a22, Slc25a23, Slc25a25, Slc25a46, Slc27a1, Slc30a9, Slc33a1, Slc35f1, Slc36a1, Slc41a1, Slc43a2, Slc44a2, Slc6a1, Slc8a1, Slc9a1,

Slc9a2, Slit2, Slitrk1, Slitrk3, Slitrk4, Slitrk5, Smad1, Smap1, Smarcd1, Smarcc2, Smarcd1, Smc1a, Smchd1, Smoc2, Sms, Snap25, Snapc1, Snrpa, Snrpn, Snurf, Son, Sos1, Spag1, Sparc, Spnb3, Spnb4, Spock1, Spon1, Sppl3, Spred2, Srp72, Srr, Ssfa2, Ssh3, Ssr1, Ssx2ip, St18, St3gal2, St5, Stac2, Stau1, Stk24, Stk35, Stox2, Stra6, Strn4, Stt3b, Stx16, Sulf2, Supt5h, Supv3l1, Sv2b, Synpo2, Syp, Syt11, Syt16, Syt17, Syt4, Syt5, Sytl5, Taf4a, Taf5, Tanc1, Tars, Tbc1d12, Tbc1d15, Tbc1d23, Tbc1d5, Tbk1, Tbp, Tbr1, Tcea1, Tcerg1, Tef12, Tcfep2, Tcfe3, Terf2, Terf2ip, Tgfa, Thoc5, Thra, Thsd7b, Tia1, Tjap1, Tjp1, Tle3, Tlk2, Tm6sf1, Tm9sf4, Tmcc2, Tmed2, Tmed7, Tmeff1, Tmem106c, Tmem115, Tmem131, Tmem144, Tmem164, Tmem168, Tmem49, Tmem64, Tmod3, Tnc, Tnks1bp1, Tnrc6a, Tomm34, Tox4, Tpbg, Trabd, Traf7, Tram1, Trib2, Trim23, Trim3, Trim35, Trim46, Trim59, Trim62, Trim9, Trip4, Trp53, Trp53i11, Trp53inp1, Trpc4ap, Trrap, Tsnax, Tspan15, Tspan2, Tsr2, Tst, Ttbk1, Ttc19, Ttc21b, Ttc28, Ttc3, Ttc5, Ttc9c, Ttll1, Ttyh1, Tubal1, Tusc1, Twsg1, Txndc5, Uap1, Uap2, Ube2d1, Ube2d2, Ube2m, Ube2q1, Ube2v1, Ubl7, Ubp1, Ugt8a, Uhm1, Unc13b, Unc13c, Upf2, Upp2, Usp11, Usp21, Usp22, Usp32, Usp38, Usp39, Usp46, Usp47, Usp9x, Ust, Utp15, Vamp1, Vamp2, Vars, Vav3, Vcl, Vegfa, Vgll1, Vps13b, Vps18, Vps39, Vps4a, Vps4b, Vps72, Vps8, Wac, Wars, Wdr26, Wdr36, Wdr37, Wdr41, Wdr45l, Wdr6, Wdr7, Wdr70, Wdr77, Wee1, Whsc1, Wipi2, Wrn, Wsb2, Ymell1, Yrdc, Ythdf3, Ywhab, Ywhaz, Zbtb1, Zbtb24, Zdhhc17, Zdhhc20, Zfp2, Zfp248, Zfp260, Zfp263, Zfp273, Zfp365, Zfp369, Zfp384, Zfp410, Zfp423, Zfp426, Zfp445, Zfp563, Zfp592, Zfp617, Zfp641, Zfp646, Zfp655, Zfp715, Zfp72, Zfp74, Zfp811, Zfp9, Zfp91, Zhx1, Zhx2, Zik1, Zkscan3, Zmym2, Zmym4, Znrf3, Zswim1, Zswim5, Zyg11b, Zzz3

B.3 APP Upregulated Genes

These genes are upregulated in mice with *APP_{NL-G-F}* genotype. Differential expression analysis was performed by Yubo Cheng.

Prl, Xist, Gm42715, Gm15446, Gm16867, mt-Tg, mt-Tr, Slc36a1, Kcnq2, Hif3a, Rgs16, Amd1, Tmem267, 0610030E20Rik, Plin4, Gm3883, Synpo2, Gm19439, Pcdha11, Pisd-ps1, Gsk3b, Hic2, Entpd4, Mid1, Fosb, C1ql2, Cebpg, Pcdha6, Sec14l5, Kif26b, Il17rd, Tspan18, Rab27a, Zbtb40, Cables1, Peg10, Fosl2, Ide, Sgk1, Ywhag, Ntng1, Tnxb, Nos1, Fn1, Zbtb16, Lrrc10b, Zfhx4, Traf3, Irs2, Bgn, 9230112E08Rik, Adamts2, Cblb, St6gal1, Cacna1i, Sik1, Kif13b, Mdga1, Dsp, Naa60, Gm45640, Spry4, Mxd4, Inhba, Doc2b, Nptx1, Parvb, Utp14b, Sipa112, Gm1043, Ncoa5, Btaf1, Soga1, Zkscan3, Gm26917, Nav1, Trp53i11, Ddr2, Kdm5c, 08-Mar, Tanc1, Tmem104, Chd7, Plch2, Plce1, Dpp8, Hdac4, Ston2, Rasd2, Cacna1c, Mycl, Dusp4, Aff1, Bsn, Klf13, Tceal3, Mical3, Dio2, Adra1d, Syn3, Eif1, Cpeb4, Ago2, Kmt2d, Itpkb, Plekha2, Chmp3, Spen, Neurl1b, Fbxl18, Lrtm2, Fkbp5, Pag1, Lhfp12, Spata13, Dock5, Cacna1h, Ttn, Pogz, Daam2, Sv2c, Elnf2, Rapgef3, Samd4b, Eif2s3x, Zdbf2, Eif4ebp2, Cspg4, Adarb1, Adamts20, Pcmt1, Sipa113, Ncor2, Kdm6b, Gse1, Prox1, Igf1r, Slc7a1, Ankrd6, Kbtbd11, Arhgap31, Shc3, Paqr8, Zdhhc23, Tmem28, Itsn1, Fgd6, Synpo, Pkd1, Foxo1, Dagla, Kmt2b, Crtc1, Slc39a14, Ctif, Panx2, Foxk1, Klhl3, Trak1, Per2, Slit1, Bcl6, Plekhm1, Dchs1, Csm2, Grin2c, Slc7a5, Sptb, Nhsl2, Homer1, Pde7b, Grm2, Per1, Gm42418, Shank3, Prdm8, Klhl29, Plxna4, Cbfa2t3,

Gpc4, Golm1, Zfp236, Pcnx, Gpt2, Gfod1, Sik2, Nrp1, Elmsan1, Sox11, Nr4a3, Ttbk1, Arhgef17, Lingo3, Slit3, Tbc1d16, Hipk2, Tns3, Zhx3, Synj2, Lrrc8a, Atxn7l3, Errfi1, 2900026A02Rik, Adecy1, Kcnc1, Ppp1r16b, Tnrc18, Unc80, Mfhas1, Lats2, Gjb6, Sel1l, Sash1, Smad3, Celsr3, Arhgap39, Plxna1, Kcna1, Adecy6, Ccdc97, C2cd3, Mkl1, Capn15, Abl2, Prkab2, Plppr2, Kcnc3, Kmt2a, Pcnx3, D10Wsu102e, Wscd2, Tnr, Phf2, Mast3, Smad7, Sbk1, Pou6f1, Galnt17, Med13l, Map1a, Jun, Pdcd11, Zfhx2, Hapln4, Bcr, Kcnip2, Stox2, Ntng2, Tln2, Chst2, Btbd9, Megf8, Auts2, Cbarp, Epb4111, Adgrb2, Arhgap23, Orai2, Foxo3, Otub2, Cpeb3, Rgs8, Lrp1, Wipf2, Adecy5, Unc5a, Zfp831, Tsc2, B3galt5, Mllt1, Zhx2, Fnip2, St3gal2, Ddi2, Stxbp6, Zfp142, Iqsec3, Adar, 5031439G07Rik, Tnik, Fbxo10, Sntb2, Helz, Tbkbp1, Sowaha, Cabp1, Lifr, Rapgef4, Kdm7a, Tnk2, Mfn2, Upf1, Camkk1, Acot11, Dlg5, Castor2, Dpp9, Prr12, Ubr4, Napepld, Kcnj10, Neurod2, Smg1, Foxn3, Ildr2, Slc38a2, Prdm2, Adecy9, Socs7, Klf9, Rtn4rl1, Slc7a14, Wdfy3, Adgrb1, Sgsm2, Ncdn, Slc41a1, Grin2b, Atxn2l, Pdzd2, Camta2, Pnmal2, Zcchc14, Nwd1, Ago3, Acin1, Nrnx2, Fam163b, Thsd7a, Shank1, Caskin1, Ubr2, Peak1, Alkbh5, Setd7, Zfp652, Kansl3, Arf3, Slc6a8, Prrc2a, Syt7, Ccdc6, Irf2bp2, Ttyh3, Ankrd11, Paqr9, Mecp2, Tet3, Rnf112, Wdtd1, Hectd4, Dapk1, Clstn2, Zswim8, Pcdh17, Brd4, Ptpnj, Prkar2a, Cbl, Fam171a1, Rptor, Plekhg5, Cacng2, Ssh2, Ski, Gpc1, Clasp1, Szt2, Dscam, Lrrtm1, Marf1, Nt5dc3, Sipal11, Ankrd52, Neurl1a, Src, Ago1, Pcdh1, Chst11, Prr14l, Nacc2, Cds2, Camta1, Med12l, Hcfc1, Mpdz, Celsr2, Cnm1, Fam168b, Cic, Pkp4, Fbxw11, Herc2, Gid4, Peg3, Disp2, Nfia, Kcnq3, Cul9, Chd3, Man2a2, Larp1, Pitpnm2, Aatk, Ryr2, Ksr2, Polr2a, Phlpp1, Fryl, Adam11, Dst, Pabpc1, Speg, Tnrc6b, Stx1b, Ddn, Ank3, Usp31, Plec, Smg7, Trrap, Rnf44, Mrs2, Prickle2, Ppp1r13b, Scn8a, Arhgef12, Map1b, Ehd3, Rere, Add2, Ppp1r9a, D430019H16Rik, Rapgef1, Atp2b2, Nova2, Scn2b, Abca1, Sbf1, Jph3, Rapgef2, Tub, Kdm2a, Mgat3, Ptpn11, Arid1b, Dixdc1, Slc8a2, Ppp1r9b, Trio, Camk2a, Dlg4, Sptbn2, Synrg, Wnk1, Rab11fip4, Sorl1, Trank1, Rnf157, Sfpq, Nfasc, Nisch, Crebbp, Huwe1, Mink1, Mapk8ip2, Syne1, Htt, Kmt2c, Cacna1a, Glg1, Kif1b

B.4 PreHS and Learning Genes

These genes are the intersect of the PreHS gene list and the learning-associated gene list.

Olfm3, Zfp248, Spon1, Zfp423, Kcnc1, Cdh11, Pacsin2, Snrpn, Ust, Ptpns, Kcnip4, Hs3st2, Col6a1, Pisd, Grm7, Heca, Lemd3, Lmo3, Gucy1b3, Dgkb, Smap1, Raver2, Kent2, Phkb, Lrrc42, Smoc2, Sh3gl2, Bai1, Cnksr3, Kif21a, Cntn1, Shank3, Lrp1b, Epb4.1l3, Qk, 1700025F22Rik, Lrrc7, Dlg5, Zdhhc17, Arntl, Bai3, Ttc28, Ctnnd2, Ak5, Mpdz, Cdh9, Cacna1g, BC024659, Nuak1, 4930506M07Rik, Rftn1, Ahi1, Dlg1, 2310035C23Rik, Slc6a1, Tnc, Rims2, Zhx2, Btre, Wrn, Ntng1, Map3k5, Thsd7b, Ncdn, 9930013L23Rik, Abcc5, Klc2, Sesn1, Cdh12, Myo18a, Smchd1, Large, Apaf1, Mitf, Dab1, Rab11fip4, Cntn6, Apba2, Gabrb3, Agpat1, Cdk8, Arnt2, Mtap7, Pclo, Vps13b, Smarcd1, Ldb2, St18, Gria4, Vav3, Hipk2, Slc8a1, Tbc1d5, Ctnnbp2, Oxr1, Zmym4, Bmpr1b, Slc35f1, Ncoa7, Nxph1, 1110012J17Rik, D15Ertd621e, Kcnab1, Trim62, Inpp4b, Accn1, Rab31, Hivep2, Plekhg1